

Review of Aeronautical Fatigue Investigations in Brazil

International Committee on Aeronautical Fatigue - ICAF 2021

Prepared by:

Carlos E. Chaves

On behalf of:

Fatigue, Fracture and Structural Integrity Committee

Brazilian Society of Engineering and Mechanical Sciences – ABCM

07/June/2021

SUMMARY

This report presents the review of fatigue and fracture investigations related to aeronautics performed in Brazil during the period from the middle of 2019 to the middle of 2021. Exceptionally, the contents of this report are not intended to be presented during any particular ICAF Conference during the year of 2021.

All papers, dissertations, theses and conference proceedings presented in this document were directly supplied by their authors, co-authors or advisors to the author of this review, and some of the works were previously presented in other conferences or are available from public sources.

CONTENTS

1. INTRODUCTION.....	10
2. CONCEPTS.....	12
3. ANALYSIS AND SIMULATION.....	16
4. METALLIC MATERIALS – FATIGUE AND FRACTURE PROPERTIES	23
5. METALLIC MATERIALS - FRETTING.....	26
6. METALLIC MATERIALS – PROCESSES.....	33
7. METALLIC MATERIALS – STRUCTURES.....	38
8. COMPOSITE MATERIALS AND STRUCTURES.....	42
9. HYBRID MATERIALS AND STRUCTURES.....	56
10. STRUCTURAL HEALTH MONITORING	65
11. LOADS.....	78
12. AIRWORTHINESS	81
13. REFERENCES.....	82

ABBREVIATIONS

3-ENF	Three Point Bend End-notched Flexure
4-ENF	Four Point Bend End-notched Flexure
ABCM	Associação Brasileira de Engenharia e Ciências Mecânicas (Brazilian Society of Engineering and Mechanical Sciences)
AFP	Automated Fiber Placement
AHM	Asymptotic Homogeneization Method
ANN	Artificial Neural Network
AR	Augmented Reality
ASTM	American Society for Testing and Materials
AZ	Adhesion Zone
BA	Bat (Optimization) Algorithm
BM	Base Metal
BVID	Barely Visible Impact Damage
CDM	Continuous Damage Mechanics
CF	Carbon Fiber Reinforced
CMOD	Crack Mouth Opening Displacement
CFRP	Carbon Fiber Reinforced Plastics
C(T)	Center Cracked in Tension (Specimen)
DCB	Double Cantilever Beam
DEN	Double-Edge Notched (Specimen)
DF	Distrito Federal
DI	Damage Index
DIC	Digital Image Correlation
EIS	Electrochemical Impedance Spectroscopy
FA	Firefly (Optimization) Algorithm
FCG	Fatigue Crack Growth
FD	Falling Dart
FDM	Fused Deposition Modeling
FEA	Finite Element Analysis
FEM	Finite Element Method

FFF	Fused Filament Fabrication
FIM	Fisher Information Matrix
FRF	Frequency Response Function
FSFT	Full-Scale Fatigue Test
FSpJ	Friction Spot Joining
FSW	Friction Stir Welding
G	Strain Energy Release Rate
GA	Genetic Algorithm
G_I	Mode I Strain Energy Release Rate
HAZ	Heat-Affected Zone
HZG	Helmholtz-Zentrum Geesthacht
IM	Inter-Metallic
LAMEF	Laboratório de Metalurgia Física
LVDT	Linearly Variable Displacement Transducer
LW	Lamb Waves
LSP	Laser Shock Process
LSPwC	Laser Shock Process without Coating
L-T	Longitudinal (Direction)
MBT	Modified Beam Theory
MCT	Multi-Continuum Theory
MG	Minas Gerais (State)
MMB	Mixed-Mode Bending
M(T)	Middle Tension (Specimen)
MWCM	Modified Wöhler Curve Method
NDT	Non Destructive Test
NZ	Nugget Zone
PA6	Polyamide 6
PAEK	Polyaryetherketone (Resin)
PDZ	Plastically Deformed Zone
PEEK	Polyether Ether Ketone (Resin)
PPS	Polyphenylene Sulfide
PR	Paraná (State)
PSD	Power Spectrum Density
R	Stress Ratio

R&D	Research and Development
RTA	Room Temperature Ambient
RTW	Room Temperature Wet
RJ	Rio de Janeiro (State)
RN	Rio Grande do Norte (State)
RS	Rio Grande do Sul (State)
RVE	Representative Volume Element
S/A	Sociedade Anônima (Corporation)
SERR	Strain Energy Release Rate
SG	Strain Gage
SHM	Structural Health Monitoring
SP	São Paulo (State)
SVET	Scanning Vibrating Electrode Technique
TCD	Theory of Critical Distances
T-L	Transverse (Direction)
TMAZ	Thermo-Mechanically Affected Zone
ULSF	Ultimate Lap Shear Force
VBM	Vibration-Based Method
VID	Visible Impact Damage

INDEX OF FIGURES

Figure 2-1 - Multiscale analysis model: (a) Two-dimensional RVE for the micro-scale analysis, (b) 3D laminated composite, (c) 2D RVE for the macro-scale analysis. Micro-scale analysis: (d) cross section of a quadratic and periodic array of circular fibers.	13
Figure 2-2 - C_{66}^* as a function of the macro failure degree θ for different values of fiber-matrix interface stiffness K_t and different sizes of the laminate interface thickness $t_{(2)}$	13
Figure 2-3 - Bi-linear traction-separation law for an equivalent mode loading.	15
Figure 2-4 - Definition of the J integral surrounding the cohesive zone.	15
Figure 2-5 - Comparison between numerical prediction for the crack growth rate and experimental results.	15
Figure 3-1 - Specimen geometry and loading conditions (dimensions in mm).	17
Figure 3-2 - Fatigue crack growth data for the specimen with peak load 20.5 kN. .	18
Figure 3-3- Equivalent plastic strain (k) along crack line. Values correspond to coordinates $y = 0$ and $z = 4.8\text{mm}$ (surface). – Equivalent plastic strain (k) along crack line. Values correspond to coordinates $y = 0$ and $z = 4.8\text{mm}$ (surface).....	18
Figure 3-4 - Finite Element model to simulate the impact test.	20
Figure 3-5 - Comparison between experimental and FE analyses: energy transferred vs. time for the $[+45^\circ/-45^\circ/+45^\circ/0^\circ/90^\circ]_s$ laminate under 5.91 J of impact.....	20
Figure 3-6 - Damage variables d_2 and d_6 for the layers of laminate $[+45^\circ/-45^\circ/+45^\circ/0^\circ/90^\circ]_s$ at the final of impact event.	21
Figure 3-7 - Contact force history for experimental, elastic and viscoelastic cases.	22
Figure 3-8 - Contact force history, for different values of contact friction.....	23
Figure 4-1- True stress–strain data and Ludwik’s model curves for AA7050-T7451 and AA7050-T6I4 conditions - True stress–strain data and Ludwik’s model curves for AA7050-T7451 and AA7050-T6I4 conditions.	24
Figure 4-2 - Experimental data and stress–life model fitting results using the maximum-likelihood estimation for AA7050-T7451 and AA7050-T6I4 conditions (unnotched specimens).....	25
Figure 4-3 - Experimental data and stress–life model fitting results using the maximum-likelihood estimation for AA7050-T7451 and AA7050-T6I4 conditions (notched specimens).....	25
Figure 5-1 - Schematic representation of the three case studies considered in the H-L loading blocks: (a) only partial slip, (b) gross slip and partial slip and (c) gross slip (including wear effects into the modelling) and partial slip.	27

Figure 5-2 - FE model, loading and geometric configurations	27
Figure 5-3 - Life estimation varying d_1 (partial slip and gross slip regime with wear).....	28
Figure 5-4 - Theory of critical distances (TCD) applied to fretting fatigue problems when wear is (a) neglected and (b) considered.	30
Figure 5-5 - Estimated vs observed fretting fatigue lives for (a) critical distance varying with life and (b) constant critical distance	31
Figure 5-6 - Photograph of fretting fatigue specimens and pads. Both specimens and pads have the same height (13 mm).....	32
Figure 5-7 - Evolution of the multiaxial index computed at the critical distance as a function of the number of cycle to failure for both specimen thicknesses.....	32
Figure 6-1 - C(T) specimens treated with two laser lines used on FCG tests. Clear dashed lines represent laser lines applied on one side; dark dashed lines represent laser lines applied on the other side.....	35
Figure 6-2 - Surface residual stresses for the two laser conditions. (a) 2 X 2 condition. (b) 2 X 4R condition.....	35
Figure 6-3 - Fatigue crack growth rate (da/dN) per stress intensity range (ΔK) for the laser-treated material. (a) 2 X 2 condition. (b) 2 X 4R condition.	36
Figure 6-4 - (a) Size and geometry of the standard M(T) specimen type, removed in the L-T and T-L direction; (b) schematic view of the experimental setup for corrosion fatigue tests in seawater solution environment.....	37
Figure 6-5 - (a) FCG curves of BM and NZ (with cracks propagating along the weld center line) in air and 3.5 wt.% NaCl solution conditions (region II) and (b) linear regression from the data extracted exclusively from Paris regime (region II).	38
Figure 7-1 - Composite curved stiffened panel manufacturing.	39
Figure 7-2 - Composite curved stiffened panel mechanical test and nonlinear finite element analysis in postbuckling under compressive load.....	39
Figure 7-3 - Embraer 190 E2 (second generation) wing full-scale fatigue test overview.....	40
Figure 7-4 - Embraer 175 E2 (second generation).....	40
Figure 7-5 - Embraer 175 E2 horizontal stabilizer overview.....	41
Figure 7-6 - Embraer 195 E2 (second generation) full-scale fatigue test overview.	41
Figure 8-1 - (a) FEM used to simulate the four-point bending test; (b) four point bending test setup for curved composite samples (dimensions in [mm]).....	43
Figure 8-2 - Failure comparison between finite element analysis via MCT model and experimental tests for the spiral composites.....	43
Figure 8-3 - Longitudinal interlaminar shear test - failure pattern progression predicted by the FE model (for plate I150-W, 0.5 mm global mesh), displacements	

of: a) 0.44 mm; b) 0.58 mm; c) 0.60 mm; d) 0.66 mm; e) 1.00 mm; and f) final aspect of specimen.	45
Figure 8-4 - Transverse compact tension test – failure pattern progression, in terms of E_{22} , predicted by the FE model (0.175 mm crack mesh), for CMODs of: a) 0.05 mm; b) 0.21 mm; c) 0.53 mm (maximum load); d) 0.85 mm; e) 1.00 m; and f) final aspect of experimental specimen.	46
Figure 8-5 - Test specimen configurations.	47
Figure 8-6 - Mode I fracture toughness prediction based on results obtained for the thermoplastic materials evaluated.	48
Figure 8-7 - Comparison between co-cured and co-bonded mode I initiation fracture toughness at each test condition.	50
Figure 8-8 - a) DCB specimen and b) 3-ENF specimen.	51
Figure 8-9 - Experimental data and Fickian approximation of the joints moisture absorption.....	52
Figure 8-10 - Mode I G-N curves for specimens with and without an environmental preconditioning.	52
Figure 8-11 - Front view of the panels tested.....	53
Figure 8-12 - Isometric view of the panels, with the Teflon™ insert depicted in red.	54
Figure 8-13 - Boundary conditions of the panels and close-up of the test rig.....	54
Figure 8-14 - Average growth of the disbanded area in the RTA and RTW panels.	55
Figure 8-15 - Crack length growth.	55
Figure 9-1 - Possible joint configurations of FricRiveting for multiple material types: a) metal-inserted, b) overlap, and c) sandwich-like joint.....	57
Figure 9-2 - Schematic representation of Direct Friction Riveting process steps....	58
Figure 9-3 - Schematic illustration of potential applications of FricRiveting in aircraft structures: a) composite floor structure, joining floor beam to floor panel, as detailed in (b); and c) composite fuselage, joining stringer to skin, as detailed in (d).....	58
Figure 9-4 - Joint S-N curves (reliabilities of 50 %, 90 %, and 99 % according to the two-parameter Weibull distribution).....	59
Figure 9-5 - Stiffness degradation curves: a) for various stress levels, and b) for 66 % of the ULSF showing the stages of damage evolution.	59
Figure 9-6 - Configuration and dimensions of the joints used for lap shear test (in mm).....	61
Figure 9-7 - Crack growth resistance curve of the friction spot joint under quasi-static mixed-mode I/II loading. The light gray rectangle represents the metallic nub region inside PDZ.....	61

Figure 9-8 - Overview of the demonstrator produced entirely with friction-based joining technologies.....	62
Figure 9-9 - Schematic of the specimen geometry of the AddJoining hybrid joints.	63
Figure 9-10 - Schematic of the boundary conditions for single lap shear testing. ...	64
Figure 9-11 - Statistically derived S-N curves at different reliability levels using the two-parameter Weibull method.	64
Figure 9-12 - Measured (a) stiffness variation, and (b) damage variation as a function of fatigue life during cyclic loading at 47% of the ULSF, corresponding to a maximum force of 5.8 kN.....	64
Figure 10-1 - Overview of the methodology used for this work.	66
Figure 10-2 - Specimen geometry used in the random vibration tests (units: mm).	66
Figure 10-3 - (a) Experimental setup and; (b) Detail of the sample with strain gage.	67
Figure 10-4 - Crack size versus time: experimental and numerical values.	67
Figure 10-5 - Basic plate dimensions and set-up.	68
Figure 10-6 - Experimental FRFs of point 40 for the intact and damaged (Levels 1, 2 and 3) conditions.....	69
Figure 10-7 Specimen assembly and test setup.....	71
Figure 10-8 - Average DI under static longitudinal loading, thickness 2 mm; b) Average DI under hydrostatic pressure at 200 kHz.....	72
Figure 10-9 - Helicopter model AS-350 and its rotor blade in detail.....	73
Figure 10-10 - Three different scenarios of induced damage on the rotor blade. ...	74
Figure 10-11 - Sensors distributed uniformly on the main rotor blade.....	74
Figure 10-12 - Graphical results of damage identification considering the objective function J_1 in all three damage cases.....	75
Figure 10-13 - Example of application of the AR tool: (a) internal view, (b) external view.....	77
Figure 11-1 - Overview of the open hole and joint specimens.....	79
Figure 11-2 - Life gain analysis in terms of overload net stress over yield strength and the total number of cycles for failure over the number of cycles for failure at base load.....	80
Figure 11-3 - Damage theory approaches comparison for two and three block loading tests.....	80
Figure 11-4 - Damage theory approaches comparison for overload tests.....	81

1. INTRODUCTION

The present document is a summary of fatigue investigations related to aerospace materials and structures performed by Brazilian organizations (or by Brazilian researchers¹) during the past two years. Originally the document contents were intended to be presented during the 37th ICAF (International Committee on Aeronautical Fatigue and Structural Integrity) Conference to be held in Xi'an, China, during the period between May 31st and June 4th 2021. However, due to the present global situation with regard to the COVID-19 pandemic, the 37th ICAF Conference will be replaced by a webinar, to be held in June 30th 2021, while the next ICAF Conference was postponed to 2023, when a new and updated report is expected to be released.

On spite of that, this report is expected to be published on the ICAF permanent website in the near term.

Some of the research works presented along this review are follow on research activities related to the ones previously presented in References [1] to [3]. While some of the contributing institutions are supplying follow-on research works and also new research works during this two year period, other institutions have faced certain difficulties (due to the pandemic).

The following Brazilian institutions have collaborated during this period with research works on fatigue and fracture mechanics related to aeronautical products, and had scientific or technological research works added to this review:

- Brazilian Society of Engineering and Mechanical Sciences (ABCM) – Rio de Janeiro - RJ
- Department of Aerospace Science and Technology (DCTA) – São José dos Campos - SP
- University of São Paulo (USP) – various campi - SP
- State University of São Paulo (UNESP) –various campi – SP
- State University of Ponta Grossa (UEPG) – Ponta Grossa - PR
- Federal University of Brasília (UnB) – Brasília - DF
- Federal University of Itajubá (UNIFEI) – Itajubá – MG
- Federal University of Minas Gerais (UFMG) – Belo Horizonte - MG
- Federal University of Ouro Preto (UFOP) – Ouro Preto – MG

¹ For the particular case of hybrid structures, the three contributions presented were developed by Brazilian researchers working in foreign institutions, with support of Brazilian agencies.

- Federal University of Rio Grande do Norte (UFRN) – Natal – RN
- Federal University of Rio Grande do Sul (UFRGS) – Porto Alegre – RS
- Federal University of São Carlos (UFSCAR) – São Carlos – SP
- Federal University of Triângulo Mineiro (UFTM)- Uberaba - MG
- Aeronautics Institute of Technology (ITA) – São José dos Campos – SP
- Embraer S/A – São José dos Campos – SP

Further, some works to be presented were developed in cooperation with foreign institutions, from which some are mentioned here:

- University of Twente– The Netherlands
- Technical University of Graz – Austria
- HZG - Helmholtz-Zentrum Geesthacht – Germany

The author of this report would like to thank to all partners from the academy and the research institutes that have collaborated with this compilation, and that will be cited along the report, and is particularly grateful to Professor Mariano Andres Arbelo, from the Aeronautics Institute of Technology (ITA) and to Professor Volnei Tita, from the University of São Paulo (USP), for their increasing support in current activities related to fatigue, fracture and structural integrity in aerospace structures and materials, and for their help during the organization of the report.

Some research works may have co-authors from institutions not mentioned among the above, from Belgium, Chile, Cuba, Portugal and even from other brazilian universities, whose collaboration is also appreciated.

The report follows the basic structure presented in References [1] to [3], with minor subject modifications. During the reporting process, some collaborations were included in certain topics according to this structure, but it is recognized that they could be also included in other similar topics (for example, “analysis and simulation with composite materials” is partially “analysis and simulation” and partially “composite materials”), and therefore it is important that the reader checks the titles of all works included in the report regardless of the chapter where they were included.

For most of the contributions, first the name of the related organizations are listed, and then a summary of the work (usually adapted with small modifications from its abstract) is presented, followed by highlights with selected information of interest.

2. CONCEPTS

Multiscale analysis for predicting the constitutive tensor effective coefficients of layered composites with micro and macro failures (Ref.[4])

This work was developed by researchers from the University of São Paulo (USP) and other institutions addressed in the reference.

Summary:

The aim of this work is to predict the effective coefficients of constitutive tensor for layered composites with delamination in macro-scale considering the influence of the debonding between fiber and matrix in micro-scale. Thus, a multiscale methodology is proposed to solve this problem. Firstly, the effective coefficients for the micro-scale level are calculated via the Finite Element Method (FEM), considering different degrees of micro failure. By using the micro-scale level homogenization results, the effective coefficients for layered composites are calculated by the Finite Element Method, as well as by Asymptotic Homogenization Method (AHM), considering different extensions of delamination (failures in macro-scale).

Results show that the macro-scale analyses are affected by the micro failure, with the most influence of the micro failure in the coefficients C_{11}^* , C_{12}^* and C_{66}^* . In addition, when the thickness of the adhesive between layers increases, the effective coefficients decrease with the macro failure (delamination). Comparisons between homogenized and heterogeneous numerical models show that for almost all effective coefficients, there are excellent convergences. Only for the values of C_{12}^* , there are relevant divergences for specific limit cases. Finally, the macro-scale results obtained via FEM and AHM are compared to evaluate the advantages and disadvantages of the proposed multiscale methodology.

Highlights:

Figure 2-1 shows a representation of the 2D multiscale analysis model, with the fibers oriented in the Y_3 direction (Figure 2-1(a)), while the laminate is assumed to be layered in the x_1 direction (Figure 2-1(b)). Figure 2-1(c) shows the 2D unit cell for a macro-scale Representative Volume Element (RVE) where θl_2 is the length of delamination (macro-scale failure), with degree imperfection θ for the interface, i.e. the extension of the damage. It is assumed to be layered in the y_1 direction. Figure 2-1(d) shows the FEM model for the RVE.

Figure 2-2 shows one example (from the ones shown in the reference) of the results obtained for different values of delamination extension combined to

different values of fiber-matrix interface stiffness K_t . The influence of the interface thickness $t_{(2)}$ was also investigated through a parametric study.

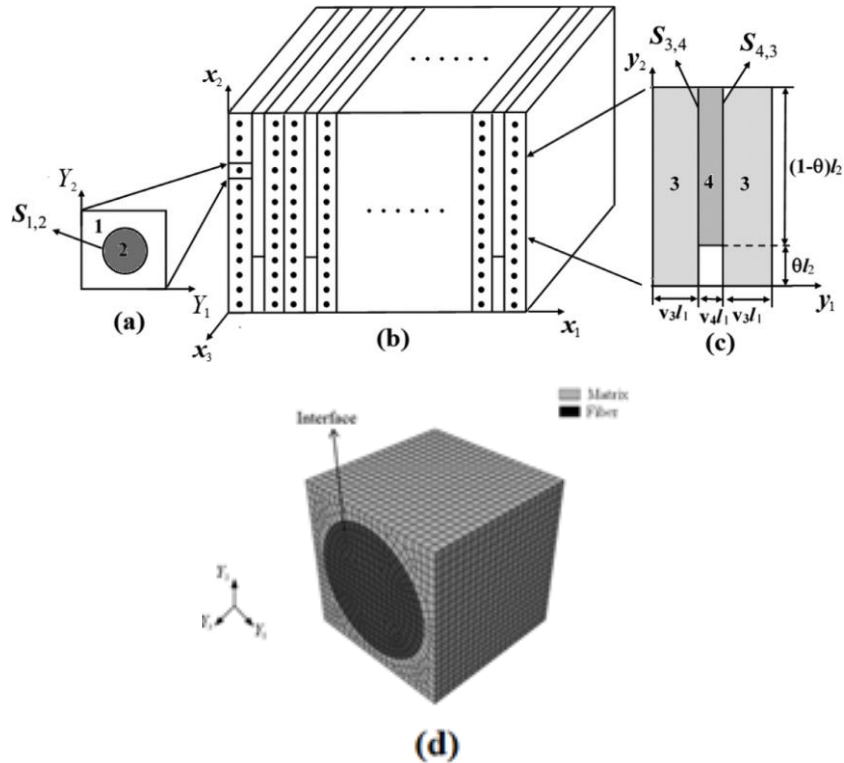


Figure 2-1 - Multiscale analysis model: (a) Two-dimensional RVE for the micro-scale analysis, (b) 3D laminated composite, (c) 2D RVE for the macro-scale analysis. Micro-scale analysis: (d) cross section of a quadratic and periodic array of circular fibers.

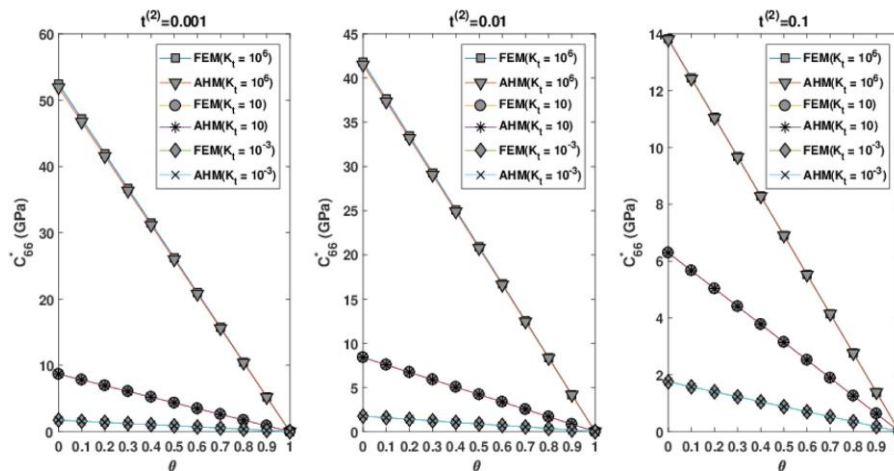


Figure 2-2 - C_{66}^* as a function of the macro failure degree θ for different values of fiber-matrix interface stiffness K_t and different sizes of the laminate interface thickness $t_{(2)}$.

A cohesive zone model to predict fatigue-driven delamination in composites (Ref. [5])

This work was developed by researchers from the Aeronautics Institute of Technology (ITA). Partial results were presented in the previous ICAF 2019 report (Ref. [3]).

Summary:

A cohesive zone model is proposed to analyse composite delamination propagation under high-cycle fatigue loading. A new method to compute the strain energy release rate at any point within the element fatigue life cycle range is presented.

The proposed scheme is based on the J-integral method evaluated at an estimated position of the crack-tip within the element, instead of the element integration points. Furthermore, a new fatigue damage evolution law is proposed to account for the unwanted quasi-static damage during the element fatigue degradation process. The model prediction capabilities were verified against experimental data available in the literature and theoretical solutions using a double cantilever beam configuration for mode I loading, four-point end-notched flexure configuration for mode II loading, and mixed-mode bending configuration for mixed-mode loading.

The simulations were performed at both constant and variable amplitude loading. The numerical predictions obtained using the proposed model correlated very well with literature's experimental data.

Highlights:

In the present work, the bi-linear traction-separation law describes the quasi-static damage evolution. Figure 2-3 illustrates the bi-linear traction-separation law.

The SERR is estimated using the J-integral method applied on the cohesive zone boundary, where the integration contour is taken at the cohesive elements surface, as shown in Figure 2-4.

The proposed formulation is implemented into ABAQUS/Explicit™ FE code within solid elements. The material properties are obtained from experimental data published previously. In this paper, three loading conditions were simulated, namely Mode I, Mode II and Mixed-mode, using DCB, 4-ENF and MMB specimen configurations, respectively. Figure 2-5 presents a comparison of the crack growth rate predicted by the proposed model and experimental results.

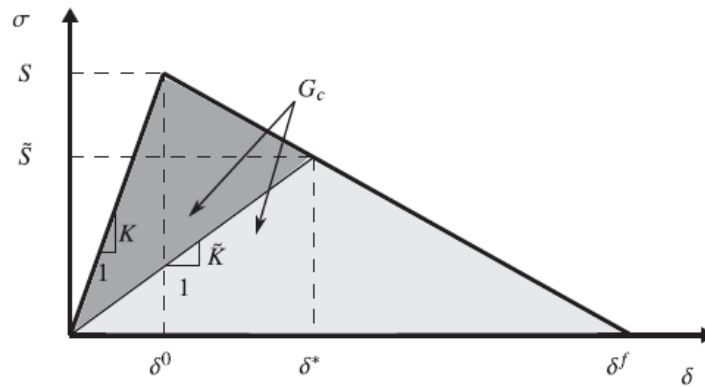


Figure 2-3 - Bi-linear traction-separation law for an equivalent mode loading.

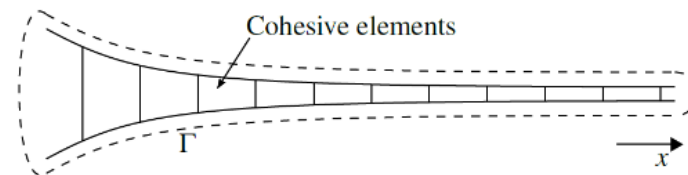


Figure 2-4 - Definition of the J integral surrounding the cohesive zone.

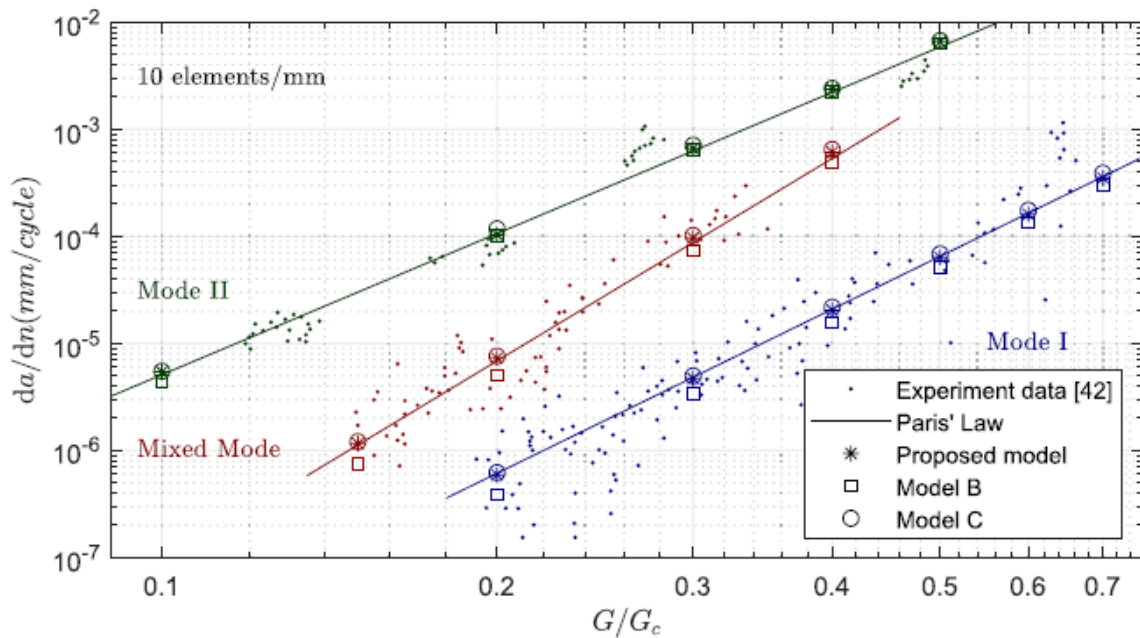


Figure 2-5 - Comparison between numerical prediction for the crack growth rate and experimental results.

Delamination analysis using cohesive zone model: A discussion on traction-separation law and mixed-mode criteria (Ref. [6])

This work was developed by researchers from the Aeronautics Institute of Technology (ITA).

Summary:

A discussion on cohesive zone model formulation for prediction of interlaminar damage in composite laminates is presented in this paper.

The degradation of interlaminar mechanical properties is analysed from a physical point of view. Firstly, the damage evolution is evaluated according to the traction-separation law and it is demonstrated that if a linear elastic unloading/reloading curve is assumed, the softening function must also be linear. Secondly, issues regarding damage onset and fracture criteria in mixed-mode loading are critically addressed and commented.

A new set of criteria is proposed, and the limitations of existing criteria are discussed.

3. ANALYSIS AND SIMULATION

Numerical model for the stress field ahead of a crack in elastoplastic regime (Ref. [7])

This work was developed by researchers from the University of São Paulo (USP) and State University of São Paulo (UNESP). The work was presented during the 3rd International Conference on Structural Integrity (ICSI 2019), held in Madeira, Portugal, in September of 2019.

Summary:

Damage-tolerant designs admit the pre-existence of defects and small cracks, which lead to stress redistribution in structural components. The accurate knowledge of the stress fields in parts under these conditions is important for damage accumulation analysis and residual life prediction. In this work, a numerical model via finite elements (FEM) is proposed to determine the stress field ahead of crack tips in a plate under cyclic loading and elastoplastic regime. The center-cracked plate analyzed simulates a M(T) specimen made of 6005-T6 extruded aluminum alloy.

From the triple symmetry condition, one eighth of the plate was discretized with tetrahedral solid finite elements of quadratic order. The refinement of the mesh

was concentrated around the crack tip region. The cyclic stress-strain curve of the material was experimentally obtained by strain-controlled fatigue tests. With this curve, elastic and plastic parameters have been determined, considering elastoplastic material with isotropic hardening governed by Swift's law. Such a model differs from most usual stress analyses in cracked components, in which the possibility of hardening is not considered.

Cyclic loading with ratios $R = 0$ and $R = -1$ has been applied from an initial crack of 11 mm in length. The crack growth was imposed by means of a simplified node release scheme.

The results showed no significant variation in terms of the equivalent stress, but considerable differences in the equivalent plastic strain. Therefore, the compressive phase in the specimen under $R = -1$ contributes to increase the equivalent plastic strain, which means that the level of yielding becomes higher even when the specimen is compressed.

Highlights:

The following Figure 3-1, Figure 3-2 and Figure 3-3 indicate the basic geometry of the specimen that was analyzed, the experimental fatigue crack growth data obtained for the same configuration, material and loading conditions, and the variation observed from analysis in the equivalent plastic strain (k) for $R = 0$ and $R = -1$ respectively.

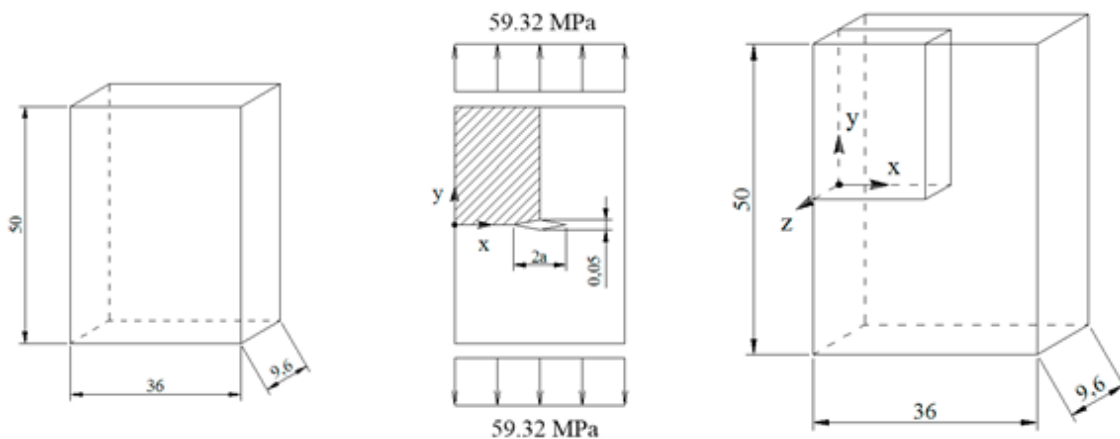


Figure 3-1 - Specimen geometry and loading conditions (dimensions in mm).

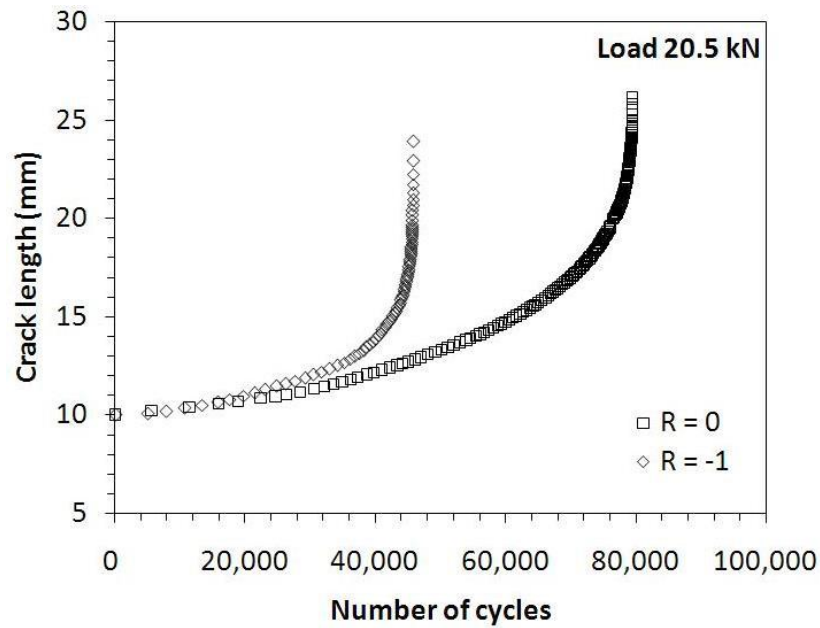


Figure 3-2 - Fatigue crack growth data for the specimen with peak load 20.5 kN.

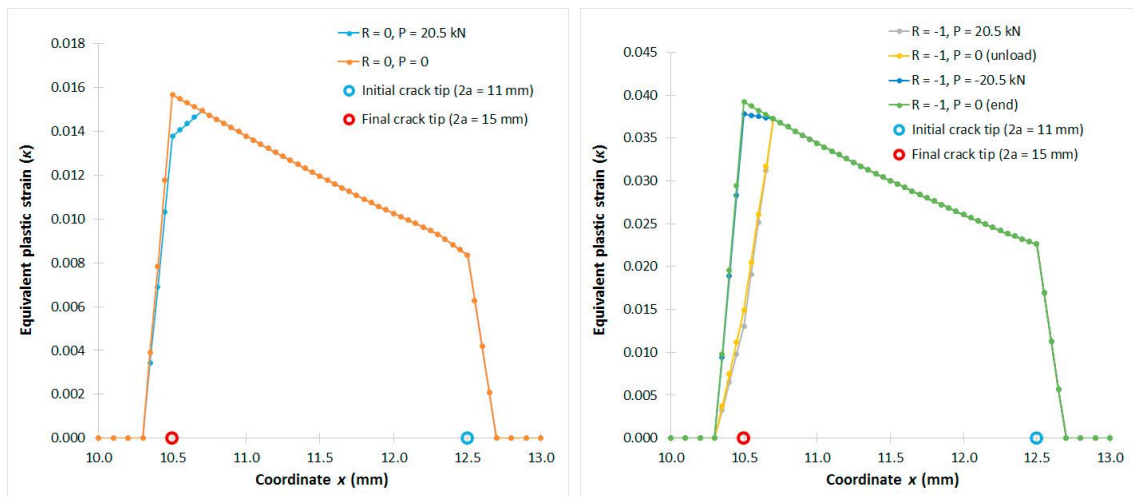


Figure 3-3– Equivalent plastic strain (k) along crack line. Values correspond to coordinates $y = 0$ and $z = 4.8\text{mm}$ (surface). – Equivalent plastic strain (k) along crack line. Values correspond to coordinates $y = 0$ and $z = 4.8\text{mm}$ (surface).

Computational analyses of composite plates under low-velocity impact loading (Ref. [8])

This work was developed by researchers from the University of São Paulo (USP). The work was presented in the 4th Brazilian Conference on Composite Materials.

Summary:

The usage of composite materials on new design structures is still very conservative, mainly due to its very complex failure behavior. Thus, the prediction

of these mechanisms requires the development of more accurate damage models. Therefore, in the present work a damage model based on Continuous Damage Mechanics (CDM) concepts is applied in order to predict intra-ply failure mechanisms in impacted carbon-epoxy laminate structures. The damage model was implemented as VUMAT (User Material Subroutine for explicit integration analyses) and linked to ABAQUS™. Several numerical analyses were performed, and the results were compared to experimental tests in order to evaluate the potentialities and limitations of the damage model application.

Highlights and Main Conclusions:

Impact tests on 120 mm composite square plates made of prepreg M10 were carried out. The tests followed ASTM D5628-96 (2001) specifications, considering FD (Falling Dart) method. For this method, the impactor has a hemispheric shape made of aluminum with mass of 51.3 g, which is added to the frame mass and the load cell. The FEM model of the setup is shown in Figure 3-4.

In Figure 3-5, for 5.91 J impact energy, the FE model simulated about 50% of the absorbed energy by the real structure (2.0 J). It is important to observe that the absorbed energy predicted by the FE model is entirely related to matrix damage mechanism, which is shown by the damage parameters d_2 and d_6 . Thus, other amount of absorbed energy is associated to the delamination mechanism (as observed in C-Scan results).

In Figure 3-6, it is observed that the damage variable d_2 was activated until the 6th layer, which is oriented at 90° , while d_6 showed a discontinuity in the 7th layer, but it is verified in 8th, 9th and 10th layers. Moreover, the shear stress acting in the matrix causes more damage than the tensile stress.

The comparisons of force vs. time history for experimental and FE analyses show that the new damage model could predict partially the impact event as matrix failures caused by transversal tensile stress and/or shear stress. Therefore, the numerical analysis consists on a very important tool to better understand the impact event on composite materials in intra-ply level, helping the design process of complex structures. However, as expected, delamination phenomenon also contributes to the absorbed energy in the low velocity impact events, mainly for cross-ply laminates. Thus, for future works, it will be included not only delamination criterion, but also delamination evolution law in order to obtain better numerical predictions.

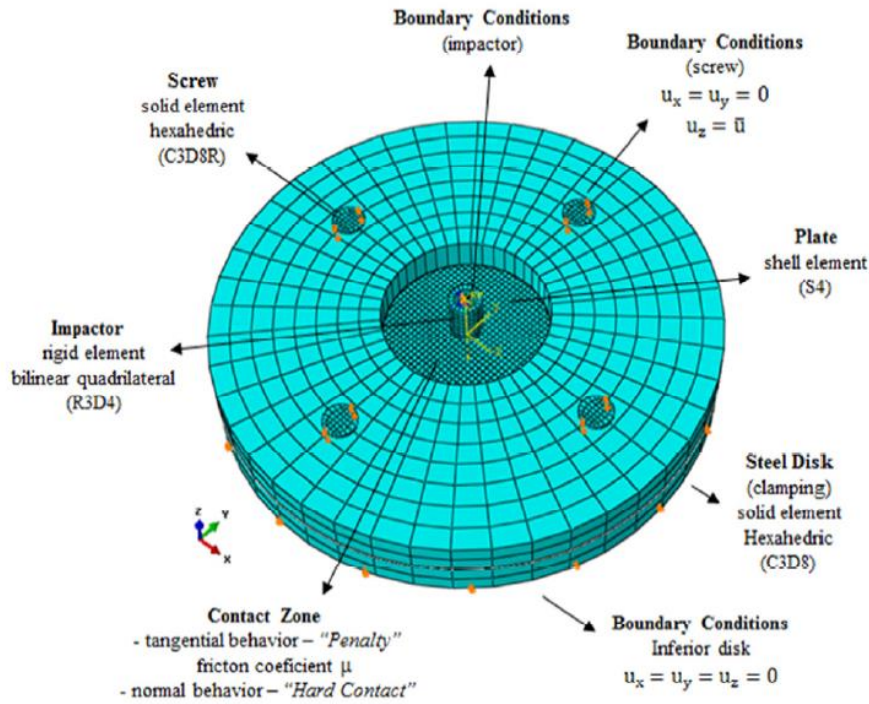


Figure 3-4 - Finite Element model to simulate the impact test.

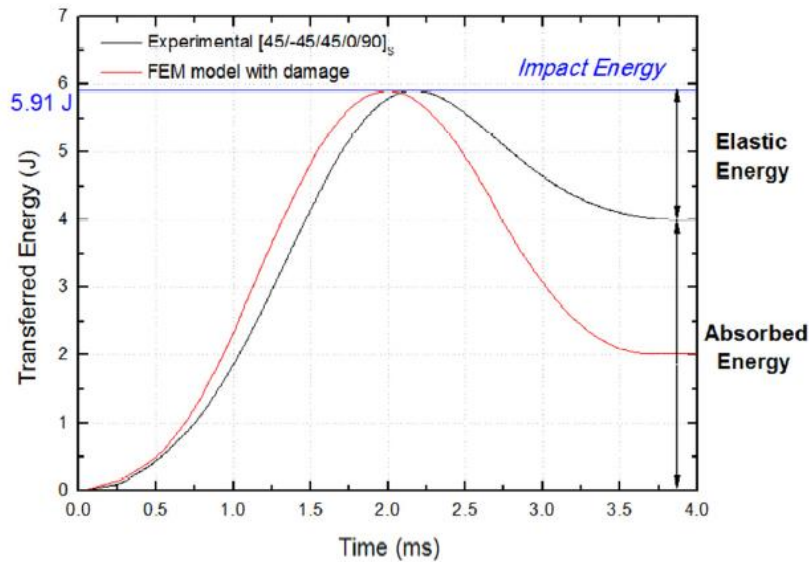


Figure 3-5 - Comparison between experimental and FE analyses: energy transferred vs. time for the $[+45^\circ/-45^\circ/+45^\circ/0^\circ/90^\circ]_s$ laminate under 5.91 J of impact.

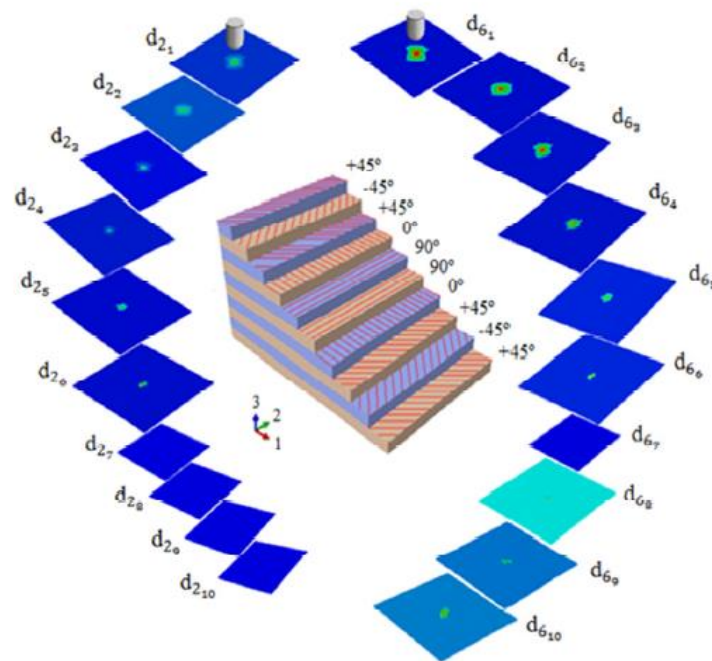


Figure 3-6 - Damage variables d_2 and d_6 for the layers of laminate $[+45^\circ/-45^\circ/+45^\circ/0^\circ/90^\circ]_s$ at the final of impact event.

Computational prediction of a composite material response to impact by using a viscoelastic damage model (Ref. [9])

This work is complementary to the previous one. It was developed by researchers from the University of São Paulo (USP).

Summary:

The use of composite materials in aeronautical industry is becoming progressively widespread nowadays, bringing special interest in their properties under impact. This interest arises with the aim of designing structural elements with increased crashworthiness, improving safety, which, in turn, requires comprehension of the complex and diverse failure modes occurring simultaneously in the material, in addition to requiring capacity of predicting impact damage size and its influence on the mechanical properties of the composite, especially on its residual strength.

Aiming for efficient and effective methodologies to predict impact damage, many authors have recently proposed constitutive damage models based on continuum mechanics, for use on finite element simulations. As many of the composites used on the aeronautical industry have polymeric matrices, viscoelastic behavior and temperature dependence are phenomena that have to be accounted for; viscoelasticity also has a direct influence on elastic wave propagation inside the material, and consequently on impact damage initiation processes.

Hence, the purpose of this work is to propose a damage model for composite materials under impact which also considers viscoelastic and temperature-dependent effects from the matrix. This damage model was tested with an impact simulation, by computationally modeling the assembly and subsequently, comparing the experimental results from that research with those obtained from the simulations. Furthermore, this work presents comparisons considering the overall influence of viscoelasticity and temperature on the results, and the influence of the model boundary conditions on the latter.

Highlights and Main Conclusions:

The FE model applied for the study is the same as presented previously in Figure 3-4.

In order to evaluate the effectiveness of the damage model and the influence of viscoelasticity on the material behavior, four cases were simulated: one purely elastic and three viscoelastic; all cases were, thus, compared with experimental results from Reference 10. The results are shown in Figure 3-7.

Likewise, results for different values of the friction coefficient, applied and modified at all contact surfaces in the model, were assessed, being presented on Figure 3-8.

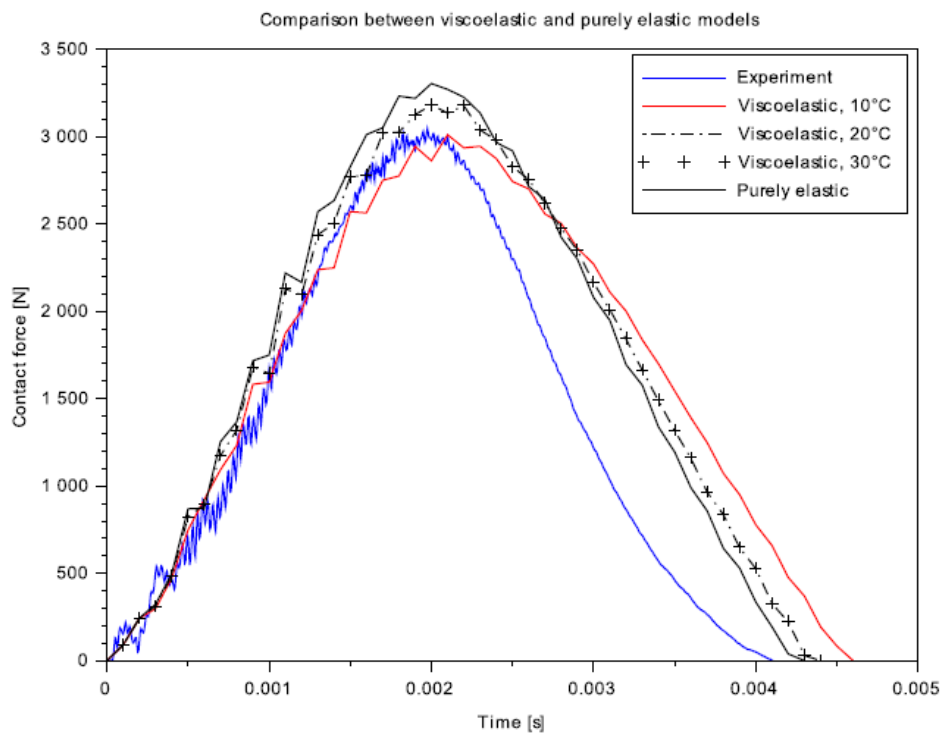


Figure 3-7 - Contact force history for experimental, elastic and viscoelastic cases.

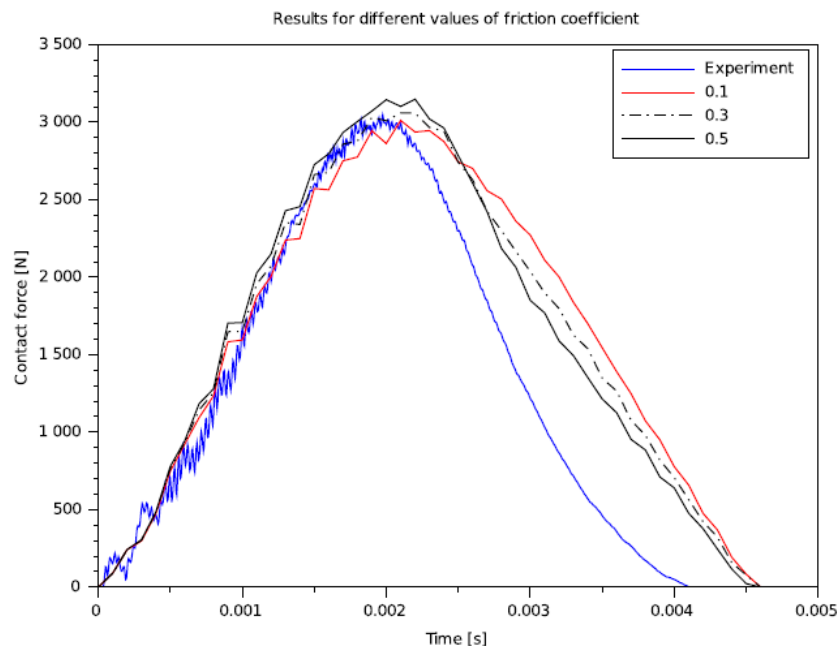


Figure 3-8 - Contact force history, for different values of contact friction.

4. METALLIC MATERIALS – FATIGUE AND FRACTURE PROPERTIES

Effect of the interrupted aging heat treatment T6I4 on the tensile properties and fatigue resistance of AA7050 alloy (Ref. [11])

This work was developed by researchers from the University of São Paulo (USP), the State University of Ponta Grossa (UEPG) and the National Center for Research in Energy and Materials (CNPEM).

Summary:

The tensile response and fatigue behavior of age-hardenable aluminum alloys are strongly influenced by factors like size, spacing and volume fraction of strengthening precipitates. In this study, the tensile properties and high-cycle fatigue behavior of two tempers of AA7050 alloy (the commercial T7451 and the interrupted aging T6I4) were investigated. Transmission electron microscopy analyses of strengthening precipitates were performed, and the results showed that AA7050-T6I4 had a higher volume fraction of strengthening precipitates with smaller size. This microstructural feature was responsible by the higher ductility and toughness shown by T6I4 temper condition while maintaining yield stress and ultimate tensile strength similar to T7451. The smooth samples rotating bending fatigue curves of both material conditions were similar. Nevertheless, the interrupted aging leads to improved notched fatigue resistance and hence lower

notch sensitivity. These results were related to the higher activity of screw dislocations and improved dislocation pinning effect during deformation promoted by T6I4 temper.

Highlights and Main Conclusions:

Compared to T7451 temper condition, the T6I4 aging heat treatment resulted in a higher density of fine strengthening precipitates. This microstructural change promotes hardness and ultimate tensile strength similar to T7451, whereas the elongation, area reduction and toughness were increased by 80, 68 and 92%, respectively. Refer to Figure 4-1.

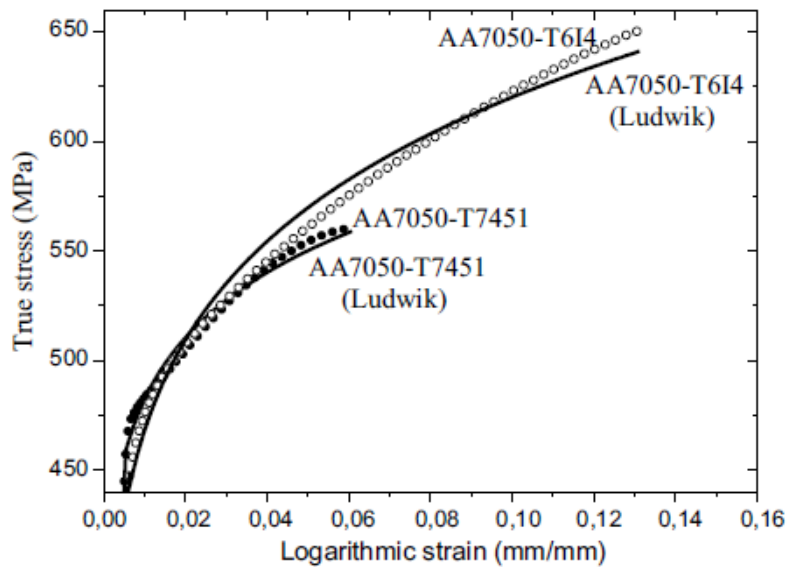


Figure 4-1- True stress–strain data and Ludwik’s model curves for AA7050-T7451 and AA7050-T6I4 conditions - True stress–strain data and Ludwik’s model curves for AA7050-T7451 and AA7050-T6I4 conditions.

The T6I4 temper condition presented higher strain-hardening exponent (n) when compared to T7451, revealing a greater ability to accommodate plastic strain during loading and a more uniform strain distribution. This result also indicates a greater capacity to cyclic hardening, which can be associated with a higher ability of dislocation pinning, loops formation and dislocation tangles configuration shown by T6I4 temper condition.

Figure 4-2 shows the results of the fatigue tests with smooth specimens for both material conditions.

Figure 4-3 shows the overlap of the experimental results from fatigue tests of notched specimens and the fitting curves using the maximum-likelihood estimation for AA7050-T7451 and AA7050-T6I4 conditions.

The smooth rotary bending fatigue strength was similar for the two temper conditions. An improvement on notched fatigue behavior was observed for AA7050-T6I4 compared to T7451. The higher fatigue strength of the T6I4 notched specimens, and consequently, the lower notch sensitivity of this temper, can be attributed to a greater cyclic hardening and capacity to accommodate strain of this condition.

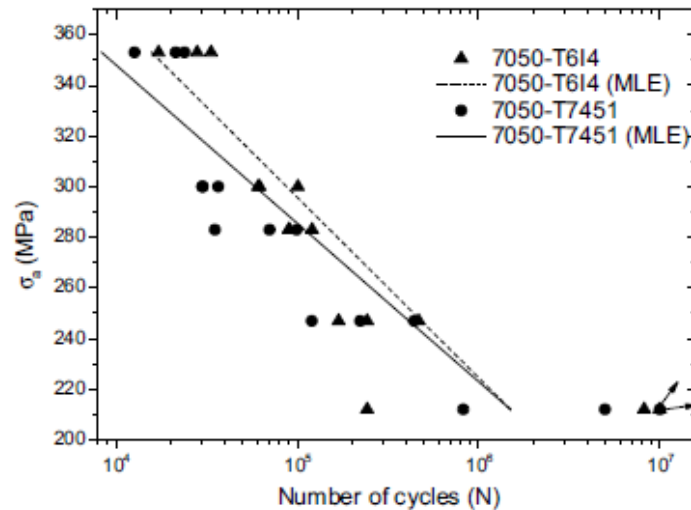


Figure 4-2 - Experimental data and stress–life model fitting results using the maximum-likelihood estimation for AA7050-T7451 and AA7050-T6I4 conditions (unnotched specimens).

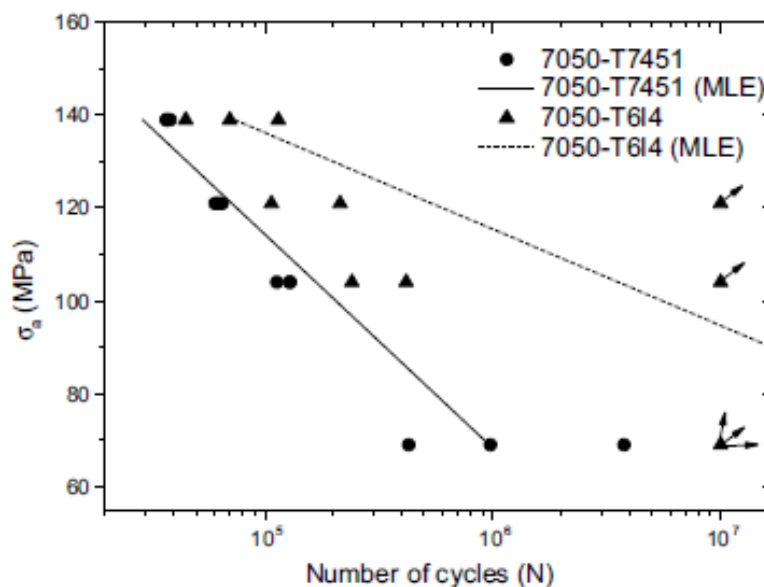


Figure 4-3 - Experimental data and stress–life model fitting results using the maximum-likelihood estimation for AA7050-T7451 and AA7050-T6I4 conditions (notched specimens).

5. METALLIC MATERIALS - FRETTING

Fretting fatigue under variable amplitude loading considering partial and gross slip regimes: Numerical analysis (Ref. [12])

This work was developed by researchers from the University of Brasília (UnB), Federal University of Rio Grande do Norte (UFRN) and KU Leuven (Belgium).

Summary:

The main aim of this work was to numerically investigate the effect of sequences of variable amplitude shear loading on contact tractions/stresses and on the development of life estimation methodologies for these more challenging loading histories. In this setting, a finite element (FE) model has been implemented in order to simulate a cylinder on plane contact problem for an aeronautical Al 7075-T651 alloy. High-Low (H-L) and Low-High (L-H) shear amplitude loading sequences under partial and gross slip conditions were considered in three different case studies. For the case studies where gross slip was involved, the proposed life estimation procedure was enhanced to include the effect of material loss due to wear. More explicitly, such procedure was based on the use of (i) the SWT (Smith-Watson-Topper) multiaxial fatigue model, (ii) the Theory of Critical Distances, (iii) Miner's cumulative damage rule and (iv) the numerical update of the contact surfaces profiles (for loading blocks under gross slip). The numerical analyses for the case studies under partial slip revealed that, when the presence of wear is neglected in the modelling, the Miner's rule provided a divergence between the expected life for the H-L and L-H loading blocks. This difference was considerably larger when gross slip took place. For the case study involving the presence of gross slip in one of the shear loading blocks, the calculated life tended to infinite when the damage generated by the high amplitude block is greater than a certain critical value. These studies are the basis for an experimental programme which will be carried out in the 4 actuators fretting fatigue rig of the University of Brasilia.

Highlights and Main Conclusions:

The paper first reviews multiaxial fatigue life estimation methods and the critical distance approach for fretting and wear models. Then the actual application of variable amplitude loading to fretting fatigue is discussed. Three different analyses are conducted to evaluate the fretting fatigue phenomenon under variable shear amplitude loading/displacement. In these three analyses, partial and gross slip conditions are investigated, refer to Figure 5-1.

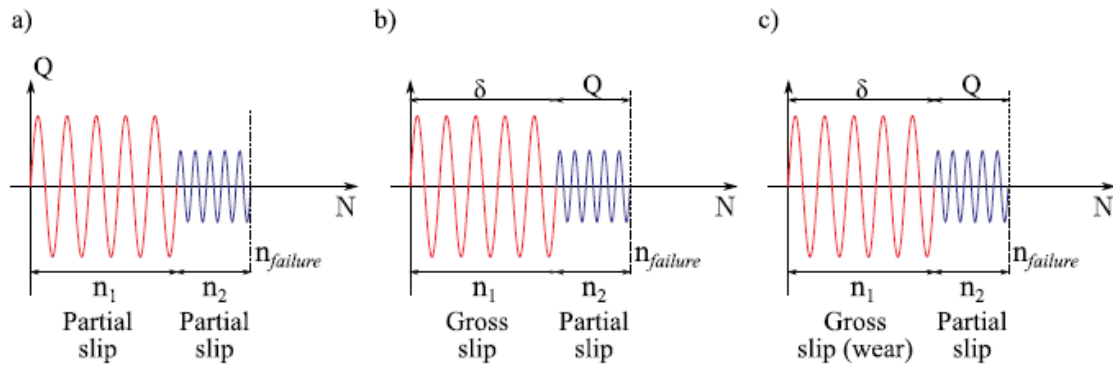


Figure 5-1 - Schematic representation of the three case studies considered in the H-L loading blocks: (a) only partial slip, (b) gross slip and partial slip and (c) gross slip (including wear effects into the modelling) and partial slip.

The geometrical model considered in this work is depicted in Figure 5-2. A pad radius $R = 70 \text{ mm}$ is considered in the analysis. The material adopted for pads and specimens is the aluminum alloy 7075-T651.

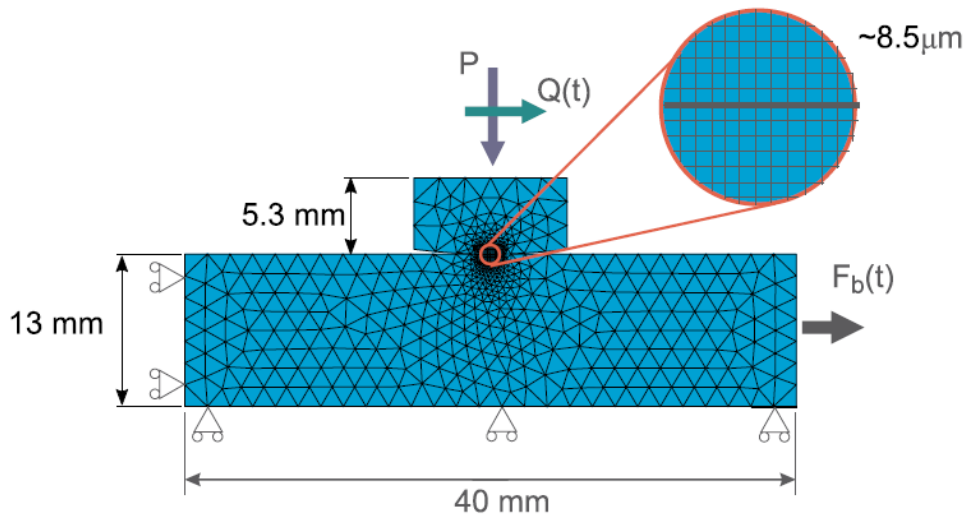


Figure 5-2 - FE model, loading and geometric configurations.

Figure 5-3, selected from various results presented along the paper, depicts the total estimated life for H-L and L-H loading sequences as a function of the damage generated by the first block d_1 , or the second block, d_2 .

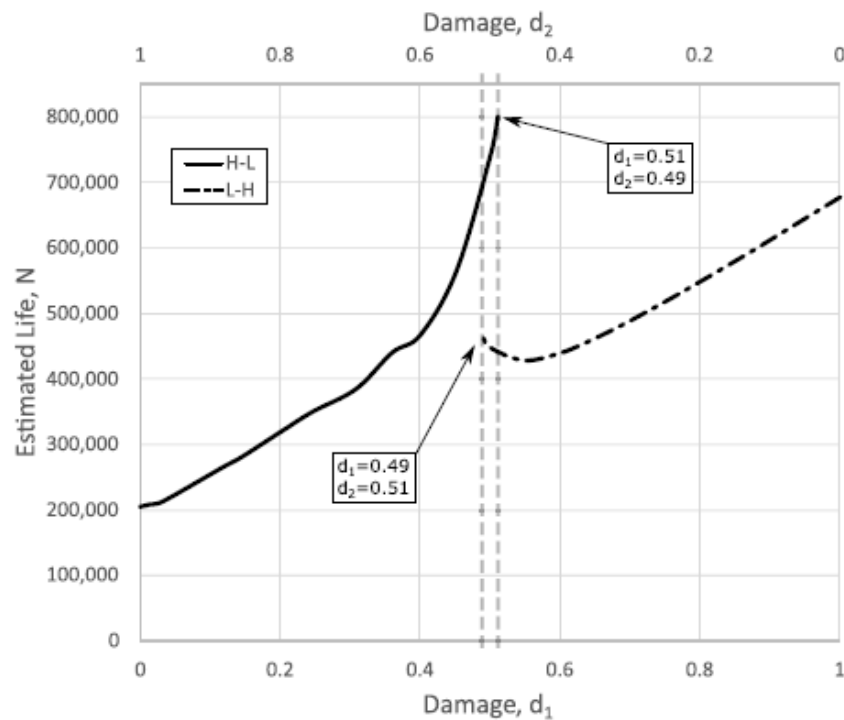


Figure 5-3 - Life estimation varying d_1 (partial slip and gross slip regime with wear).

This seems to be the first time that fretting fatigue cases under variable amplitude loading are assessed in terms of life estimates also including wear effects. This work was aimed to develop a methodology to predict fretting fatigue life under such conditions. Up to this point, it is not possible to measure the accuracy of the present approach due to the lack of experimental data including the literature, however, in a future work to be published soon, an extensive set of fretting fatigue tests reproducing study cases similar to the ones presented here will be carried out. After that, it is expected to answer some open questions such as:

- (i) Miner's linear rule is capable of dealing with fretting variable amplitude loading? If not, can a nonlinear version of it be more adequate?
- (ii) Will be the loading history effect observed in the numerical model also verified in the experiments?
- (iii) Do wear have such a great influence on fatigue lifetime such as verified in the numerical tests?
- (iv) With experimental data in hands, can the use of a variable critical distance parameter improve the quality of the results?

Fretting life of the Al7050-T7451 under out-of-phase loads: Numerical and experimental analysis (Ref. [13])

This work was developed by researchers from the University of Brasília (UnB).

Summary:

This study investigates the effect of the phase angle between fretting and fatigue loads on the life of Al7050-T7451 aluminum alloy specimens. Tests with phase angles of 0°, 45°, 90° and 135° are carried out using a biaxial system which permits the distinct control of fretting and fatigue loads. A numerical stress analysis for the in phase condition is developed and compared with the closed form solution to provide a benchmark for the study. Life is estimated using three different critical plane criteria coupled with extended versions of the Theory of Critical Distances. Results show that the introduction of a phase angle between loads plays a significant role on the fatigue life of this alloy.

Investigation of crack initiation path in AA7050-T7451 under fretting conditions (Ref. [14])

This work was developed by researchers from the University of Brasília (UnB) and Federal University of Rio Grande do Norte (UFRN).

Summary:

Early crack orientation in 7050-T7451 aluminum alloy was investigated under fretting conditions. New tests were performed in the partial slip regime to observe the influence of the tangential load amplitude, mean bulk stress, and pad radius on the crack orientation. Three critical plane fatigue parameters were combined with different stress averaging methods to estimate the crack initiation direction. The normal stress-based Smith–Watson–Topper parameter provided better crack orientation estimates than the shear stress-based parameters.

The experimental observations indicated a small increase in the early crack angle when the tangential load amplitude was raised.

Life prediction in multiaxial high cycle fretting fatigue (Ref. [15])

This work was developed by researchers from the University of Brasília (UnB) and Federal University of Rio Grande do Norte (UFRN).

Summary:

The aim of this work is to show that multiaxial fatigue modeling can be successfully adapted to estimate crack initiation life of mechanical assemblies under fretting conditions. The paper is divided into two parts. In Part I, the focus is on the study

of size and gradient effects but considering the influence of incorporating fretting wear on the life estimation procedure. New data for a Ti-6Al-4V cylindrical on plane contact configuration were produced to assess the analyses. It is shown that critical plane criteria, coupled with a critical distance which varies with life, are capable to provide accurate estimates of fretting fatigue life in the medium high cycle regime. The inclusion of wear in the modeling did not significantly improved the life estimates but increased a lot the computational cost. In Part II, the paper extended this life estimation approach to the contact of wires taken from overhead conductors. Fretting fatigue data of AA1350-H19 wires and new tests on the more resistant AA6201-T81 corroborated the successful use of the life methodology to other materials and applications.

Highlights and Main Conclusions:

The first part of this paper details the differences in multiaxial life estimation approaches where the wear is considered and where the wear is neglected. When neglecting wear, life can be directly estimated by evaluating the multiaxial fatigue criterion at the center of the fatigue process zone (point method), which is located at a distance $L/2$ from the contact trailing edge (hot spot), Figure 5-4(a). On the other hand, when wear takes place, Miner's rule needs to be considered. Besides, the hot-spot point at the contact surface is not fixed over the fretting cycles due to the changes in the contact surface geometry. In this case, the strategy here adopted is to cumulate increments of Miner's damage parameter but only considering points $L/2$ vertically distant from the contact surface, Figure 5-4(b).

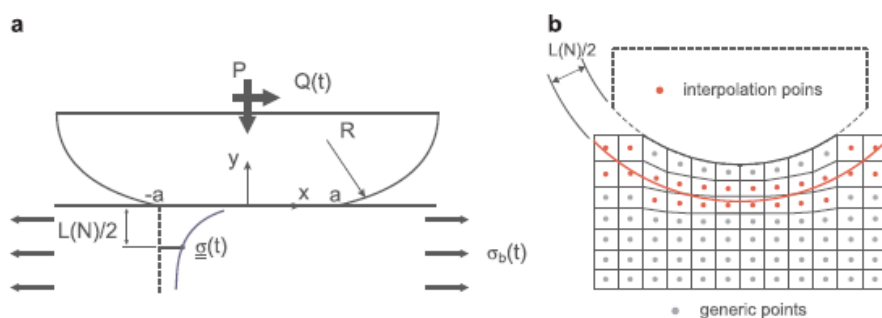


Figure 5-4 - Theory of critical distances (TCD) applied to fretting fatigue problems when wear is (a) neglected and (b) considered.

With the experimental data for Ti-6Al-4V and the numerical model previously presented in Figure 5-2, the estimated and observed fretting fatigue lives for critical distance varying with life and constant critical distance are presented in Figure 5-5.

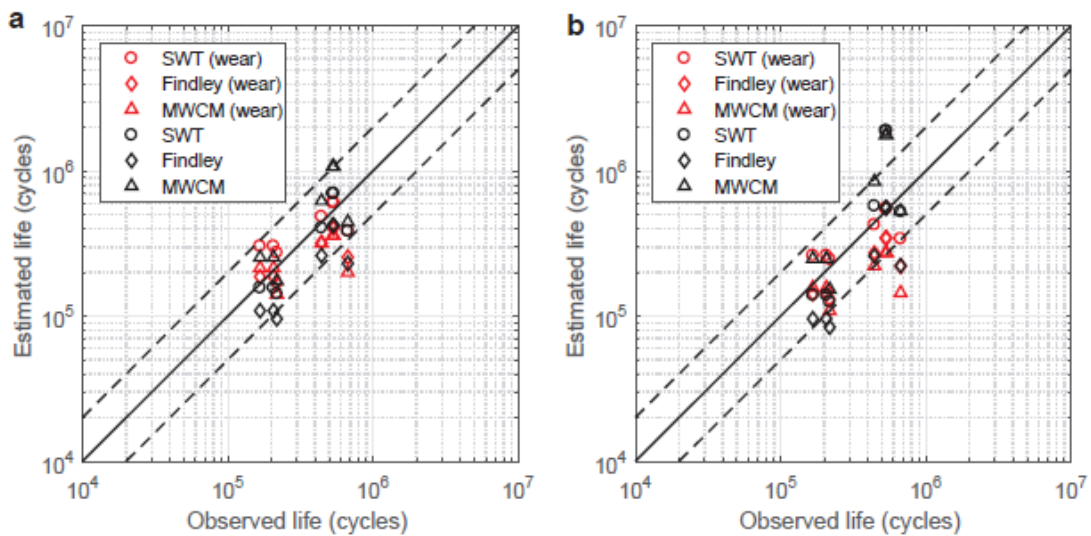


Figure 5-5 - Estimated vs observed fretting fatigue lives for (a) critical distance varying with life and (b) constant critical distance.

Study of size effects in fretting fatigue (Ref. [16])

This work was developed by researchers from Federal University of Rio Grande do Norte (UFRN), from the University of Brasília (UnB), from Université Paris-Saclay and from Snecma Villaroche, France.

Summary:

The aim of this work is to carry out an experimental campaign to study the size effect on fretting fatigue. Tests were carried out on a two vertical-actuators fretting-fatigue rig at the University of Brasilia.

The study of the size effect was divided into two parts. First, the influence on fretting fatigue life of the volume of material stressed under the contact was investigated. For so, the thickness of the specimens were reduced while maintaining the variation of a multiaxial fatigue parameter with the distance from the surface and the damaged area within the slip zones constant. In addition, the influence of the damaged area within the slip zones was also investigated by reducing it while maintaining all other experimental parameters constant, i.e. bulk fatigue load and tangential load per unit length. These two experimental campaigns were designed and analyzed by applying a multiaxial fatigue criterion in conjunction with the Theory of the Critical Distances (TCD). It was found that none of these two parameters seems to have a significant influence on the fretting fatigue resistance for the Ti-6Al-4V alloy here investigated.

Highlights and Main Conclusions:

The paper addresses multiaxial through the fatigue and the Modified Wöhler Curve Method (MWCM) criterion and Theory of Critical Distances. The experimental procedure focuses on Ti-6Al-4V specimens whose characteristics are presented in Figure 5-6.

Many details about the fretting fatigue device are presented, The fretting fatigue results are plotted in two groups, the first addressing volume effects (group a) and the second addressing the area effect (group b). Figure 5-7 presents the Evolution of the multiaxial index computed at the critical distance as a function of the number of cycle to failure for both specimen thicknesses (i.e., for group a).



Figure 5-6 - Photograph of fretting fatigue specimens and pads. Both specimens and pads have the same height (13 mm).

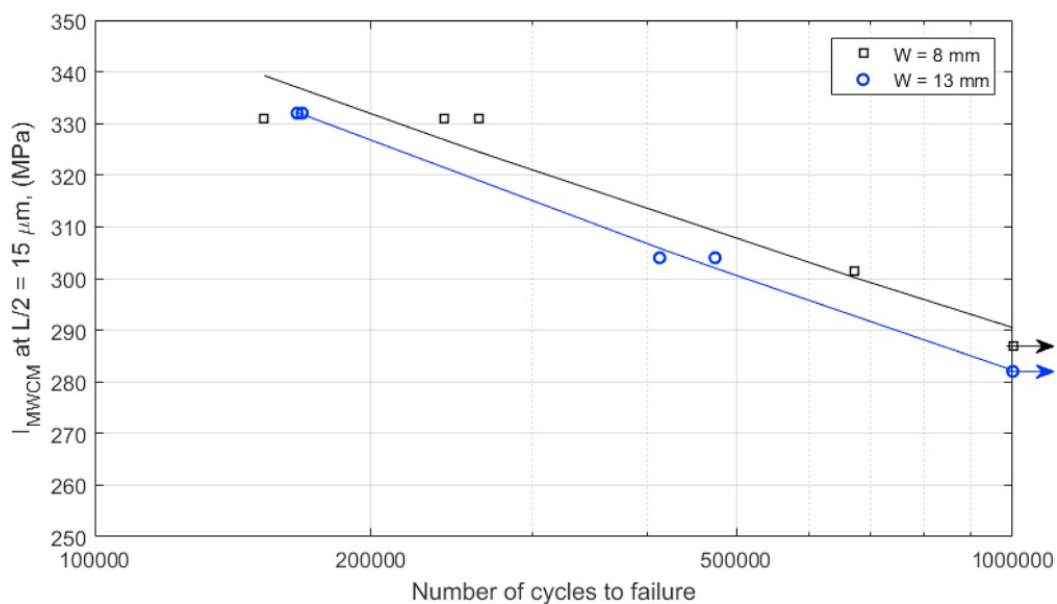


Figure 5-7 - Evolution of the multiaxial index computed at the critical distance as a function of the number of cycle to failure for both specimen thicknesses.

6. METALLIC MATERIALS – PROCESSES

Fatigue crack growth behavior of laser-shock processed aluminum alloy 2024-T3 (Ref. [17])

This work was developed by researchers from the University of São Paulo (USP) and from the Department of Aerospace Science and Technology (DCTA). It is a follow-on work from similar activities presented in Reference [3]. The work was presented during the 3rd International Conference on Structural Integrity (ICSI 2019) held in Madeira, Portugal in September of 2019.

Summary:

Laser shock processing (LSP) is a surface modification technique aimed at enhancing the resistance to wear, corrosion and fatigue of structural alloys. Recently, LSP without coating (LSPwC) has been gaining ground, using lasers with lower energies, shorter pulse duration, smaller laser spots and higher surface coverage per shot. In the present work, LSPwC treatment was performed in both sides of pre-cracked compact tension specimens of aluminum alloy 2024-T3. A pulsed (9 ns) Nd:YAG laser system operating in the second harmonic (532 nm) at 10 Hz repetition rate and with pulse energy of about 270 mJ was positioned with a 500 mm focal distance lens in order to conduct LSPwC with an estimated power density of 5.2 GW/cm² and two distinct overlapping rates: 50% and 75%. The objective of the work was to investigate the effect of the LSPwC and cyclic load condition on the crack closure and fatigue crack growth (FCG) behavior shown by the samples.

Highlights and Main Conclusions:

No significant effect due to the overlapping rate was observed in the surface analyses. Constant amplitude FCG tests were performed with two distinct load ratios: $R = 0.2$ and $R = 0.5$. A small increase in the crack closure loads ($P_{cl} \approx 1.1-1.2 P_{min}$) was evinced for the samples tested at $R = 0.2$ compared to the untreated ones, whereas negligible effect ($P_{cl} < 1.05 P_{min}$) was observed in the $R = 0.5$ results. With regard to the number of cycles for crack growth, the three laser treated samples tested at $R = 0.2$ presented an increased number of cycles compared to both of the untreated specimens, whereas no gain was verified for the treated samples tested at $R = 0.5$; on the contrary, a decrease in the number of cycles was observed. It seems that for the higher R tests, where no crack closure occurs, a deleterious effect of laser treatment prevails, possibly due to surface damage.

The results presented indicate that the increase in overlapping rate is not effective for the adopted LSPwC conditions. In further efforts it is intended to use higher

pulse energy laser in order to achieve superior peening effect aiming to improve the FCG behavior of LSPwC treated samples.

Effect of different forms of application of a laser surface treatment on fatigue crack growth of an AA6013-T4 aluminum alloy (Ref. [18])

This work was developed by researchers from the Federal University of Ouro Preto (UFOP), Federal University of Minas Gerais (UFMG) and Department of Aerospace Science and Technology (DCTA).

Summary:

This work analyzes the effect of surface-localized laser heating treatment on the fatigue crack growth (FCG) rate on region II of the sigmoidal $da/dN \times \Delta K$ curve of an aerospace-grade AA6013-T4 aluminum alloy sheet with 1.3 mm thickness. The influence on microstructure changes is also evaluated. Aiming to improve the FCG resistance without changing the mechanical behavior of the alloy, a Yb: fiber laser beam is defocused to generate a laser spot diameter of 2 mm, using 200 W power and a laser speed of 2 mm/s. Two laser lines are applied over fatigue C(T) specimens in two different forms: on only one surface and on both lateral specimen surfaces. Guinier–Preston zones, dispersoids and coarse constituent particles are found on the base material. On the heat-treated material, the same precipitates and also β' and Q' precipitates are found. These microstructural variations due to the laser thermal cycle, together with the presence of induced compressive residual stresses, improved the fatigue behavior of the material. The FCG retardation is optimized when two laser lines were applied on both lateral surfaces of the specimen.

Highlights and Main Conclusions:

Figure 6-1 presents the overview of the C(T) specimens subjected to the two conditions evaluated through the laser process, named 2 X 2 condition (where 2 beams were applied in one side) and 2 X 4R condition (where 4 beams were applied, two per each side).

The laser heating lines caused a significant microstructural change in the aluminum alloy, mainly for the 2 X 4R condition, with the presence of precipitates that characterize an aging state near to the equilibrium state.

Microhardness profiles performed along the laser lines showed that the verified microstructural changes caused local softening, which is more evident for the 2 X 4R condition.

Residual stresses were present around the laser lines, with distinct profiles for the two studied conditions. Before the first heating line, a compressive residual stress

was created in both cases. For the 2 X 2 condition, tensile stresses were observed between the two heating lines. For the 2 X 4R condition, the induced stresses between the lines are close to zero. Refer to Figure 6-2.

4. The microstructural changes together with the induced residual stresses caused a retardation in the fatigue crack propagation, due to the appearance of a plasticity crack closure mechanism. These changes are more evident in the 2 X 4R condition, as this situation showed a strong behavior toward the crack retardation. Refer to Figure 6-3.

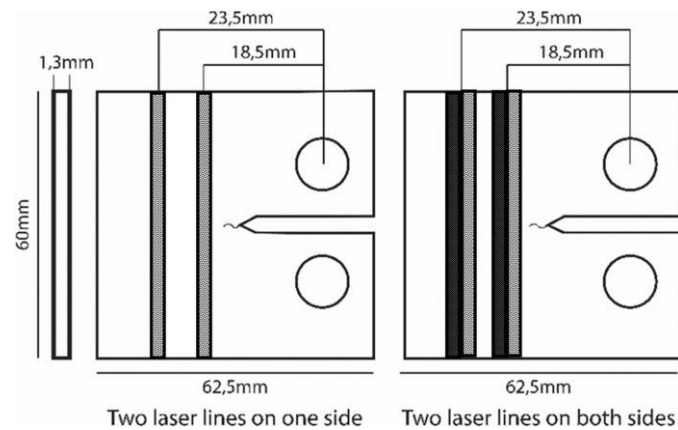


Figure 6-1 – C(T) specimens treated with two laser lines used on FCG tests. Clear dashed lines represent laser lines applied on one side; dark dashed lines represent laser lines applied on the other side.

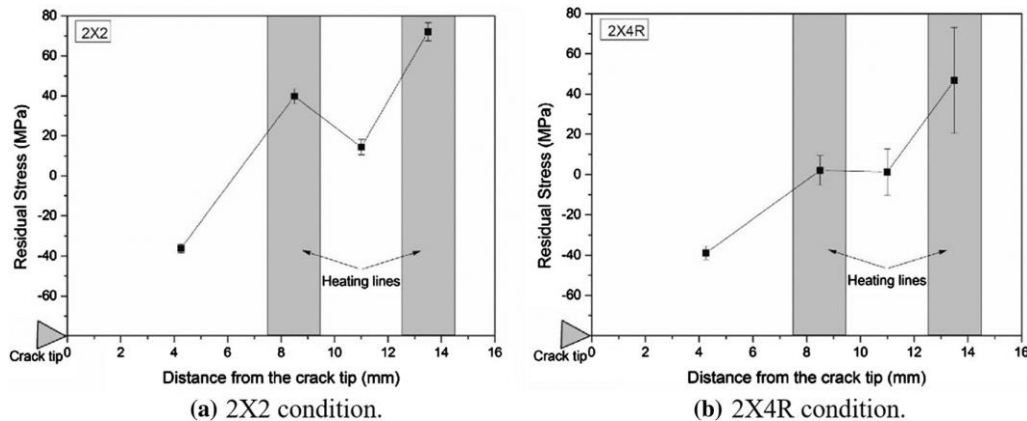


Figure 6-2 – Surface residual stresses for the two laser conditions. (a) 2 X 2 condition. (b) 2 X 4R condition.

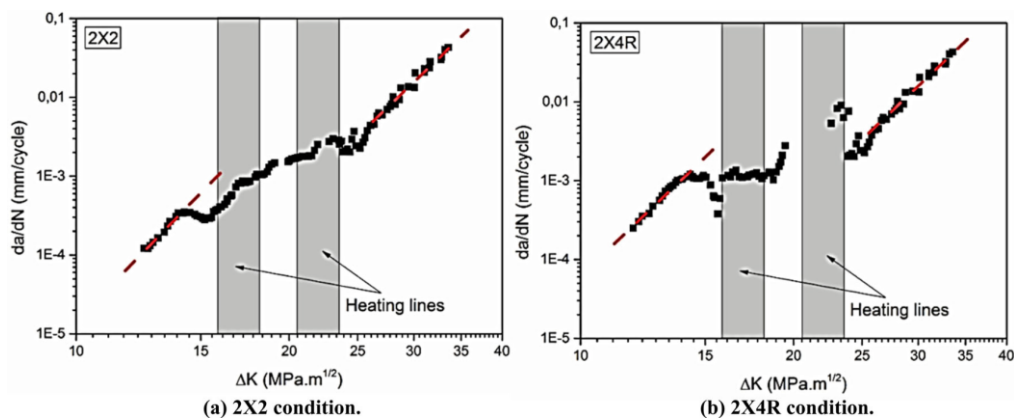


Figure 6-3 - Fatigue crack growth rate (da/dN) per stress intensity range (ΔK) for the laser-treated material. (a) 2 X 2 condition. (b) 2 X 4R condition.

Corrosion and corrosion-fatigue synergism on the base metal and nugget zone of the 2524-T3 Al alloy joined by FSW process (Ref. [19])

This work was developed by researchers from the Federal University of Triângulo Mineiro (UFTM) and the University of São Paulo (USP) and the University of Lisbon, in Portugal.

Summary:

The corrosion processes and its influence on the FCG curves of the 2524-T3 alloy joined by FSW was studied in the nugget and BM. To assess the corrosion process, SVET, pH micro-potentiometry and EIS were used. The localised corrosion results showed similar BM and nugget zone electrochemical behaviour, while the TMAZ/HAZ region was electrochemically the weakest zone, susceptible to anodic dissolution. The FSW process and saline environment was found to modify the BM and nugget FCG resistance, being more detrimental for the BM due to the primary IM particles that are not present in the nugget, making it chemically more homogeneous.

Highlights and Main Conclusions:

The corrosion and corrosion-fatigue behaviour of industrially important 2524-T3 Al alloy welded by FSW has been investigated in aggressive medium containing NaCl solution. Figure 6-4 presents an overview of the M(T) specimens geometry and a schematic view of the experimental setup for corrosion fatigue tests in seawater solution environment. Besides, the FSW process was successfully performed on plates of 2524-T3 Al alloy.

In agreement with the results of EIS, the combination of SVET and pH micro-potentiometry demonstrated that there was no significant difference between electrochemical behaviour of nugget and base material. The dissolution of the alloy

matrix in 0.05 mol L^{-1} NaCl solution was predominantly electrochemical. The region TMAZ/HAZ was found to be the most susceptible to anodic dissolution in the studied system, while nugget and base material remained slightly cathodic during the entire time of immersion;

In air environment, the NZ presented lower FCG resistance than the BM mainly as result of its smaller grain size and strengthening precipitates lower density and size (underage), making more effective crack deflection (zig-zag) in the BM, refer to Figure 6-5.

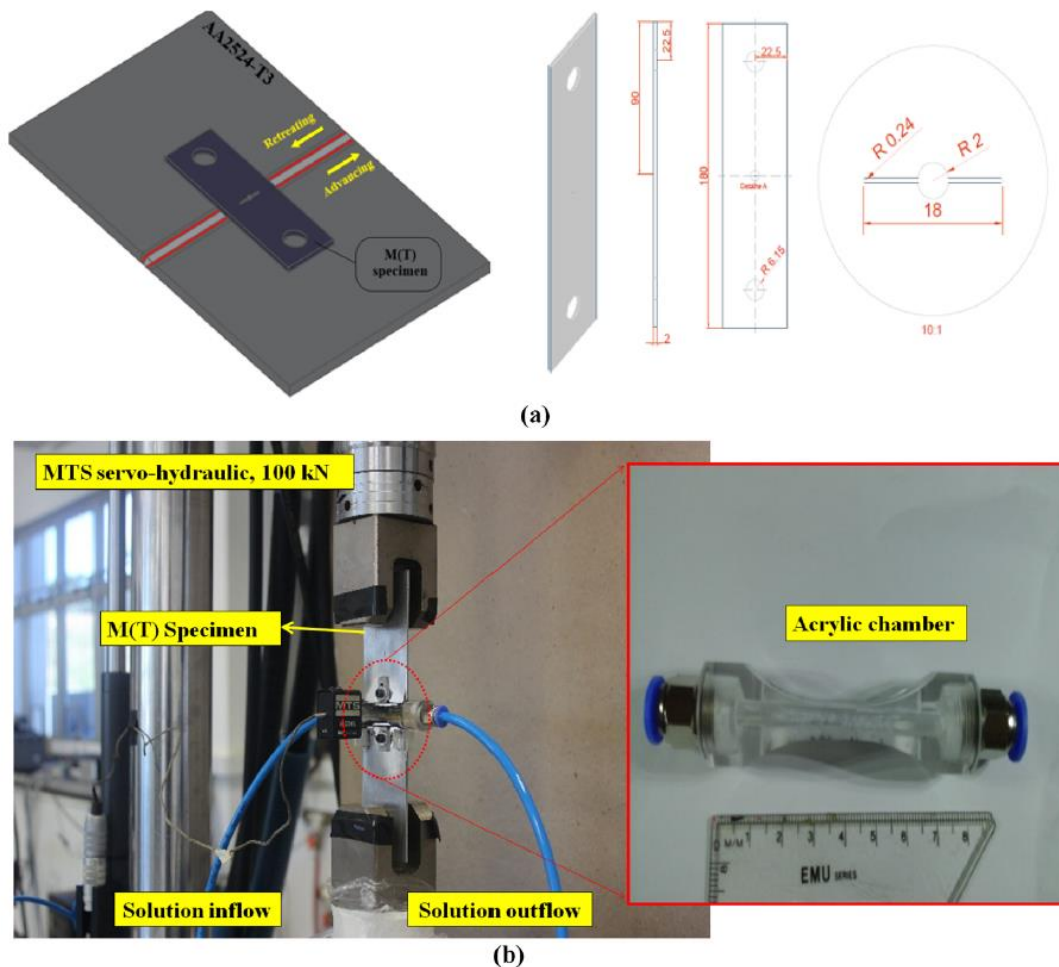


Figure 6-4 – (a) Size and geometry of the standard M(T) specimen type, removed in the L-T and T-L direction; (b) schematic view of the experimental setup for corrosion fatigue tests in seawater solution environment.

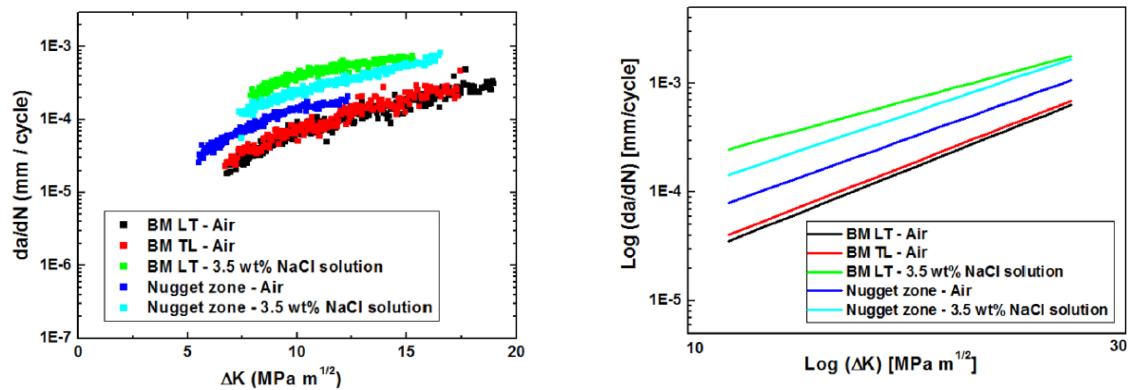


Figure 6-5 – (a) FCG curves of BM and NZ (with cracks propagating along the weld center line) in air and 3.5 wt.% NaCl solution conditions (region II) and (b) linear regression from the data extracted exclusively from Paris regime (region II).

7. METALLIC MATERIALS – STRUCTURES

Fatigue and Damage Tolerance Evaluation of Composite Curved Stiffened Panels in Postbuckling under Compressive Loads

Embraer R&D Group concluded structural tests to evaluate the effects of typical damage scenarios over damage tolerance and residual strength capability of composite curved stiffened panels in the postbuckling state under compressive loads.

This effort was developed in the context of a cooperation project between Embraer R&D and IPT (Institute for Technological Research of the State of São Paulo) for development of a composite rear fuselage technological demonstrator. For this purpose, the project encompassed the development of new design solutions using up to date manufacturing processes as well as the validation of structural analysis methodologies.

The specimens were designed and sized in order to represent curved stiffened panels located in regions of critical compressive loads of the composite rear fuselage. Closed hat-section stringers co-cured to the skin were adopted as design solution in order to take advantage of their high torsional stiffness and their resulting capability to delay skin buckling.

The panels were manufactured and tested at IPT facilities, using Automated Fiber Placement (AFP) process for skin lamination and hand-layup over elastomeric bladders for the closed section stringers (Figure 7-1).

Several panel configurations were evaluated, including an intact that served as baseline and others containing typical damage scenarios like barely visible (BVID) and visible impact damages (VID), manufacturing small defects, one-bay through-

the-thickness crack in the skin and two-bay through-the-thickness crack with a broken middle stiffener. The tests demonstrated that the proposed configurations provided damage tolerance and residual strength compatible with aeronautical industry's requirements, even in postbuckling state at load levels slightly below typical design load conditions (Figure 7-2).

Furthermore, those results were used for validation of methodologies and numerical simulations for the prediction of buckling and postbuckling behavior as well as the collapse load of composite curved stiffened panels.



Figure 7-1 - Composite curved stiffened panel manufacturing.

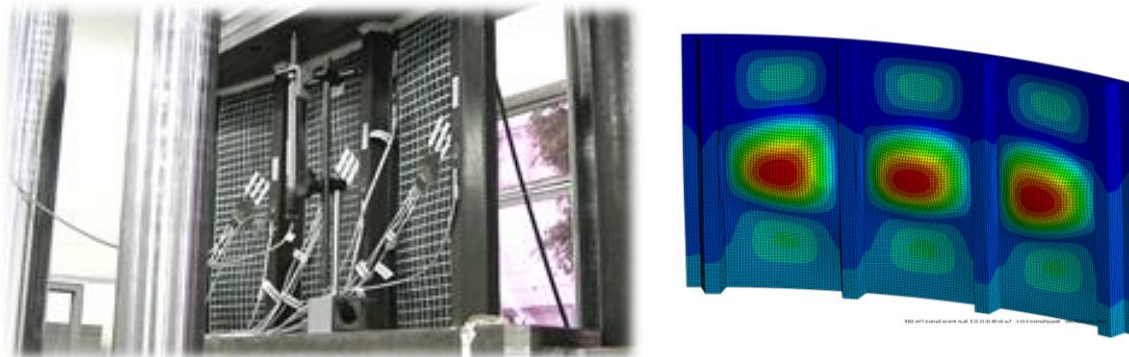


Figure 7-2 - Composite curved stiffened panel mechanical test and nonlinear finite element analysis in postbuckling under compressive load.

Component fatigue tests

Parallel to the Embraer 195 E2 full-scale fatigue test, this development test is being performed for verification of the Embraer 190 E2 wing fatigue behavior. This is because while the fuselage of the Embraer 190 E2 and Embraer 195 E2 have very similar constructions, their wings present some differences. Figure 7-3 shows the overview of this test, that is currently being performed.



Figure 7-3 - Embraer 190 E2 (second generation) wing full-scale fatigue test overview.

The empennage fatigue test for these aircraft has completed three lifetimes without relevant findings.

The landing gear tests for Embraer E2 aircraft as well as the KC-390 are currently being performed in Embraer facilities, in São José dos Campos, Brazil.

Additionally, the Embraer 175 E2 aircraft (outlined in Figure 7-4) is currently under the certification process, and the horizontal stabilizer of this aircraft, that is made of composite materials, is being subjected to dedicated full-scale static and fatigue tests in Brazil, according to related certifications requirements. An overview of the horizontal stabilizer test specimen is presented in Figure 7-5.



Figure 7-4 - Embraer 175 E2 (second generation).



Figure 7-5 - Embraer 175 E2 horizontal stabilizer overview.

Full-scale fatigue tests

Currently there are two full-scale fatigue tests being performed. The KC-390 multi-mission aircraft test specimen, presented in the previous ICAF report, and the Embraer 195 E2 (second generation) aircraft test specimen, whose test overview is presented in Figure 7-6 below.



Figure 7-6 - Embraer 195 E2 (second generation) full-scale fatigue test overview.

8. COMPOSITE MATERIALS AND STRUCTURES

Composite spirals and rings under flexural loading: Experimental and numerical analysis (Ref. [20])

This work was developed by researchers from the Federal University of Santa Maria (UFSM) and the University of São Paulo (USP).

Summary:

Recent improvements in pultrusion and filament winding have allowed the manufacturing of spirals and rings composite profiles for applications such as fuselage reinforcements of small aircrafts. However, the behavior of curved carbon fiber components is complex and hard to predict, and still demands deeper understanding. In this work, progressive damage and cohesive zone numerical models were used to simulate the behavior of unidirectional curved composite structures under flexural loading.

Four point bending tests were carried out on curved samples monitored by strain gages for model validation. The results have demonstrated a strong influence of delamination on samples with well-defined resin-rich areas. In contrast, curved structures with more homogeneous fiber distribution, i.e. those manufactured by curved pultrusion, showed increased flexural strength. Maximum stresses from numerical and experimental analyses were compared and the maximum difference found was below 3.5%.

Highlights:

Figure 8-1 and Figure 8-2 show an overview of the tests and analyses performed and a qualitative comparison for the failure. More details about modelling strategies, boundary conditions and loading, displacements and strain measurements may be found in the reference.

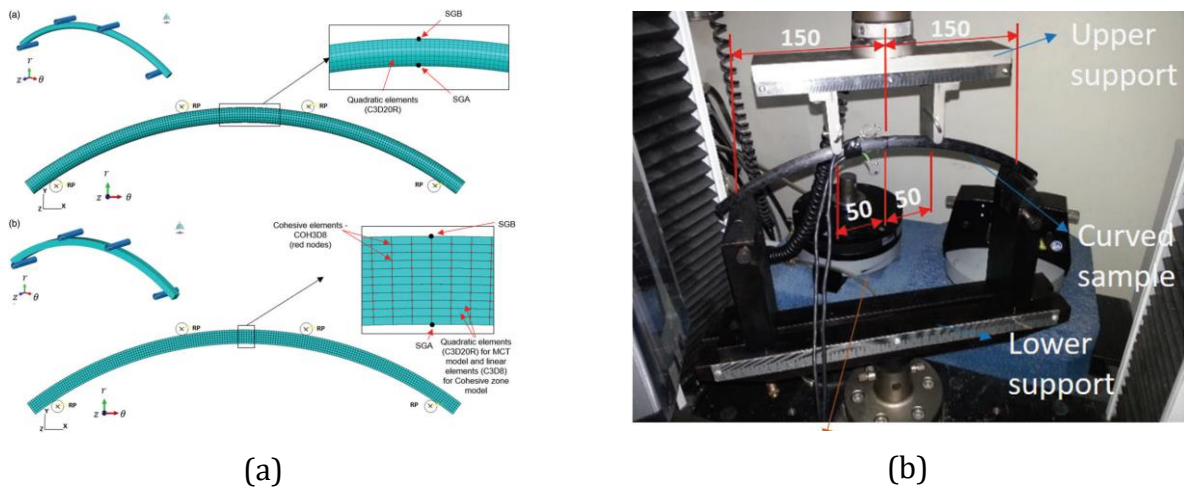


Figure 8-1 – (a) FEM used to simulate the four-point bending test; (b) four point bending test setup for curved composite samples (dimensions in [mm]).

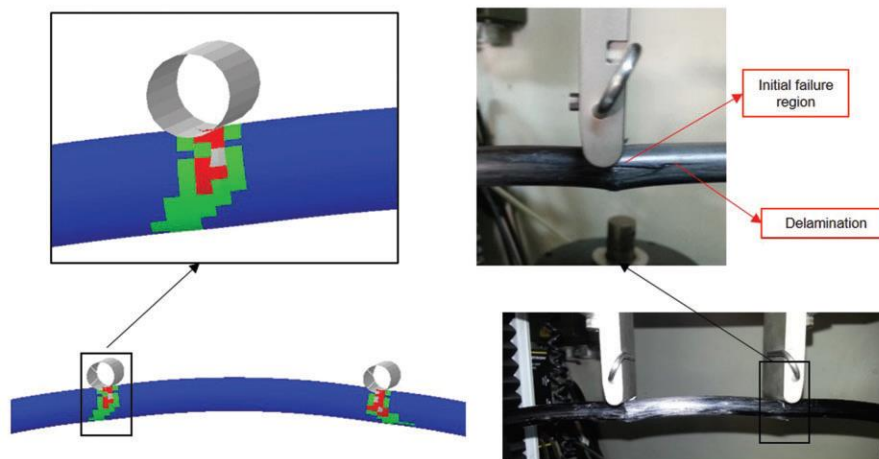


Figure 8-2 - Failure comparison between finite element analysis via MCT model and experimental tests for the spiral composites.

Novel progressive failure model for quasi-orthotropic pultruded FRP structures: Formulation and calibration of parameters (Part I) (Ref. [21])

Novel progressive failure model for quasi-orthotropic pultruded FRP structures: Application to compact tension and web-crippling case studies (Part II) (Ref. [22])

Summary:

The first part of this paper presents a novel progressive failure model for the 3D simulations of pultruded FRP structures which allows the modelling of the laminates as a homogeneous material. The failure initiation model proposed requires only the strength in each direction as input, combining them to retrieve

in-plane and out-of-plane failure indexes. The damage propagation model can be divided in two main stages: (i) damage progression and (ii) constant stress beyond a limit strain. The former stage uses the in-plane and out-of-plane failure indexes to determine the damage progression, using different parameters in each direction to account for the different damage responses, while the latter is characterized by a constant stress after a limit strain is reached, also different for each direction. FE models were developed with the proposed damage propagation model, requiring as input the strengths obtained from standardized experimental material coupon testing, the results of which, namely the load/stress vs. displacement/strain curves, are used to calibrate all the parameters needed to establish the model. The results show that the proposed damage propagation model, using a homogenized material, is well able to predict the experimental behaviour even for very complex cases such as interlaminar shear tests. Furthermore, in a companion paper the accuracy and limitations of the model are further assessed in the simulation of transverse compact tension and web-crippling tests.

Part II presents the application of that (calibrated) model to the simulation of two case studies: (i) transverse compact tensile (C(T)) tests; and (ii) web-crippling tests for two load configurations, external two-flanges (ETF) and internal two-flanges (ITF). The CT test, which is often used to determine the (tensile) fracture energy of FRP materials, is especially interesting as it allows assessing the quality of the simulations for a combination of in-plane transverse tensile and shear stresses in a geometry with a sharp singularity. The web-crippling test, on the other hand, is often used to determine the strength of FRP shapes under concentrated transverse loads, a real structural problem involving combined in-plane compressive and shear stresses. These two relatively complex case studies are used to assess the quality of the simulation in the presence of combined in-plane stresses. The numerical results showed an excellent agreement with their CT test counterparts; the simulation of these experiments were also used to demonstrate the need for using a mesh regularization scheme when modelling problems with singularities. The models were also well able to simulate both web-crippling load configurations, only slightly underestimating the maximum load – this was likely due to the slight underestimation of shear strength for combined in-plane shear and moderate transverse compressive stresses, as discussed in Part I, and/or non-quasi-orthotropic behaviour of the web-flange junction.

Overall, the numerical results showed a good agreement with the experimental data, even for relatively coarse meshes, attesting the feasibility and precision of the proposed damage progression model.

Highlights:

The papers are extensive and supply details about the formulation of the proposed damage progression model, FE implementation, calibration of parameters,

analysis, results and discussion for various test configurations. Figure 8-3 shows one example of qualitative correlation between FE analysis and experiments for a longitudinal interlaminar shear test, presented in Part I, while Figure 8-4 presents the damage progression for the transverse compact tension specimen evaluated in Part II of this study.

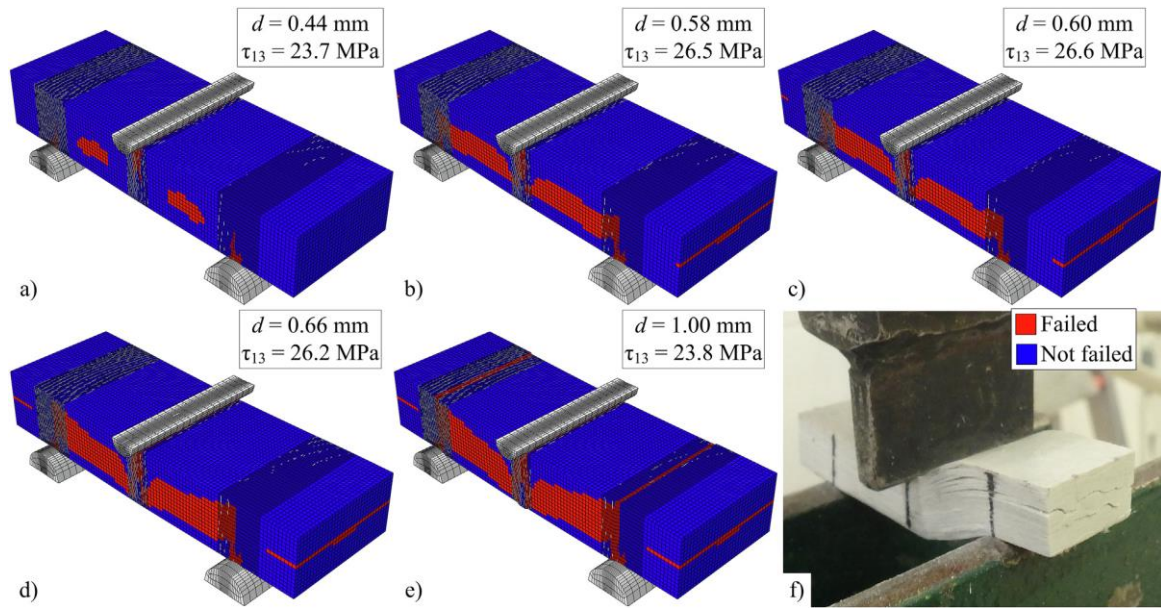


Figure 8-3 - Longitudinal interlaminar shear test – failure pattern progression predicted by the FE model (for plate I150-W, 0.5 mm global mesh), displacements of: a) 0.44 mm; b) 0.58 mm; c) 0.60 mm; d) 0.66 mm; e) 1.00 mm; and f) final aspect of specimen.

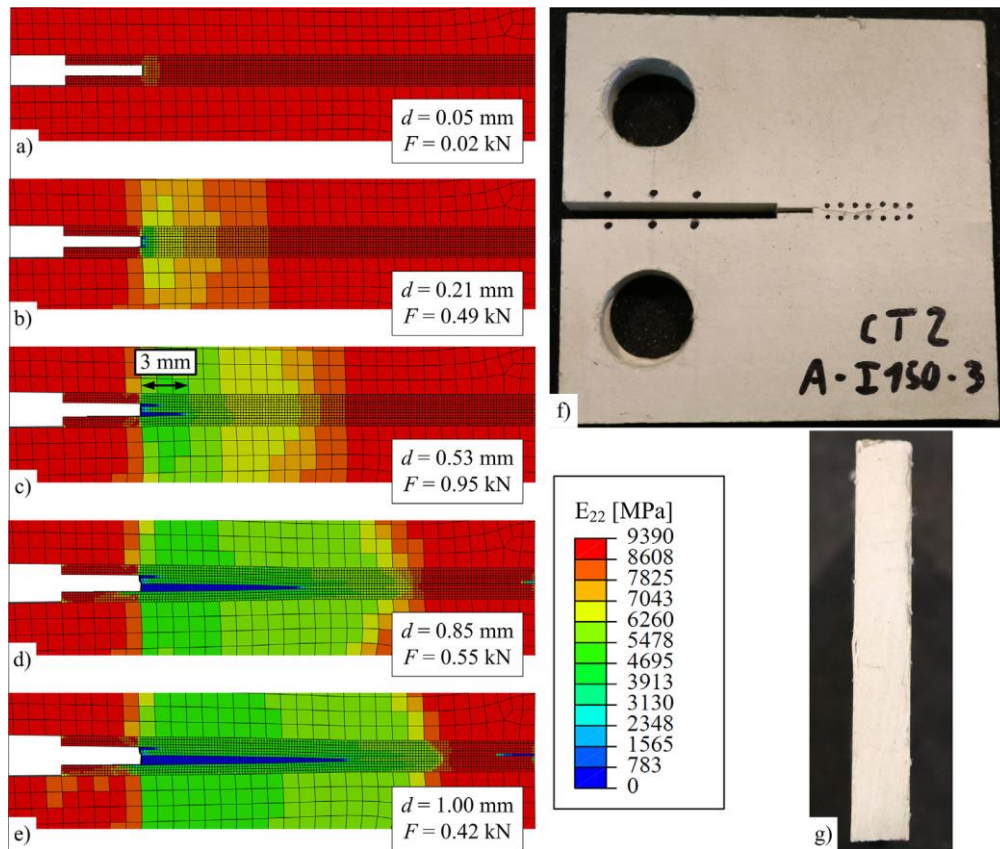


Figure 8-4 - Transverse compact tension test – failure pattern progression, in terms of E_{22} , predicted by the FE model (0.175 mm crack mesh), for CMODs of: a) 0.05 mm; b) 0.21 mm; c) 0.53 mm (maximum load); d) 0.85 mm; e) 1.00 m; and f) final aspect of experimental specimen.

Quasi-static translamellar fracture behavior of additively manufactured continuous carbon fiber reinforced thermoplastics (Ref. [23])

Summary:

The aim of this work is to study the translamellar fracture behavior of a 3D printed continuous carbon fiber reinforced thermoplastics. This investigation was made by experimental tests and numerical modeling by the finite elements method. The specimen type chosen was the double-edge notched (DEN) with unidirectional and cross-ply layup configurations and the composites coupons were manufactured by the fused filament fabrication (FFF) technique with the commercial carbon fiber filament from Markforged®.

The DEN tensile test results were assessed by the equations from the ASTM STP 410 standard, linear elastic finite elements simulation and strain calculations with video gauge data over Digital Image Correlation (DIC). Fractography analyses were also performed for a better perception of the failure mechanisms.

This work contributes with the quantification of critical translamellar fracture toughness K_{Ic} and critical energy release rate G_{Ic} for unidirectional and cross-ply 3D printed laminates as well as for single laminae at 0° and 90° . It also comments on material behavior in the microscopic scale through fractography. The results show properties not known before for FFF carbon fiber composite, considering layup with laminae at 0° and 90° , demonstrating fracture toughness for this composite in the range of K_{Ic} between polymers and metals values, depending of layup configuration. Furthermore, the behavior of a failure surface after an unstable crack in an opening mode for the 3D printed carbon fiber composite is described.

Highlights:

Figure 8-5 presents the geometry of the specimens tested, where a is crack size, W is the width, H_t is the total height and H is the effective height.

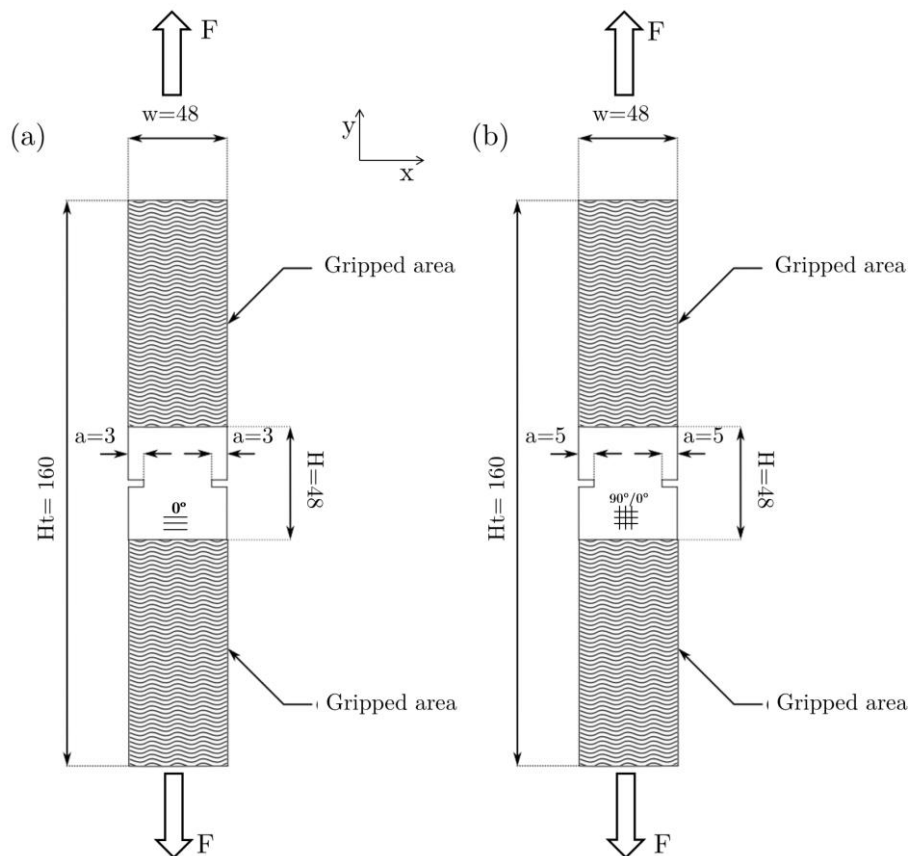


Figure 8-5 - Test specimen configurations.

Table 8-1 shows the fracture toughness results for the tests performed for the FFF carbon fiber filament composites during this work. Following the work premises and results presented, combining the layup information of a cross-ply structure, the fracture toughness in Mode I can be predicted. The graph is shown in Figure 8-6 - Mode I fracture toughness prediction based on results obtained for the

thermoplastic materials evaluated. with the respective standard deviation region of indicated values (shaded region).

Table 8-1 - Fracture toughness results summarized.

Layers	Technique	$K_{Ic}[MPa\sqrt{mm}]$	CV[%]
Lamina 90°	(DIC Unidirectional)	94.65	15.0
	(DIC Cross-Ply)	73.98	16.0
	(FE)	83.05	14.0
Lamina 0°	(DIC Cross-Ply)	882.50	18.0
	(FE)	1037.31	5.0
Laminate Unidirectional	(DIC)	73.74	15.0
	(FE)	61.72	14.0
	(ASTM)	65.73	14.0
Laminate Cross-Ply	(DIC)	361.06	17.0
	(FE)	421.21	5.0
	(ASTM)	443.08	5.0

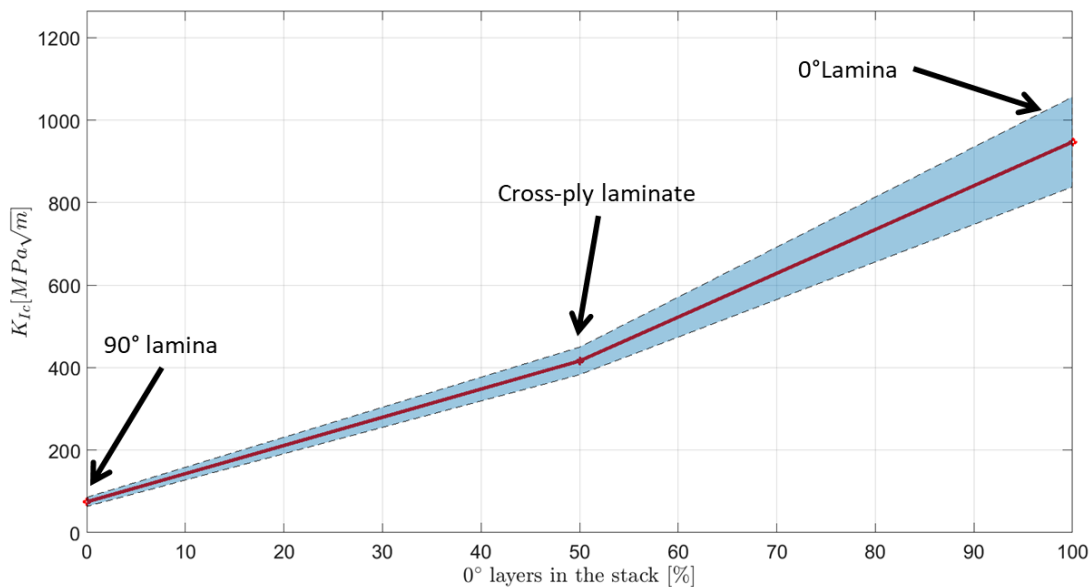


Figure 8-6 - Mode I fracture toughness prediction based on results obtained for the thermoplastic materials evaluated.

Effects of temperature and moisture on the fracture behaviour of composite adhesive joints (Ref. [24])

This work was developed by researchers from the Aeronautics Institute of Technology (ITA) and the State University of São Paulo (UNESP). The first author is presently a PhD candidate in TU Delft.

Summary:

Mode I interlaminar fracture toughness of CFRP joints co-cured and co-bonded was experimentally characterised under several environmental conditions. Two test campaigns were carried out: one with as-received specimens tested at $-54\text{ }^{\circ}\text{C}$ and $25\text{ }^{\circ}\text{C}$, and another with hygrothermally aged samples tested at $25\text{ }^{\circ}\text{C}$ and $80\text{ }^{\circ}\text{C}$. Dynamic mechanical analysis and scanning electron microscopy were used to explain distinct results. For co-cure, the propagation onset for as-received samples started at the interlayer region between the two adherends before migrating deeper into the adherend, while for as-received co-bonded samples, propagation onset was mainly cohesive. After aging, both bonding techniques failed directly in the adherend, in a fibre-tear fashion. Thus, the aging process presented a higher influence on failure mechanisms than the testing temperature. Regarding performance, mode I fracture toughness did not present a great variation for co-cured samples, since failure locus was always in the adherend. However, the initiation mode I fracture toughness of co-bonding decreased between as-received and aged samples. This difference is attributed to the presence of the adhesive in co-bonded systems, which showed to be more affected by environmental conditions than systems formed by fibre and matrix only, such as co-cured ones.

Highlights:

The paper describes the materials and methods, the procedure for moisture absorption and the Mode I fracture toughness tests. Further, it shows details about the microscopic and fractographic analyses performed in order to obtain a deeper evaluation on the distinct characteristics that occurred during each failure process.

Figure 8-7 brings one of the principal results of this work, that is the comparison between co-cured and co-bonded mode I initiation fracture toughness. The reader may consult the reference in order to obtain more details about the test specimens and testing conditions.

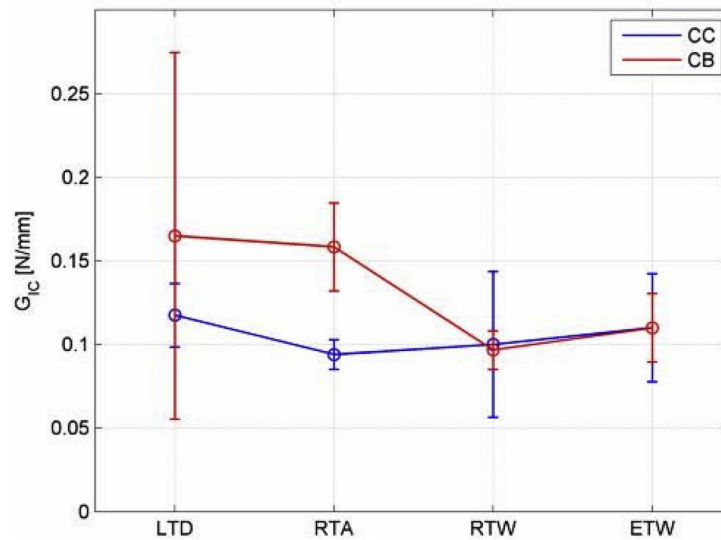


Figure 8-7 - Comparison between co-cured and co-bonded mode I initiation fracture toughness at each test condition.

Experimental characterization of mode I interlaminar fracture toughness in low-melt PAEK thermoplastic composite material (Ref. [25])

This work was developed by researchers from the Aeronautics Institute of Technology (ITA).

Summary:

Mode I fracture is one of the most widely studied fracture modes in fiber-reinforced polymer structural composites research. On the other hand, fracture properties of thermoplastic structural composites have not been studied extensively. This paper presents the determination of opening Mode I strain energy release rate (G_I) for a reinforced thermoplastic laminate made by a semipreg plain-5H satin weave fabric and a semi-crystalline engineered polyaryletherketone (PAEK) resin. Interlaminar fracture toughness was calculated based on Modified Beam Theory (MBT) method considering a perfectly built-in double cantilever beam. Experimental procedure and calculations to characterize Mode I interlaminar fracture toughness was performed according to Double Cantilever Beam (DCB) test method described in ASTM D5528-13 using end blocks to introduce opening forces. Comparisons with analytical solution using simple beam theory analysis was carried out to verify the obtained results. Finally, a fractography analysis was carried out in the tested samples to determine the failure mechanisms involved during the fracture process. Results demonstrated that thermoplastic composites usually present enhanced fracture toughness compared to thermosets. This improved fracture behavior is justified mainly due to the higher fracture resistance of crystalline polymers in comparison to amorphous polymers.

Hygrothermal effects on the fatigue delamination growth onset in interlayer toughened CFRP joints (Ref. [26])

This work was developed by researchers from the Aeronautics Institute of Technology (ITA) and the State University of São Paulo (UNESP). Partial results were presented in the previous ICAF report.

Summary:

Aeronautic structures are exposed to a great variety of temperatures and humid environments during service. Nowadays, it is known that the combined influence of moisture and temperature induces further detrimental effects on the fatigue behavior of bonded joints when compared to the influence of each isolated condition. The effect of hygrothermal pre-conditioning on the fatigue delamination growth onset of different bonded technologies was investigated.

This paper provides a material database for composite-joints tested under different environments and gives important insights on the failure mechanisms observed under cyclic loadings. This information can be latter used to validate analytical and numerical models.

Highlights:

Two test campaigns were performed to analyze the influence of a hygrothermal pre-conditioning on the fatigue delamination growth onset of CFRP bonded joints under modes I and II. Figure 8-8 shows an outline of the test specimens.

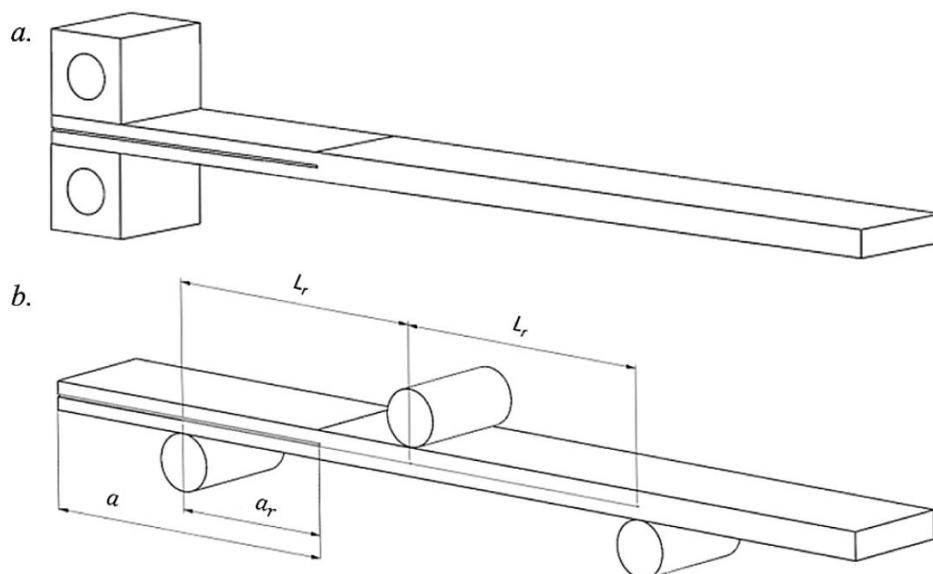


Figure 8-8 - a) DCB specimen and b) 3-ENF specimen.

Figure 8-9 shows the experimental data for moisture absorption for the specimens, where a Fickian behavior equation was applied to adjust the absorption trends.

Among various test results presented along the paper, Figure 8-10 was selected, that shows the trends of Mode I G-N curves for specimens with and without environmental preconditioning.

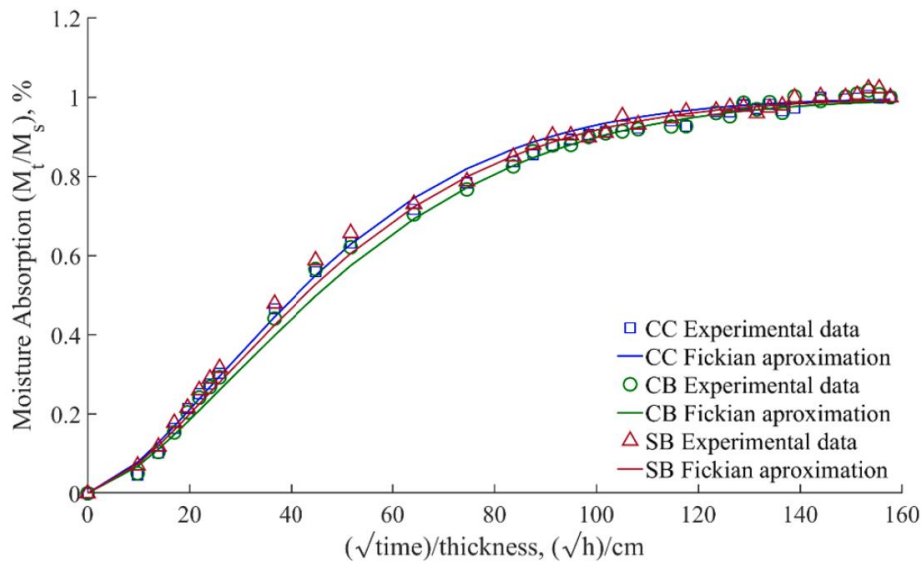


Figure 8-9 - Experimental data and Fickian approximation of the joints moisture absorption.

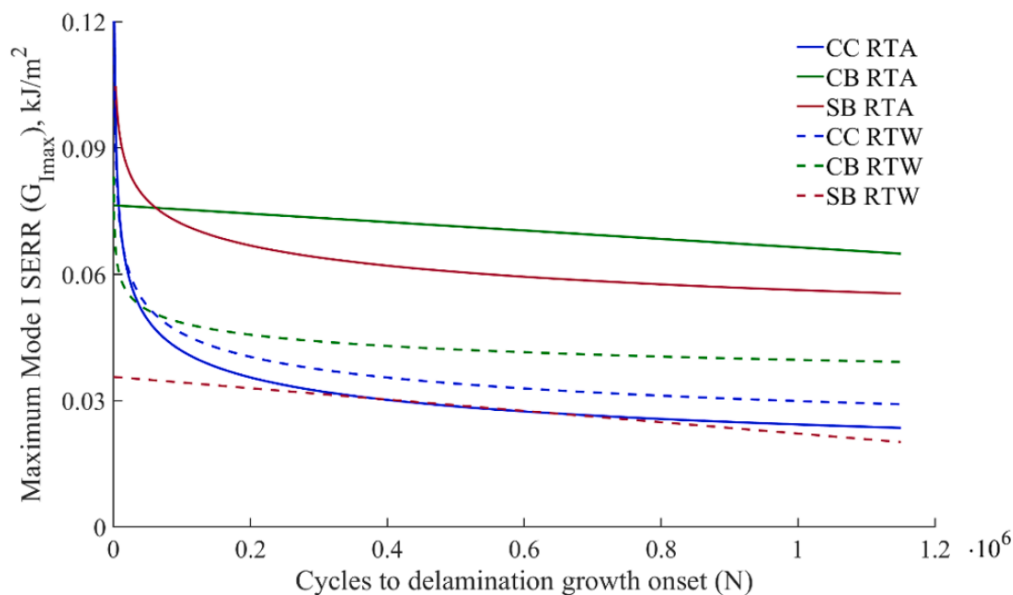


Figure 8-10 - Mode I G-N curves for specimens with and without an environmental preconditioning.

The influence of hygrothermal aging on the fatigue behavior and residual strength of post-buckled co-bonded stiffened panels subjected to compressive loading (Ref. [27])

This work was developed by researchers from the Aeronautics Institute of Technology (ITA) and from the University of Twente (The Netherlands).

Summary:

Adhesively bonded composite structures, if designed properly, have proven to be stiffer and to possess a higher specific strength than their mechanically fastened counterparts. To increase the applicability of these bonded joints in the aircraft industry, a study was performed to investigate the influence of hygrothermal aging on co-bonded composite stiffened panels with an initial disbond under cyclic compression loading. Experiments showed that hygrothermal aging led to a decrease in disbond growth throughout cyclic loading. The decreased disbond growth was likely caused by the increased ductility of the bond due to the presence of moisture. A higher ductility can lead to crack blunting and stress relaxation, resulting in higher fracture toughness of the bond. Furthermore, it was shown that hygrothermal aging did not influence the residual strength and stiffness of the panels after cyclic loading. The experiments were simulated numerically to gain a better understanding of the crack growth behavior and to aid future numerical crack growth predictions.

Highlights and Main Conclusions:

Some selected information from this work is presented below. Figure 8-11 shows the front view (cross section) of the panels tested, while Figure 8-12 shows the isometric view with the artificial damage inserted. Figure 8-13 shows how the specimens were assembled for the static, fatigue and residual strength tests, including some auxiliary devices, such as anti-buckling plates, strain gages and LVDTs.

Figure 8-14 and Figure 8-15 show the disbond area and the disbond length growth respectively as function of the number of cycles for the post-buckling cyclic tests.

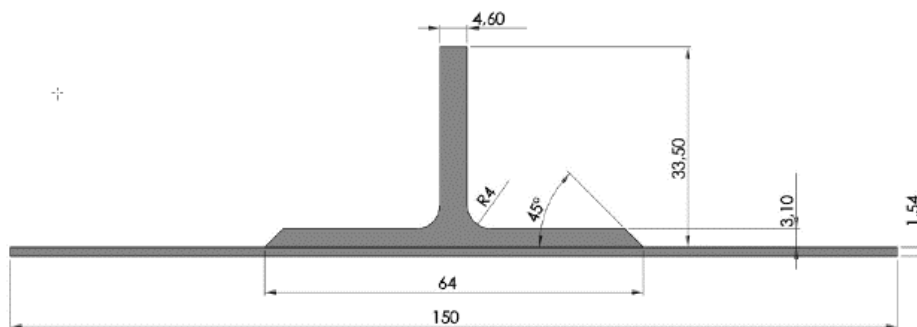


Figure 8-11 - Front view of the panels tested.

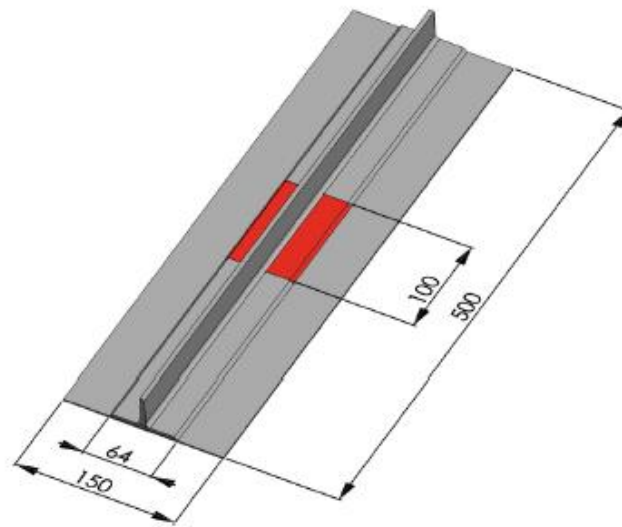


Figure 8-12 - Isometric view of the panels, with the Teflon™ insert depicted in red.

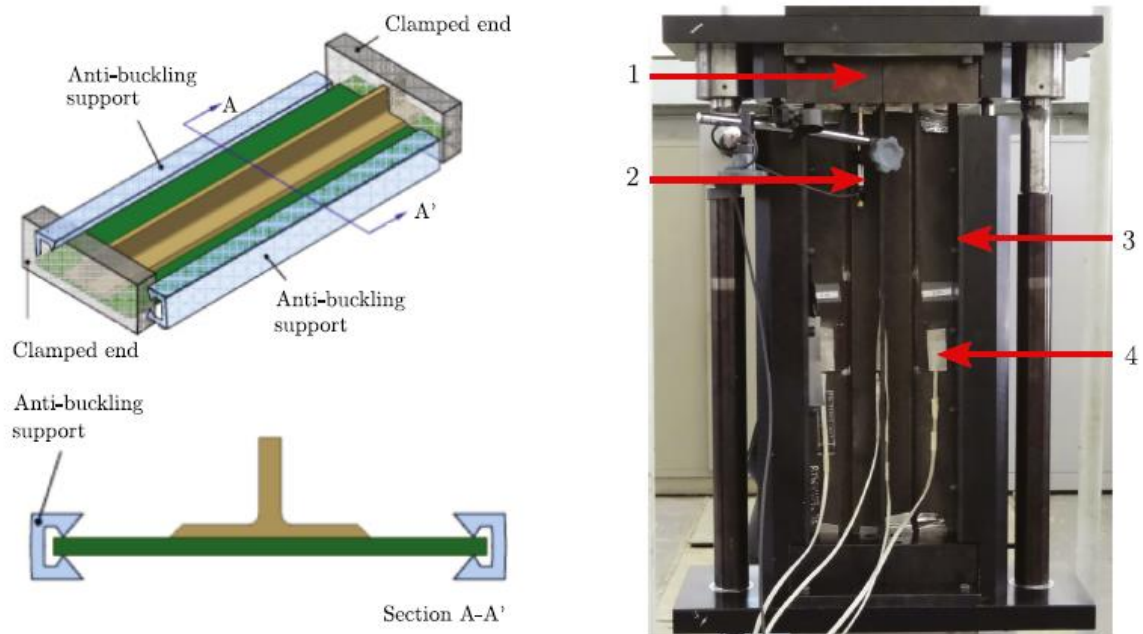


Figure 8-13 - Boundary conditions of the panels and close-up of the test rig.

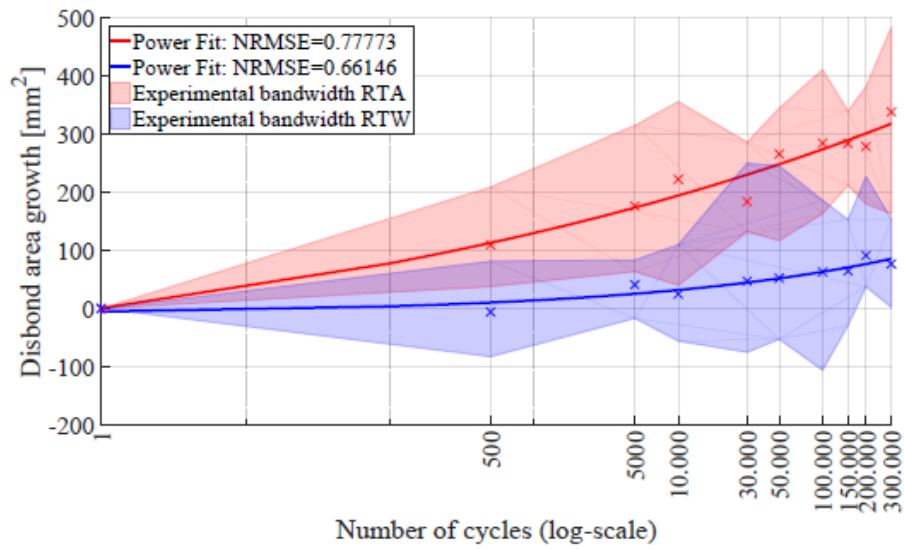


Figure 8-14 - Average growth of the disbonded area in the RTA and RTW panels.

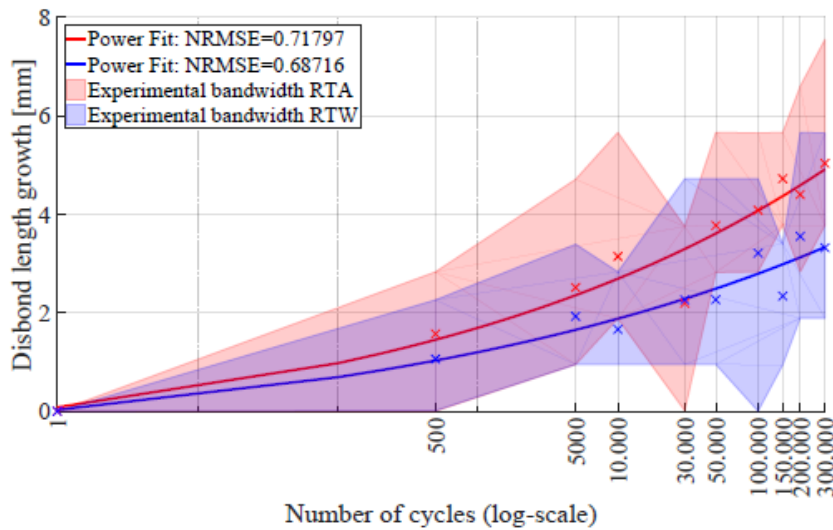


Figure 8-15 - Crack length growth.

9. HYBRID MATERIALS AND STRUCTURES

Design and mechanical integrity of friction riveted joints of thermoplastic composite (Ref. [28])

Hydrothermal aging of friction riveted thermoplastic composite joints for aircraft applications (Ref. [29])

Low-velocity impact response of friction riveted joints for aircraft application (Ref. [30])

Mechanical integrity of friction-riveted joints for aircraft applications – Ref. [31]

This series of works, resulting in a PhD thesis, were developed by Natascha Zocoller Borba, from Federal University of São Carlos (UFSCar) and co-workers from German and Austrian organizations. Her PhD degree was obtained in the Technical University of Hamburg.

We are particularly grateful to Dr. Jorge dos Santos, from HZG, and Dr. Sergio de Traglia Amancio-Filho, from the Technical University of Graz (Austria) for their support through these valuable contributions.

Summary:

Thermoplastic composites have attracted increasing interest as alternative materials for primary and secondary structures of the next aircraft generation, owing to their fast processability and good reparability. The employment of these materials has triggered research in the fields of durability, fatigue, and damage tolerance, and prompted the development of alternative joining solutions that mitigate the dissimilarity between them and the remained metal parts in the aircraft. Among these technologies, Friction Riveting (FricRiveting) is an innovative, friction-based joining process suitable for polymers, composites and hybrid metal-composite structures.

This PhD work was devised to fill in gaps in scientific and technological knowledge, with a focus on further develop and understand the fundamentals of the FricRiveting process, joint design, and mechanical integrity. Case study overlapped joints were produced using a titanium alloy Ti6Al4V rivet and woven carbon fiber reinforced polyether ether ketone (CF-PEEK) parts relevant to aviation.

Although FricRiveting presented inferior quasi-static mechanical performance compared to reference lock bolting, the fatigue life of the joints showed an improvement up to 88 %, fulfilling aircraft industry requirements. The sensitivity of the friction riveted joints to impact damage and its propagation under quasi-static and cyclic loading was investigated through drop weight impact testing as

well as microstructural characterization and post-impact single lap shear and fatigue testing. The joint strength and fatigue life were not compromised by barely-visible impact damage, which did not indicate a nucleation of critical delamination. However, visible impact damage introduced both delamination and premature failure at the metal-composite interface, leading to a 40% decrease of quasi-static mechanical strength and the fatigue limit reached at load level of 58% of the quasi-static joint strength. The residual quasi-static strength of those joints surviving 10^6 cycles of fatigue was evaluated revealing no critical damage accumulation at the examined load level for unimpacted and impacted joints.

The durability of the joints was assessed under hydrothermal and saline aging. With hydrothermal aging a 23% increase of joint mechanical performance was observed after 28 days of exposure, as a result of PEEK post-crystallization. With saline aging a decrease up to 23% of the quasi-static mechanical performance could be explained by corrosion induced in the external tightening elements, which no longer contributed to redistribution of the compression stress through the composite surface.

This PhD work succeeds in further developing the FricRiveting process by covering complex and relevant issues from scientific and engineering perspectives for the introduction of thermoplastic composites and providing a new joining solution for aircraft manufacturing.

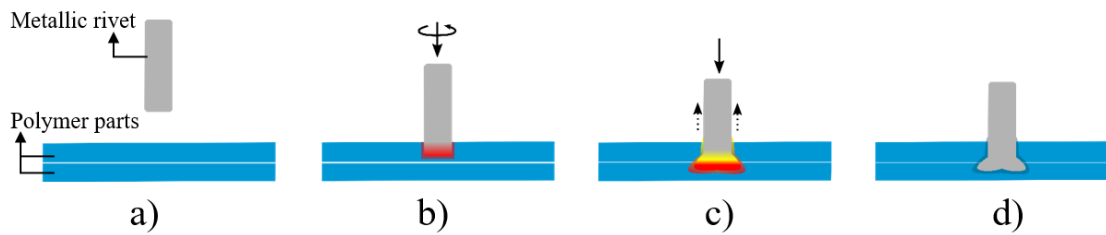
Highlights:

Figure 9-1 shows some possible configurations for the FricRiveting process, while in Figure 9-2 it is presented an schematic overview of the friction riveting process steps. Figure 9-3 shows some potential applications for this technology in aircraft structures.

Selected among a large amount of results presented in the above references, Figure 9-4 shows the SN behavior of FricRiveting joints, and Figure 9-5 shows the stiffness degradation of joints tested for various stress levels, with 66% of the ultimate lap shear force (ULSF).



Figure 9-1 - Possible joint configurations of FricRiveting for multiple material types: a) metal-inserted, b) overlap, and c) sandwich-like joint.



(a) positioning of the joining parts

(b) friction phase (plunging of the rotating rivet through the upper part)

(c) forging phase (plunging of the rivet through the lower part and rivet plastic deformation)

(d) joint consolidation.

Figure 9-2 - Schematic representation of Direct Friction Riveting process steps.

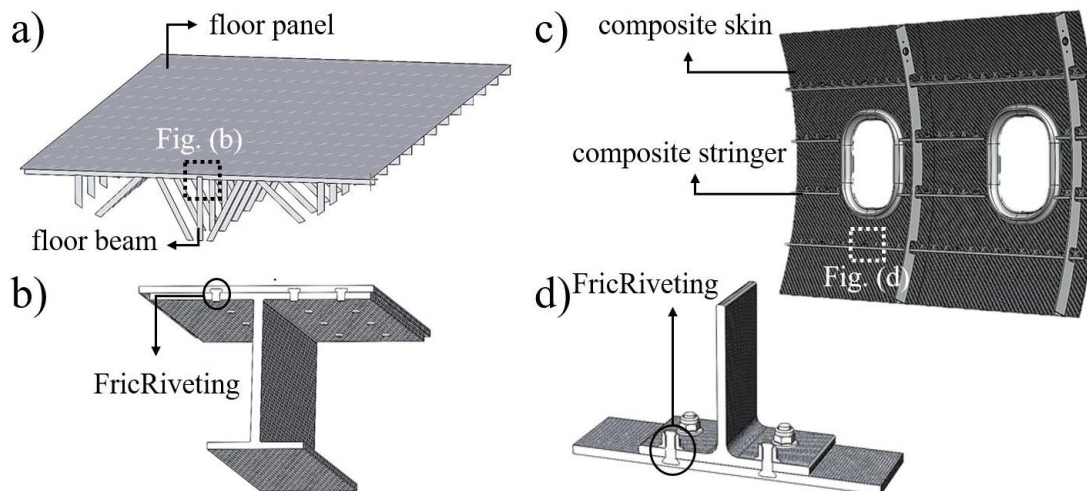


Figure 9-3 - Schematic illustration of potential applications of FricRiveting in aircraft structures: a) composite floor structure, joining floor beam to floor panel, as detailed in (b); and c) composite fuselage, joining stringer to skin, as detailed in (d).

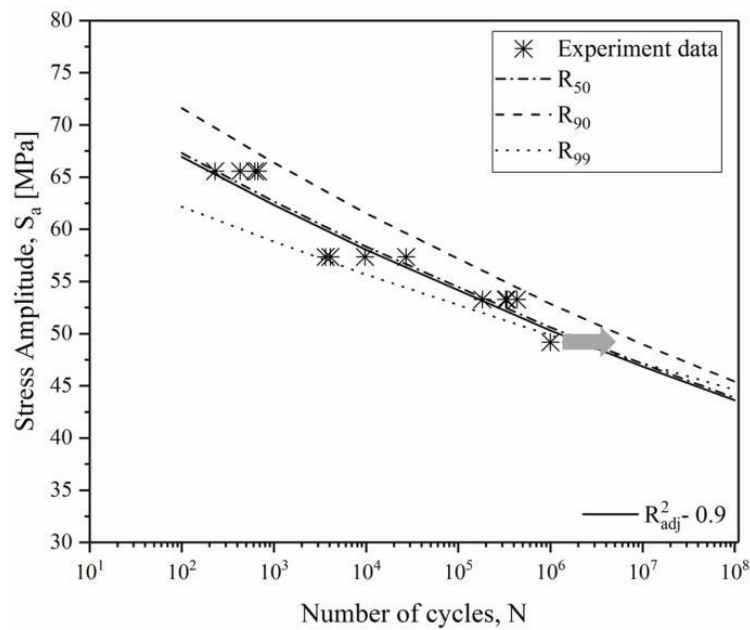


Figure 9-4 - Joint S-N curves (reliabilities of 50 %, 90 %, and 99 % according to the two-parameter Weibull distribution).

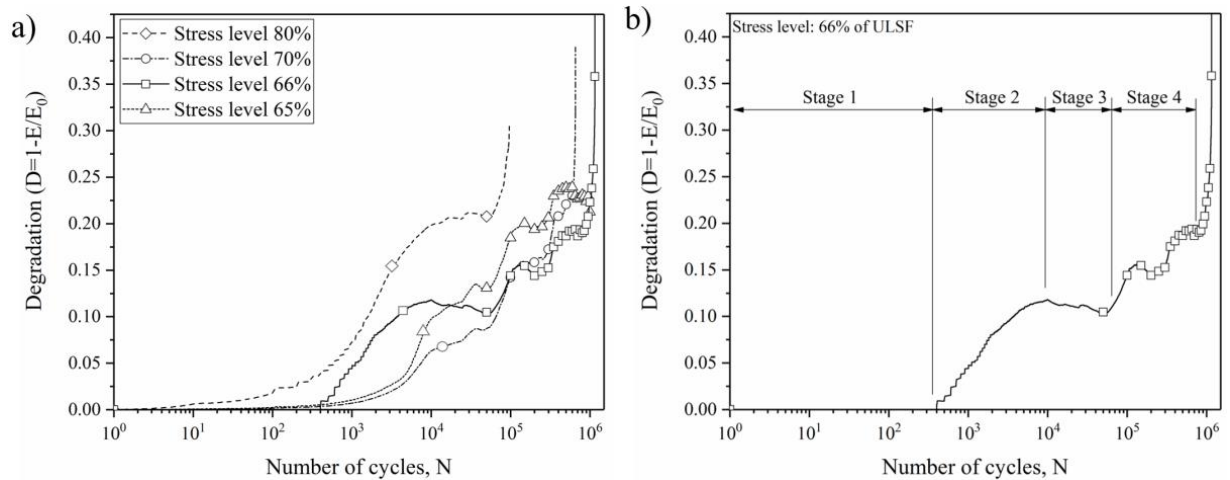


Figure 9-5 - Stiffness degradation curves: a) for various stress levels, and b) for 66 % of the ULSF showing the stages of damage evolution.

Mechanical integrity and corrosion behavior of metalcomposite hybrid joints produced with Friction Spot Joining (Ref. [32])

This PhD work was developed by Natalia Manente André, under supervision of Dr. Prof. Dr. Sergio de Traglia Amancio-Filho, from the Technical University of Graz (Austria).

Summary:

The combination of fiber-reinforced polymer composites and lightweight alloys has emerged as a lightweight solution for the transportation sector, mainly due to the optimal specific strength and stiffness associated with these materials. The possibility of joining metals and composites is an important topic for the cost-effectiveness of hybrid structures in mass production. Friction Spot Joining (FSpJ) is an alternative solid-state joining technique for hybrid structures. This technology has demonstrated its potential as a joining solution for metal-composite structures by attaining high mechanical and durability performances in previous investigations. Nevertheless, the industrial transferability of such new technology requires further assessment regarding the mechanical integrity and corrosion behavior of the joints.

Therefore, this thesis is dedicated to understand the damage evolution at the interface of AA2024-T3/CF-PPS friction spot joints. For this purpose, finite element modelling was applied and the bonding zones of the joints were discretized using the traction-separation law. It was demonstrated that the damage in friction spot joints initiates at the AZ (adhesion zone) and then propagates as a symmetric linear front from the edges towards the center of the joined area. Nevertheless, as the damage advances inside the PDZ (plastically deformed zone), its propagation became an asymmetrical linear front that evolves preferably from the free edge of the composite part due to the higher peeling stresses in this region (asymmetrical secondary bending of the structure took place due to differential stiffness of materials). Based on the findings of this study, modifications were proposed to the failure theory previously stated for friction spot joints.

In addition, the fatigue damage tolerance of the joints was evaluated under mixed-mode I/II loading. The AZ presented low crack growth resistance, while the PDZ demonstrated to be the most damage tolerant zone of the joints. The fatigue crack growth of the friction spot joints was dictated by the bonding zones and occurred in three well-defined stages: initiation, linear region, and unstable crack growth. Steady crack growth rates were found for AZ and PDZ. This shows that the main bonding zones of these joints have defined properties. Thereby, the mechanical behavior of the joints can be tailored by their zones. Moreover, the friction spot joints generally present inferior and more stable fatigue crack growth rates when compared to adhesive bonded joints.

The impact resistance of the joints was also investigated using the drop weight test. Further, the corrosion behavior of the joints was investigated during six weeks of salt spray exposure.

Finally, as a first step for the upscaling of the FSpJ technology, a fuselage sub-component was constructed using FSpJ in combination with other friction-based technologies. A reduction of 20% in weight was reached in comparison with the

full-metallic and bolted design, thereby successfully demonstrating the potential of FSpJ as a joining solution for hybrid aircraft structures in the future.

Highlights:

From the extensive campaign of tests performed from this work, Figure 9-6 shows the general configuration of the joints used for damage tolerance tests. As one example of the results obtained, Figure 9-7 shows the crack growth resistance curve of the friction spot joint under quasi-static mixed-mode I/II loading.

Regarding the applications of the FSpJ process, Figure 9-8 shows an overview of the demonstrator produced entirely with friction-based joining technologies. This demonstrator also includes the FricRiveting technology previously addressed.

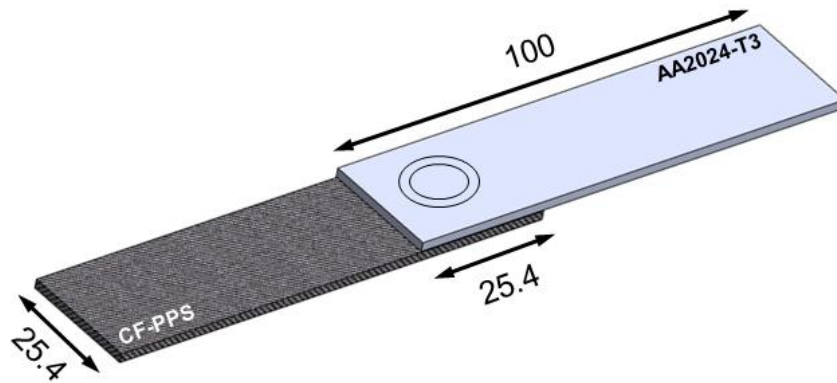


Figure 9-6 - Configuration and dimensions of the joints used for lap shear test (in mm).

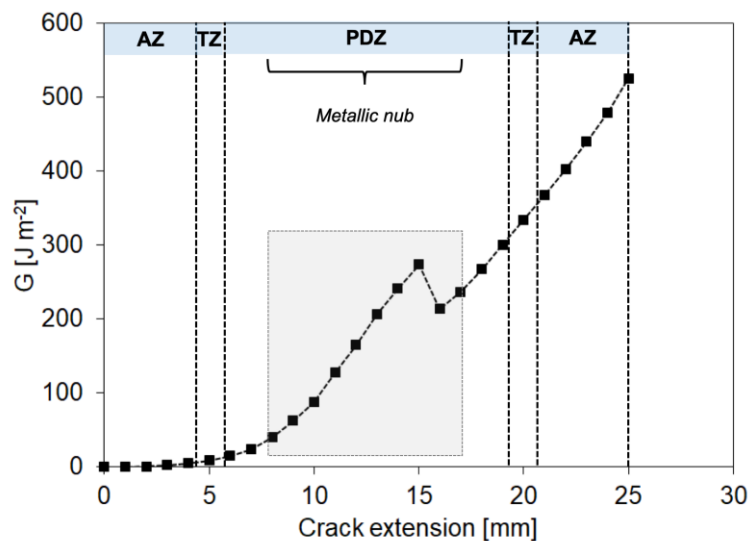
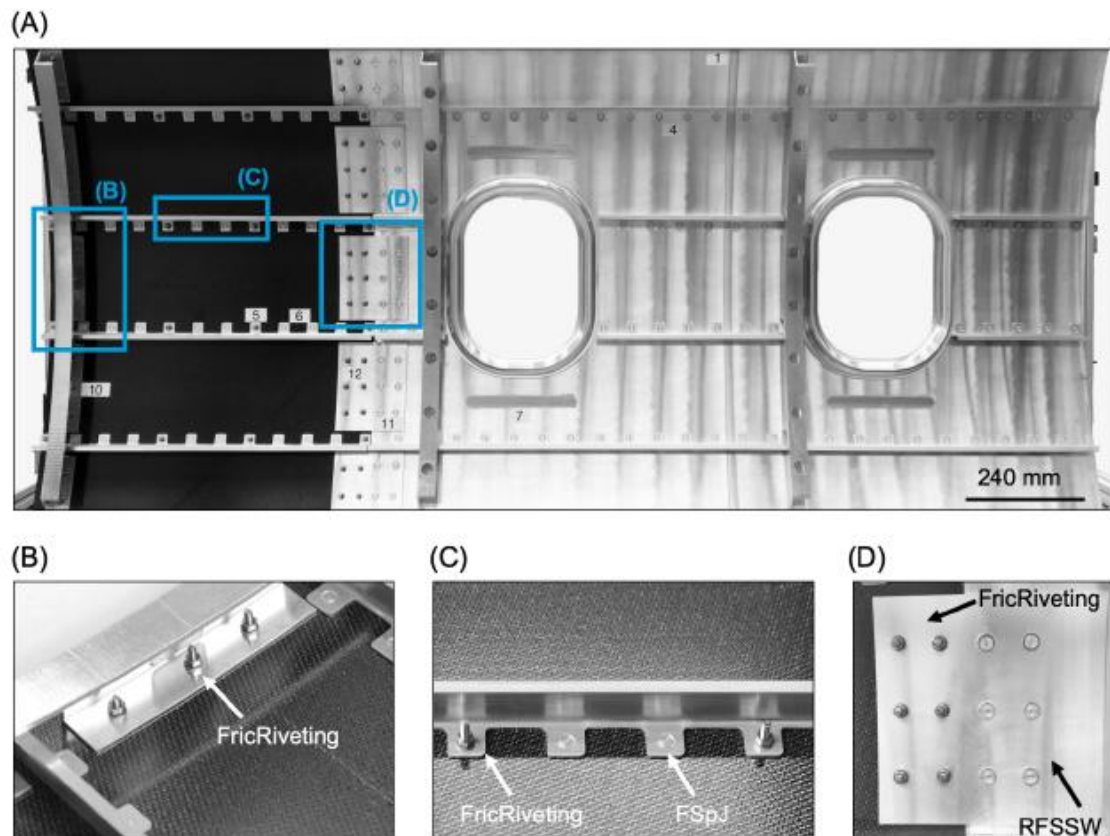


Figure 9-7 - Crack growth resistance curve of the friction spot joint under quasi-static mixed-mode I/II loading. The light gray rectangle represents the metallic nub region inside PDZ.



(A) overview of the demonstrator.

Hybrid connections:

(B) composite skin-metallic frame joined by FricRiveting,

(C), composite skin-metallic stringer joined by FSpJ

(D) composite skin-metallic doubler joined by FricRiveting and RFSSW.

Figure 9-8 - Overview of the demonstrator produced entirely with friction-based joining technologies.

A new additive manufacturing technique for layered metal-composite hybrid structures (Ref. [33])

This PhD work was developed by Rielson M. M. Falck, under supervision of Dr. Prof. Sergio de Traglia Amancio-Filho, from the Technical University of Graz (Austria). The PhD scholarship was supported by Conselho Nacional de Desenvolvimento Científico e Tecnológico – CNPq (Brazil).

Summary:

There is an increased interest in recent advances in the field of additive manufacturing (AM). These offer the flexibility to produce complex geometric parts, such as sandwich structures with AM honeycomb cores. Combining the

principles of joining and polymeric AM is the main aim of the present doctoral thesis, which introduces AddJoining, a new technique that was co-invented by the author to contribute to the manufacturing options for joining multi-material parts. The process was inspired by additive manufacturing and joining technology principles, and this new technique uses polymer 3D printing, e.g., fused filament fabrication, FFF (also known as fused deposition modeling, FDM), to add layers of polymer or composite to a metal substrate. The AddJoining process has a potential to produce structures with geometric flexibility, such as honeycomb cores. As an early phase of this technology this PhD work was devised to understand and develop the fundamentals of the AddJoining process by joining transportation grade lightweight aluminum 2024-T3 with a combination of unreinforced polyamide 6 (PA6) and carbonfiber reinforced polyamide 6 (CF-PA6).

The mechanical performance of AddJoining hybrid joints was assessed by a wide range of mechanical tests. An interfacial intralaminar failure mode was observed with quasi-static loading. Compared to adhesively bonded joints there was a significant increase in ultimate lap shear force (ULSF). In addition, the S-N curves obtained from fatigue testing indicated outstanding results and the hybrid joints produced reached their fatigue limits (10^6 cycles) with loading levels corresponding to 30 % of ULSF. By monitoring stiffness degradation, it was seen that damage evolution was dominated mostly by fiber rupture throughout fatigue life due to the high stiffness stability of hybrid joints.

Highlights:

From the extensive campaign of tests performed from this work, Figure 9-9 shows the general configuration of the joints used for damage tolerance tests and Figure 9-10 shows schematically the boundary conditions for the for single lap shear tests performed.

Figure 9-11 shows the S-N behavior of AddJoining hybrid joints, and Figure 9-12 shows the stiffness degradation of joints tested under cyclic loading for 47% of the ultimate lap shear force (ULSF).

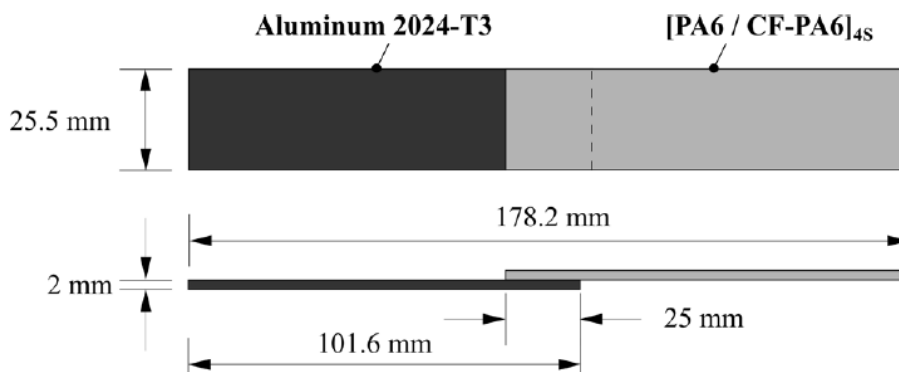


Figure 9-9 - Schematic of the specimen geometry of the AddJoining hybrid joints.

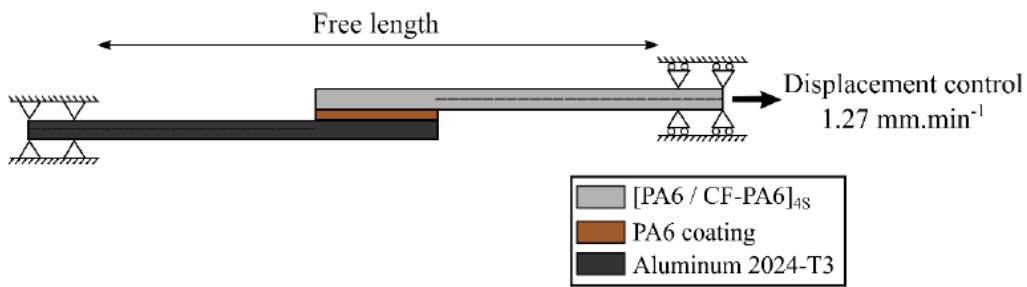


Figure 9-10 - Schematic of the boundary conditions for single lap shear testing.

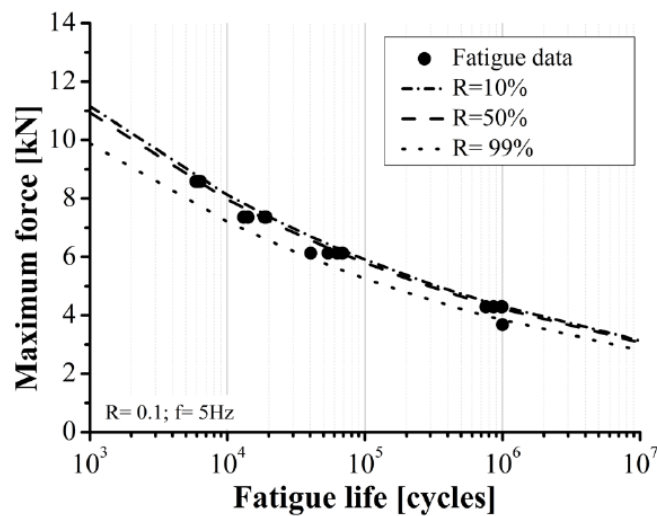


Figure 9-11 - Statistically derived S-N curves at different reliability levels using the two-parameter Weibull method.

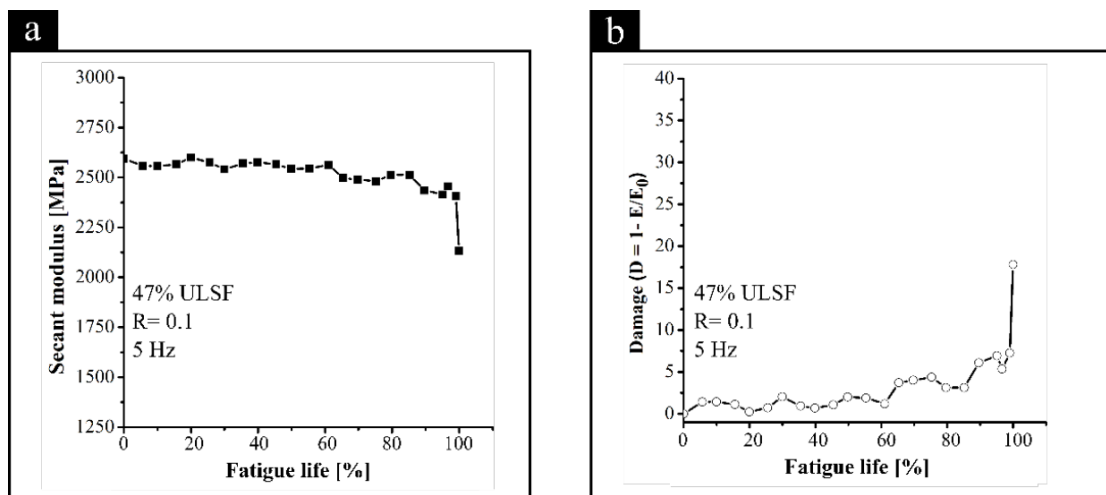


Figure 9-12 - Measured (a) stiffness variation, and (b) damage variation as a function of fatigue life during cyclic loading at 47% of the ULSF, corresponding to a maximum force of 5.8 kN.

10. STRUCTURAL HEALTH MONITORING

Damage detection and fatigue life estimation under random loads: A new structural health monitoring methodology in the frequency domain (Ref. [34])

This work was developed by researchers from the University of São Paulo (USP) and from KU Leuven, Belgium.

Summary:

This paper presents a methodology for structural health monitoring of fatigue cracks under stationary random loads. The methodology is composed of two parts: an empirical correlation to monitor the evolution of damage indices and a numerical scheme for fatigue life estimation. The damage indices are based on the variation of the vibrational response of the structure due to crack propagation.

Two damage metrics are studied, and the methodology is verified for a cantilever beam subjected to random base excitation. The case study validates the effectiveness of the methodology and shows that both metrics have the potential for damage detection. For the numerical estimation of the fatigue life, the proposed framework uses the probability density function of the stress, which is obtained from frequency-domain methods, and an equivalent stress approach based on the Walker's equation for fatigue crack growth. Excellent agreement is found between the predicted fatigue life and the experimental values.

Highlights and Main Conclusions:

The objective of this research is to integrate a methodology based on VBM for damage detection and fatigue life estimation of structures under spectrum loads. Two different DIs are used for damage quantification, and an empirical correlation is developed to relate the DI values to the fatigue life of the structure. Besides the empirical correlation, a numerical framework is presented for the estimation of fatigue crack growth using a frequency domain approach and an equivalent stress concept. Figure 10-1 summarizes the methodology.

A case study is examined, using an aluminum sheet in Al7075-T6. The geometry is a cantilever beam with 1.27-mm thickness, while the other dimensions are shown in Figure 10-2. Figure 10-3(a) shows one of the specimens mounted on top of the electromechanical shaker and Figure 10-3(b) shows the intact specimen with a strain gage attached.

Among various results obtained from this work, such as the stress histograms in the frequency domain (prediction and experimental data), and damage indexes

obtained via different methods for fatigue , Figure 10-4 was selected, showing the correlation between prediction and experimental data in terms of crack growth.

Since the method is based on frequency domain, there is no need for heavy calculations of stress history, which makes this solution easy to implement, turning it a good tool that could be readily generalized and employed on SHM systems for fatigue life estimation of structures under spectrum loads.

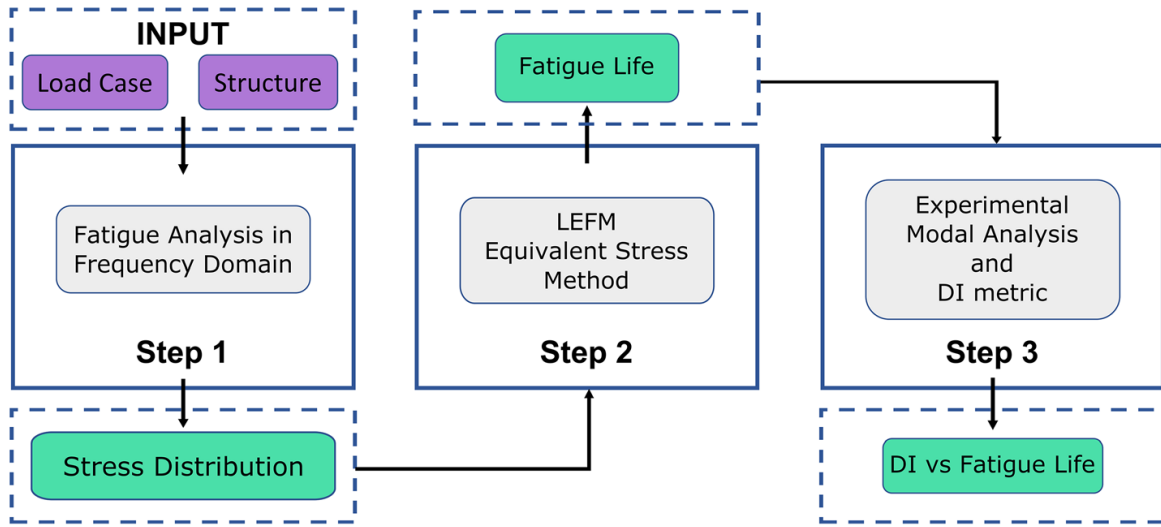


Figure 10-1 - Overview of the methodology used for this work.

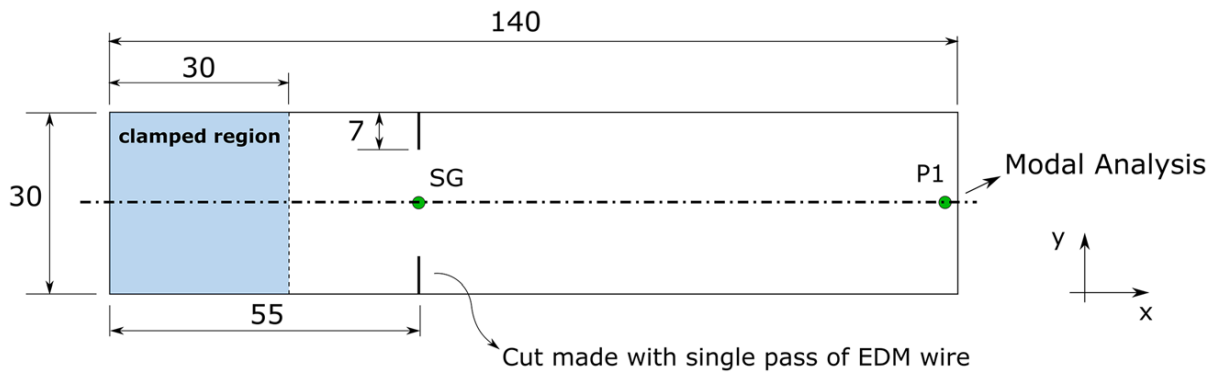


Figure 10-2 - Specimen geometry used in the random vibration tests (units: mm).

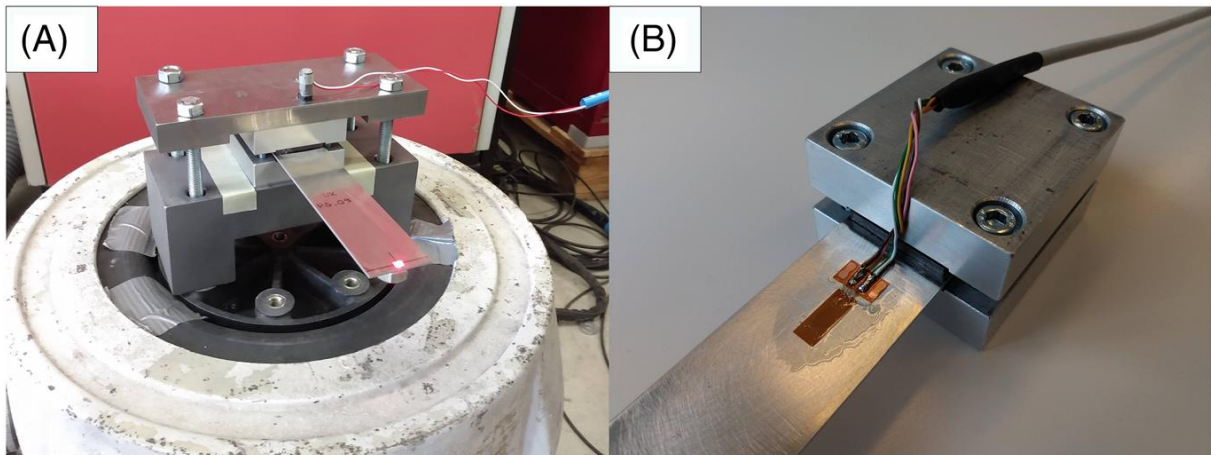


Figure 10-3 - (a) Experimental setup and; (b) Detail of the sample with strain gage.

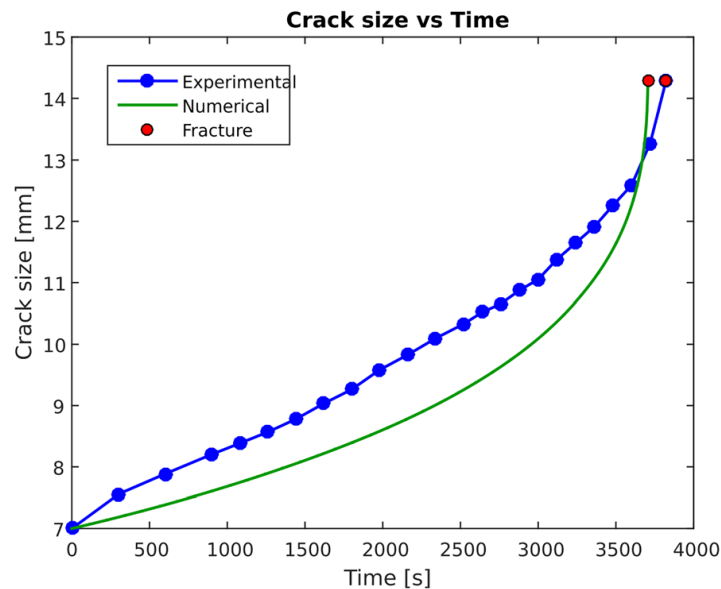


Figure 10-4 - Crack size versus time: experimental and numerical values.

Sensitivity analysis and damage identification in composite plates (Ref. [35])

This work was developed by researchers from the University of São Paulo (USP) and the State University of São Paulo (UNESP).

Summary:

The presence of composite materials in primary and secondary aircraft structures has increased over the years, combined with the use of Structural Health Monitoring (SHM) systems for the monitoring and assessment of the real conditions of the structure.

In this work, vibration-based methods and damage metrics are employed to monitor composite plates subjected to a controlled damage. A sensitivity analysis is also carried out to determine how much uncertainties in the mechanical properties of the structure can affect its modal response and the results are used to create an envelope for the expected frequency response of the plate. An experimental modal analysis was conducted in the plate in its intact condition and later three levels of damage were introduced in the plate and new modal analyses were carried out. The results were used to evaluate the performance of three different damage metrics.

Highlights and Main Conclusions:

The structure analyzed in this work is a plate made of carbon fiber reinforced polymer (CFRP). The laminate is made of carbon fibers in a polymeric matrix of polyphenylene sulfide (PPS). The stack configuration is $[0^\circ/90^\circ]_7$. The plate has dimensions of 390 mm x 365 mm and an average thickness of 2.19 mm. The plate was initially in a pristine condition, but for later analysis, damages was introduced in the plate via the insertion of two cuts with 2.3 mm thick on the border of the plate, and three levels of damage were evaluated (namely with cutting sizes L_c equal to 30 mm, 60 mm and 90 mm). Figure 10-5 shows (a) the plate and damage geometry and (b) the set-up of the experimental modal identification test highlighting the position of the four points, which were used in the sensitivity analysis.

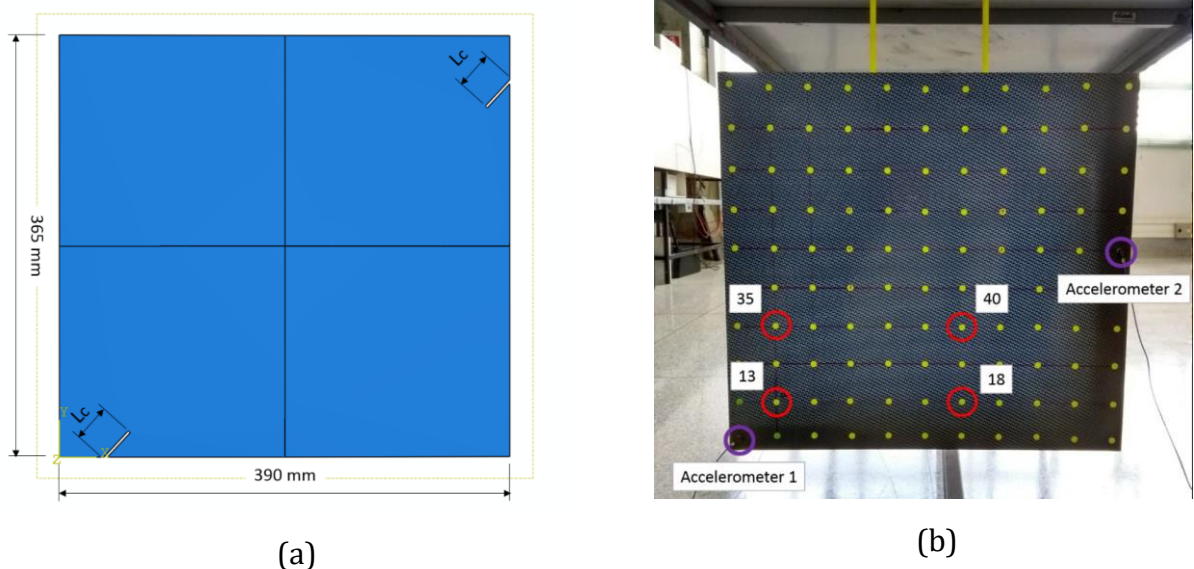


Figure 10-5 - Basic plate dimensions and set-up.

There are several techniques that can be used for damage identification from vibrational tests. The simplest one is the direct comparison of natural frequencies from the damaged structure with its natural frequencies from the pristine condition. Although easy to implement, this method has typically low sensitivity because shifts in natural frequency are usually associated with high levels of damage.

As an example, Figure 10-6 shows the FRFs of point H40 for the intact condition and for all the three damage levels. It can be observed that large differences in the FRF appear only for the highest damage level studied (that is, Damage Level 3).

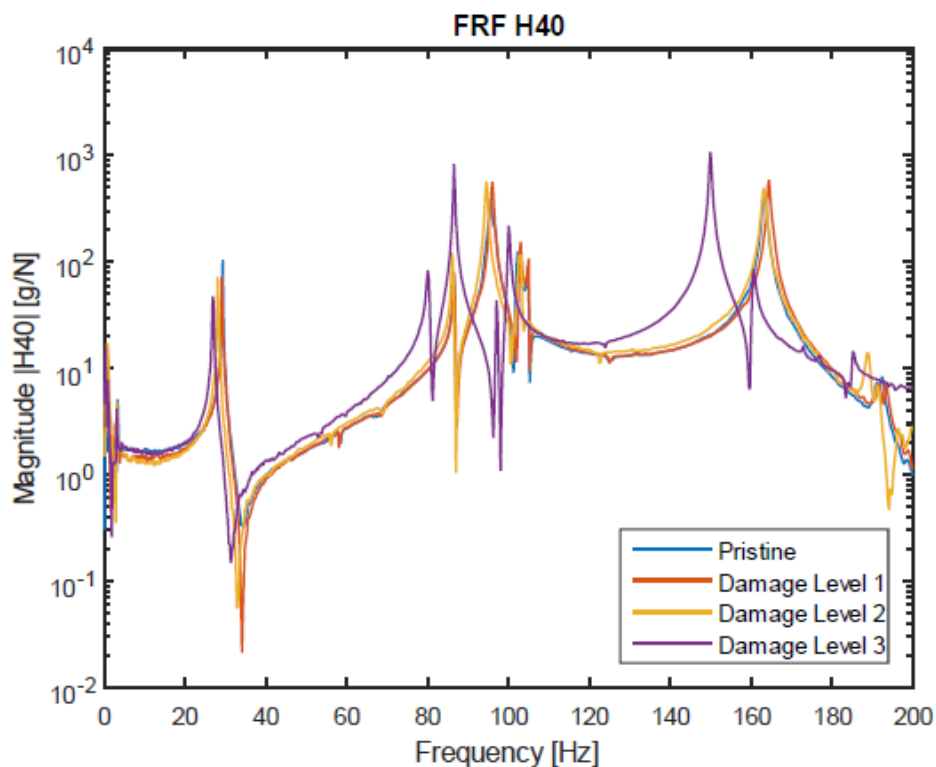


Figure 10-6 - Experimental FRFs of point 40 for the intact and damaged (Levels 1, 2 and 3) conditions.

Reliability of Lamb Wave SHM systems: influence of hydrostatic pressure, mechanical loading and fatigue on the value of a damage index (Ref. [36])

This work was developed by researchers from the Federal University of Rio Grande do Sul (UFRGS) and from Embraer R&D department.

Summary:

Structural Health Monitoring (SHM) systems can cause changes in paradigms in industrial maintenance, such as a move from time-based to condition-based

maintenance, where the integrity of a structure would be continuously monitored and analysed.

Lamb Waves (LW) are one of the most promising technologies for SHM since it is able of monitoring a relatively large area with a relatively small number of sensors, especially when compared to other techniques such as conventional ultrasound and eddy current. However, there is a need to evaluate the reliability of such systems under operating conditions. So, there are several research programs which aim to investigate the LW response variability when faced with temperature changes, mechanical load cycling and other physical effects.

This study is part of a collaboration program between LAMEF and Embraer R&D department. This paper presents initial results and discussions on the influence of different scenarios on lamb waves systems. Several laboratory tests have been conducted in order to evaluate the influence of conditions commonly imposed on aircraft structures on the signals, such as tension, compression or hydrostatic loads (found in fuel tanks).

Additionally, a study of structure settling under a cyclic loading was performed. The results show that each kind of load has a different influence on the signals, and it was also observed that the influences may change depending on excitation frequency.

In addition to analyzing the signals, the authors also observed the behaviour of a damage index (DI), which is the energy of a signal under the test conditions compared to the energy of a baseline signal. Signal comparison is a common method of detecting damage to a structure, but there is a need to separate the difference in signals from being caused by an operating condition or a damage.

These studies will be a key part to increase confidence on the SHM applications, providing the necessary knowledge for a successful future application in the aviation industry.

Highlights and Main Conclusions:

The sample sizes were kept the same for all tests. The specimens have 3 thickness: 3.4 mm, 6.35 mm and 12.7 mm. Piezoelectric transducers were bonded with 150 mm in between, in the same position for all samples and tests as shown in Figure 10-7.

Regarding mechanical loading, the results of the averaged DI are shown in Figure 10-8(a), the lowest value are at 0 kN applied as expected because the baseline are at this load. As the load increases its amplitude, the DI is also increased in a monotonic way.

The frequency of 200 kHz seems to be more sensitive to signal variation, and consequently it presents a greater variation of DI. The higher frequencies appear to

have less variation. This can be explained by the fact that it is taken from the ratio between the measured signal and the baseline signal, if these signals are saturated, there is less variation of the energy between them.

The result of the hydrostatic pressure test is shown in Figure 10-8(b), it shows the average values for the samples with same thickness acquired with central frequency of 200 kHz. It shows that an increase in the water column from the baseline state infers little change in the DI, however complete water removal greatly increases the DI value. In addition, thicker samples showed less sensitivity to pressure variation as well as absence of water. This may indicate that for the SHM system to be applicable in reservoirs it is always necessary the presence of fluid inside.

The paper also presents DI results for cyclic loading.

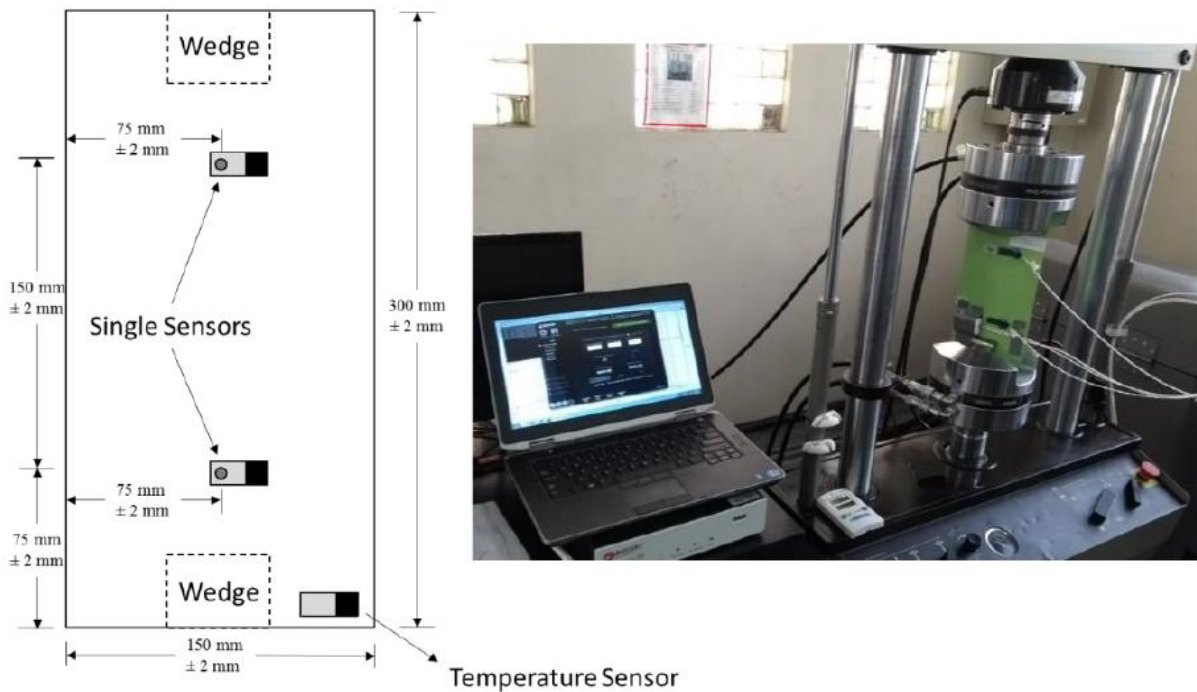


Figure 10-7 Specimen assembly and test setup.

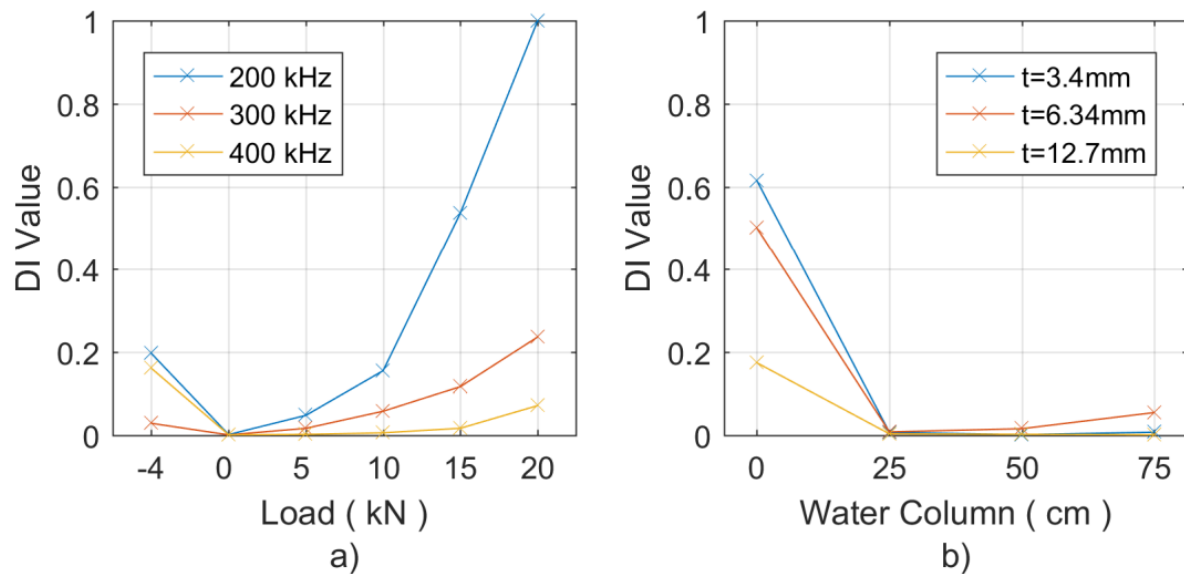


Figure 10-8 - Average DI under static longitudinal loading, thickness 2 mm; b) Average DI under hydrostatic pressure at 200 kHz.

An inverse damage location problem applied to AS-350 rotor blades using bat optimization algorithm and multiaxial vibration data (Ref. [37])

This work was developed by researchers from the Federal University of Itajubá (UNIFEI).

Summary:

In this study, a damage identification method is proposed using both the finite element method and the bat optimization algorithm applied to the AS-350 helicopter main rotor blade. First, the structure is numerically modeled and evaluated with and without the presence of induced damages. In a second approach, an inverse problem of optimization is constructed in order to identify certain damages in terms of its position and severity level.

Three different objective functions are evaluated according to the modal parameters of the rotor blade (vibrations in x, y and z directions). Numerical results, through analysis of variance, showed that local damage significantly modifies the modal response into a non-linear aspect. The modal response used was able to identify, with great efficiency, the actual (noise simulated) damages induced in terms of location and severity. Accordingly, a damage identification method is developed in order to better handle any measurement data (to find/regarding) structural changes (or damages) in complex aerospace structures.

The results from these numerical examples indicate that the proposed approach can be used for detection of true damage locations and estimation of damage magnitudes with satisfactory accuracy, even under high measurement noise.

Highlights:

This paper first presents a summary of vibration-based damage identification methods in aeronautic field, and an explanation about the Bat Optimization Algorithm (BA). Then, the proposed application is discussed, that is the AS-350 rotor blade (Figure 10-9).



Figure 10-9 - Helicopter model AS-350 and its rotor blade in detail.

Three different scenarios damage scenarios were evaluated, as shown in Figure 10-10. These distinct scenarios address damage at different positions along the blade and with different intensities of damage. An inverse problem is a method that seeks to obtain a physical data from observed measurements by mathematical framework. In this study, a total of 10 (virtual) sensors are used in the rotor blade evenly distributed in its area excluding the support as shown in Figure 10-11.

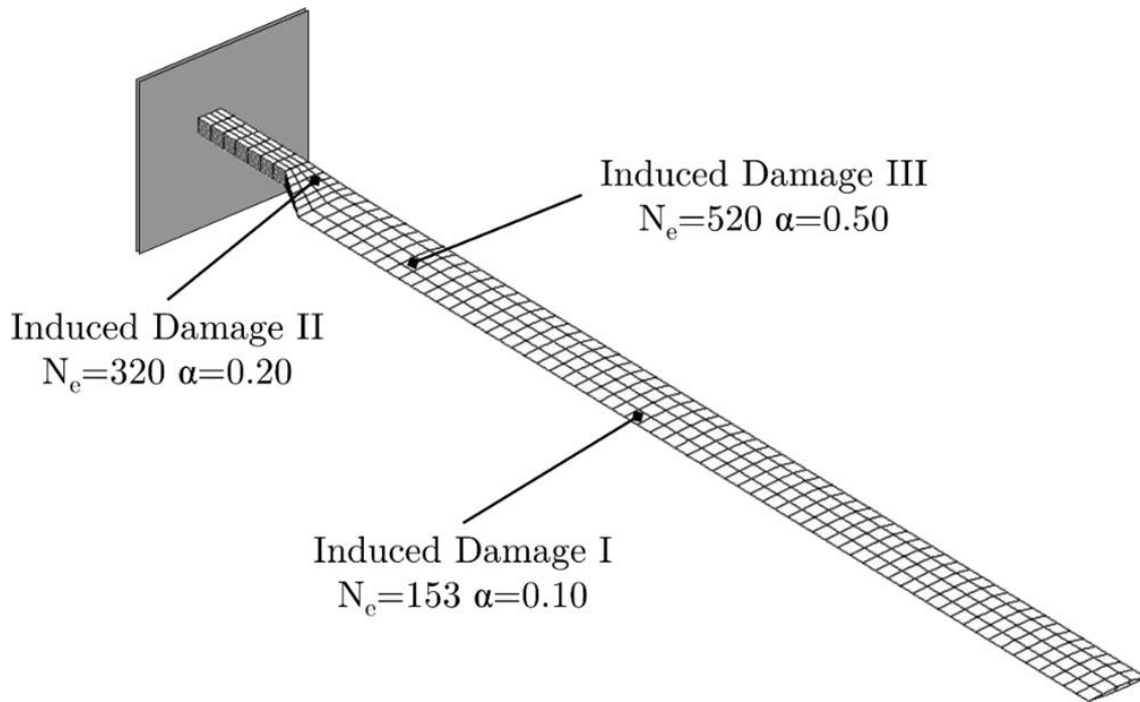


Figure 10-10 - Three different scenarios of induced damage on the rotor blade.

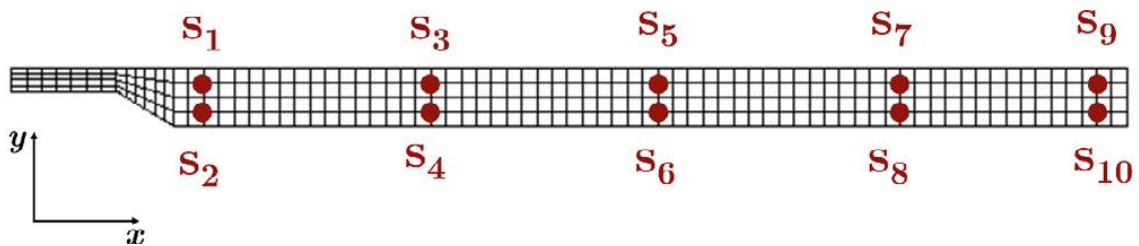


Figure 10-11 - Sensors distributed uniformly on the main rotor blade.

For each objective function and induced damage, the BA algorithm was run 10 times, and of these results, it was taken the average for the damage rate and the mode for the damaged element, that is to say, the most frequent result. Three objective functions J_1 , J_2 and J_3 were evaluated. Figure 10-12 shows results of damage identification considering the objective function J_1 , where α is a damage severity parameter.

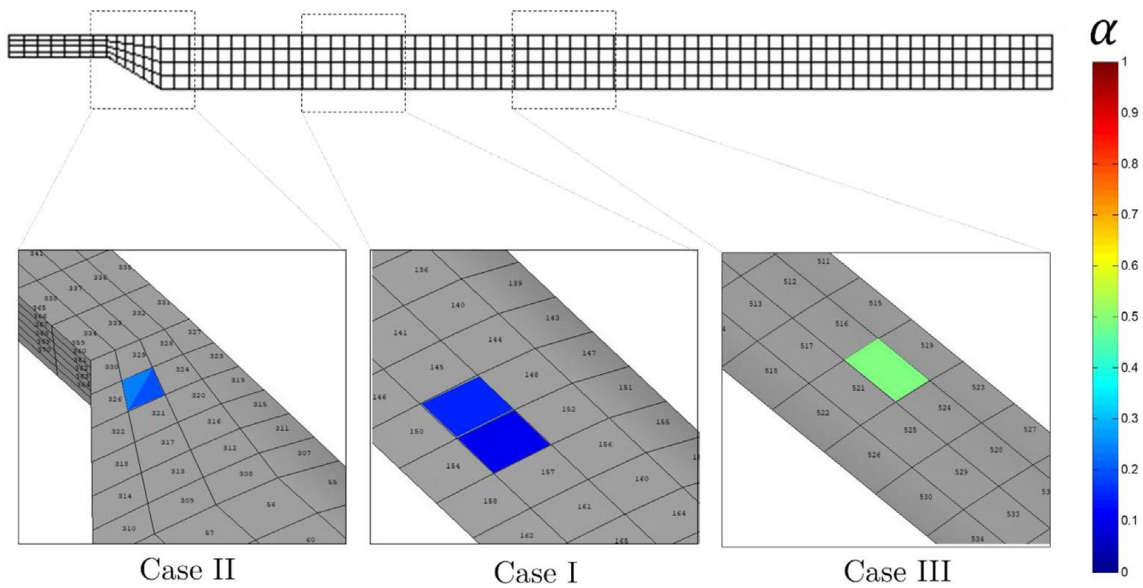


Figure 10-12 - Graphical results of damage identification considering the objective function J_1 in all three damage cases.

Sensor placement optimization and damage identification in a fuselage structure using inverse modal problem and firefly algorithm (Ref. [38])

This work was developed by researchers from the Federal University of Itajubá (UNIFEI).

Summary:

To overcome limitations of traditional non-destructive inspections (NDIs), damage identification techniques have been developed from global indicators, mainly those based on modal data.

In this study, damages are identified by solving an inverse problem. A fuselage model of a regional aircraft is considered and the firefly algorithm (FA) metaheuristic is applied to solve the inverse problem in order to identify structural damages (location and severity). The method is then solved in two main fronts: (1) the direct problem using finite element analysis and (2) the inverse problem by minimizing an objective function.

Evaluating modal response at many points on a large-scale structure can become prohibitive. For this, a method of optimizing sensors is performed using the Fisher information matrix (FIM). Results are compared considering the sensor placement optimization problem. It is noticed that optimized sensors contribute to an improvement in the identification of damages, mainly for complex and large-scale structures. The proposed optimized damage identification process using FIMFA has the potential to be extended to a wide range of SHM applications in complex structures. Hence, traditional NDIs have many shortcomings due to the complexity

of large-scale structures as well as modern design structures and may not be practicable if the structure has restricted access. Accordingly, an enhanced damage identification method is developed in order to better handle measurement data to find structural changes (or damages) in complex aerospace structures.

Optimized damage identification in CFRP plates by reduced mode shapes and GA-ANN methods (Ref. [39])

This work was developed by researchers from the Federal University of Itajubá (UNIFEI).

Summary:

Delamination is one of the most common failure modes in laminated composites that leads the separation along the interfaces of the layers. The structural performance can be significantly affected by this degradation. Such damages are not always visible on the surface and could potentially lead to catastrophic structural failures. The existence of delamination alters the vibration characteristics of the laminated structures, so if they are detected and measured previously, they can be used as indicator for quantifying health and the potential risk of catastrophic failures.

In this study, an optimized methodology for delamination identification on laminated composite plates involving the use of reduced mode shapes and computational tools, i.e., Genetic Algorithm (GA) and Artificial Neural Networks (ANN) is performed. In a first step, the sensor distribution on the surface of the structure was optimized using Fisher Information Matrix (FIM) criteria. After, GA and ANN were applied in order to identify and predict delamination location. A feed-forward based neural network is used in order to detect damage on the laminated plate using data obtained from Finite Element Analysis (FEA).

The present methodology identifies damage localization in structures and also quantifies damage severity. The applicability of the technique is demonstrated on laminated plates and results are compared with numerical algorithms. This paper shows the effectiveness of GA and ANN as tools for delamination damage identification problem. The algorithms in their inverse formulations are capable of predicting accurately delamination position in plates-like structures.

Developments on Augmented Reality

Embraer, together with SENAI CIMATEC, developed an experimental Augmented Reality (AR) tool to support maintenance activities and the Full Scale Fatigue Test (FSFT) Structural Testing team.

The tool was developed to assist in the location of events, principal structural elements (PSE) and display the location of the aircraft frames and stringers. Figure 10-13 shows one example of the AR images over the aircraft fuselage structure.

The project included the participation of the Structural Testing on Ground, Maintenance Engineering and Technical Information areas, among others.



(a)



(b)

Figure 10-13 - Example of application of the AR tool: (a) internal view, (b) external view.

Participation in ReMAP - Real-time Condition-based Maintenance for Adaptive Aircraft Maintenance Planning

Embraer R&D is currently involved in the ReMAP initiative (Ref. [40]), working on "Sensor technologies for SHM" e "Structural Health Management – Diagnostics & Remaining Useful Life Prognostics".

11. LOADS

A modified cumulative damage approach accounting for plasticity effects on fatigue life (Ref. [41])

Summary:

This work proposes a new methodology of cumulative fatigue damage calculation in structures subjected to overload that causes plastic deformations at notches. This new approach was based on overload tests performed with open-hole and riveted lap-joint specimens manufactured of the aluminum 2524-T3 alloy.

Fatigue tests with constant amplitude loads were carried out in order to fit the S-N curve for both specimens. In addition, block load spectrum tests were important to observe the material behavior when blocks that cause plasticity at the notch root were applied. Finally, the tests of single overload together with the calculation of stresses at the notch root based on the Neuber's methodology supported the new method of calculating the cumulative fatigue damage proposed.

The results of the overload tests in open-hole plate specimens showed that the higher the plasticity level at the notch root, the greater the increase in fatigue life is, regardless of the moment when the overload was applied (with previous damage or not). In addition, observations on the behavior of the riveted lap-joint specimens in constant amplitude loads showed that the severity factor (SF) calculation method together with the S-N curve extrapolation method provides a good approximation of the fatigue behavior for this type of structure.

The new proposal compared to other methodologies for calculating cumulative fatigue damage obtained the same estimates as Miner's approach for constant and block loading, not standing out among the other approaches. However, for the open hole single overload tests, the new approach presented fatigue life estimations closer to experimental results than the other approaches. The new approach to cumulative fatigue damage shows promising results since it takes into account the plastic effects at the notch root resulted from overloads.

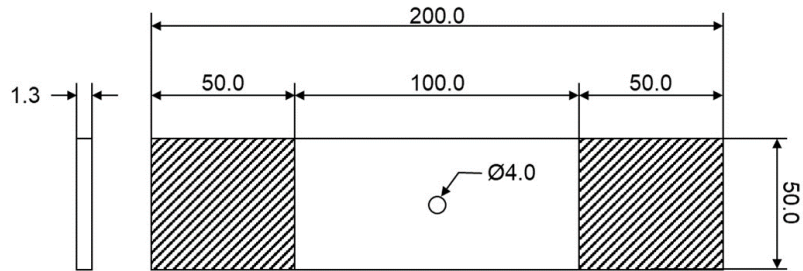
Highlights and Main Conclusions:

Figure 11-1 shows the typical test specimens used in this development, that nearly follow ASTM and SAE standards.

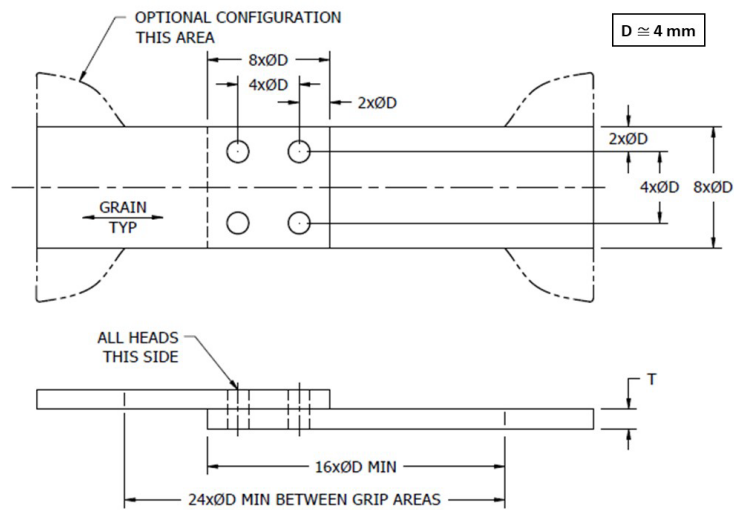
From the test campaign, some overloads lead to life increases higher than 15 times when compared to the baseline constant amplitude loading, as it can be seen in Figure 11-2.

Regarding the new methodology that was proposed (whose details may be found in the reference), Figure 11-3 and Figure 11-4 show the adhesion of this

methodology to experimental results. In the first case, the comparison is presented for for two and three block loading tests, while in the second plot the comparison is presented for single overload tests. There results were obtained with the open hole specimens.



(a)



(b)

(a) Open-Hole specimen dimensions

(b) Lap-Joint specimen dimensions and characteristics.

Figure 11-1 - Overview of the open hole and joint specimens.

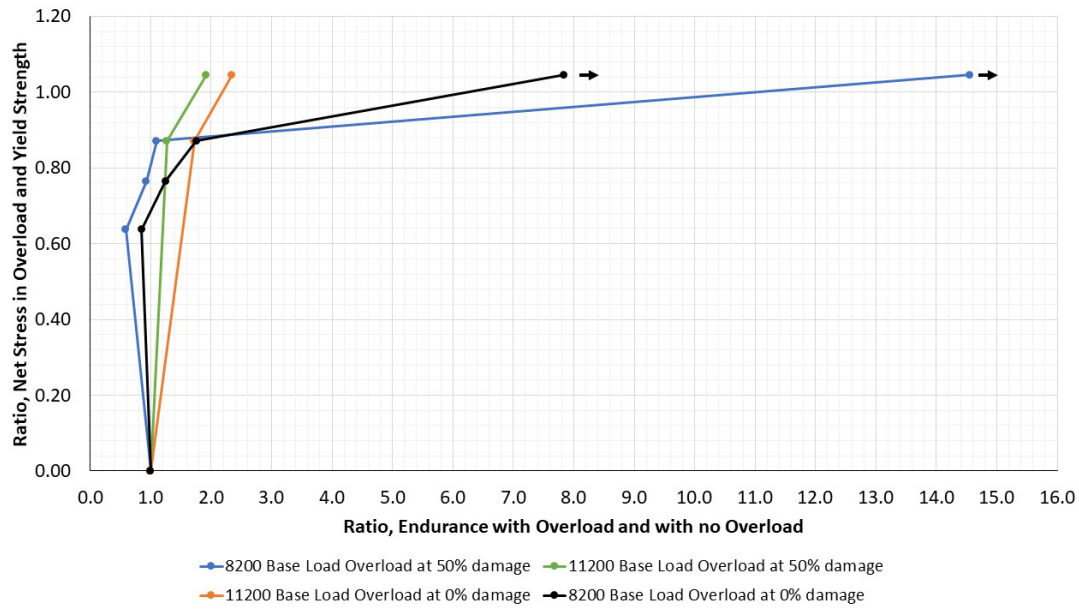


Figure 11-2 - Life gain analysis in terms of overload net stress over yield strength and the total number of cycles for failure over the number of cycles for failure at base load.

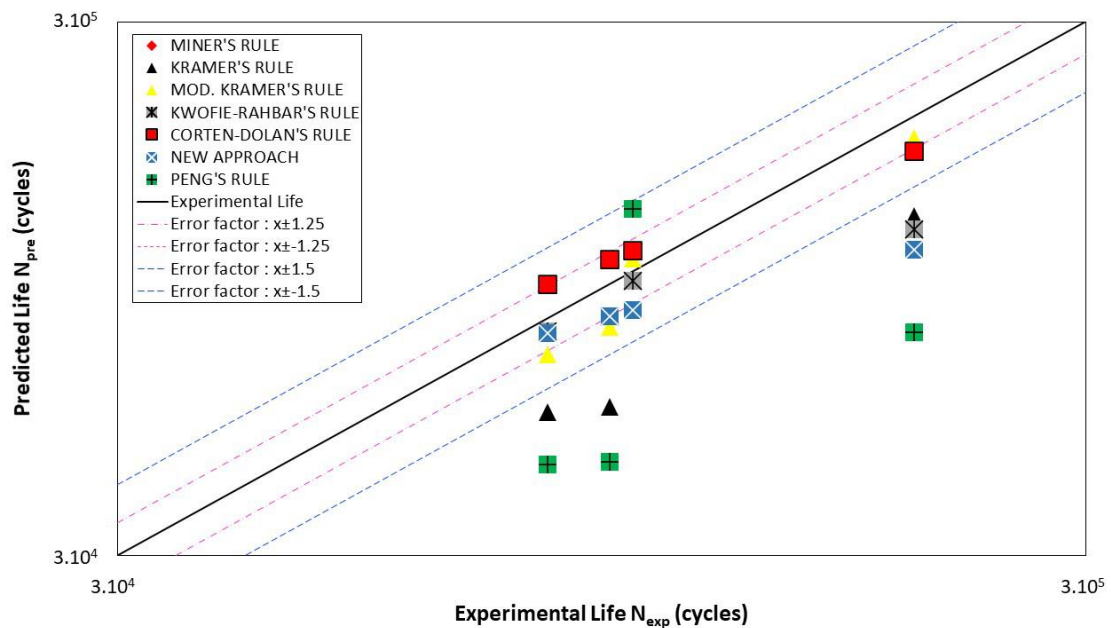


Figure 11-3 - Damage theory approaches comparison for two and three block loading tests.

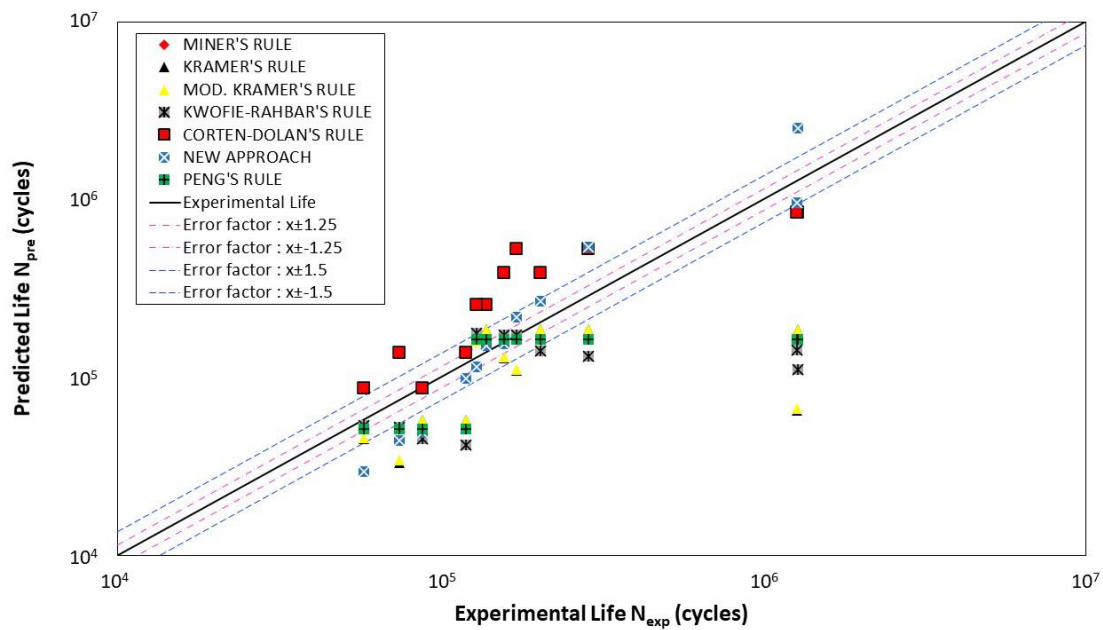


Figure 11-4 - Damage theory approaches comparison for overload tests.

12. AIRWORTHINESS

EASA Part 26 Requirements

In 2021, EASA is releasing Part 26 Ageing Aircraft Requirements. There are many categories of aircraft affected by this requirement, including families of commercial and executive jets made in Brazil.

Most of the requirements present commonality with previous FAA and ANAC Part 26 requirements. Others may require additional documentation for compliance.

This is a long term work, and some activities may last until 2026 or later.

13. REFERENCES

General

1. Chaves, C. E., *A review of aeronautical fatigue investigations in Brazil*, International Committee on Aeronautical Fatigue and Structural Integrity (ICAF), Helsinki – Finland – June, 2015.
2. Chaves, C. E., *A review of aeronautical fatigue investigations in Brazil*, International Committee on Aeronautical Fatigue and Structural Integrity (ICAF), Nagoya - Japan – June, 2017.
3. Chaves, C. E., *A review of aeronautical fatigue investigations in Brazil*, International Committee on Aeronautical Fatigue and Structural Integrity (ICAF), Krakow – Poland – June, 2019.

Concepts

4. Brito-Santana, H., Thiesen, J. L. M., Medeiros, R., Ferreira, A. J. M., Rodriguez-Ramos, R., Tita, V., *Multiscale analysis for predicting the constitutive tensor effective coefficients of layered composites with micro and macro failures*, Applied Mathematical Modelling 75 (2019) 250-266.
5. De Oliveira, L. A., Donadon, M. V., *A cohesive zone model to predict fatigue-driven delamination in composites*, Engineering Fracture Mechanics 235 (2020) 107124.
6. De Oliveira, L. A., Donadon, M. V., *Delamination analysis using cohesive zone model: A discussion on traction-separation law and mixed-mode criteria*, Engineering Fracture Mechanics 228 (2020) 106922.

Analysis and Simulation

7. Pascon, J. P., Torres, M. A. S., Baptista, C. A. R. P., *Numerical model for the stress field ahead of a crack in elastoplastic regime*, Procedia Structural Integrity 17 (2019) 411-418.
8. Ferreira, G. F. O., Ribeiro, M. L., Ferreira, A., J. M., Tita, V., *Computational analyses of composite plates under low-velocity impact loading*, Materials Today: Proceedings 8 (2019) 778-788.
9. Urzedo Quirino, M., Tita, V., Ribeiro, M. L., *Computational prediction of a composite material response to impact by using a viscoelastic damage model*, Proceedings of the 7th International Symposium on Solid Mechanics - MECSOL 2019, ABCM, Brazil.

10. Ribeiro, M. L., Angélico, R. A., Medeiros, R., Tita, V., *Finite element analyses of low velocity impact on thin composite disks*, International Journal of Composite Materials, Vol.3(6B) 59-70.

Metallic Materials – Fatigue and Fracture Properties

11. Antunes, A. M. B. S., Baptista, C. A. R. P., Barboza, M. J. R., Carvalho, A. L. M., Mogili, N. V. V., *Effect of the interrupted aging heat treatment t6i4 on the tensile properties and fatigue resistance of AA7050 alloy*, Journal of the Brazilian Society of Mechanical Sciences and Engineering (2019) 41:319.

Metallic Materials - Fretting

12. Pinto, A. L., Cardoso, R. A., Talemi, R., Araújo, J. A., *Fretting fatigue under variable amplitude loading considering partial and gross slip regimes: Numerical analysis*, Tribology International 146 (2020) 106199.
13. Gailliegue, T., Doca, T., Araújo, J. A., Ferreira, J. L. A., *Fretting life of the Al7050-T7451 under out-of-phase loads: Numerical and experimental analysis*, Theoretical and Applied Fracture Mechanics 106 (2020) 1024492.
14. Almeida, G. M. J., Pessoa, G. C. V., Castro, F. C., Araújo, J. A., *Investigation of crack initiation path in AA7050-T7451 under fretting conditions*, Tribology International 144 (2020) 106103.
15. Araújo, J. A., Castro, F. C., Cardoso, R. A., *Life prediction in multiaxial high cycle fretting fatigue*, International Journal of Fatigue 134 (2020) 105504.

16. Cardoso, R. A., Ferry, B., Montebello, C., Meriaux, J., Pommier, S., Araújo, J.A., *Study of size effects in fretting fatigue*, Tribology International 143 (2020) 106087.

Metallic Materials - Processes

17. Baptista, C. A. R. P., Lima, M. S. F., Riva, R., Siqueira, R. H. M., *Fatigue crack growth behavior of laser-shock processed aluminum alloy 2024-T3*, Procedia Structural Integrity 17 (2019) 324-330.
18. Gonçalves, C. M., Godefroid, L. B., Lima, M. S. F., Sampaio, N. P., *Effect of different forms of application of a laser surface treatment on fatigue crack growth of an AA6013-T4 aluminum alloy*, Journal of Materials Engineering and Performance (2019) 28:5832-5842.
19. Moreto, J. A., dos Santos, M. S., Ferreira, M. O. A., Carvalho, G. S., Gelamo, R. V., Aoki, I. V., Taryba, M., Bose Filho, W. W., Fernandes, J. C. S., *Corrosion and corrosion-fatigue synergism on the base metal and nugget zone of the 2524-T3 Al alloy joined by FSW process*, Corrosion Science 182 (2021) 109253.

Composite Materials and Structures

20. Tonatto, L. P., Tita, V., Amico, S. C., *Composite spirals and rings under flexural loading: Experimental and numerical analysis*, Journal of Composite Materials, 2020, Vol. 54(20) 2697-2705.
21. Gonilha, J. A., Silvestre, N., Correia, J. R., Tita, V., Martins, D., *Novel progressive failure model for quasi-orthotropic pultruded FRP structures: Formulation and calibration of parameters (Part I)*, Composite Structures 255 (2021) 112974.
22. Gonilha, J. A., Silvestre, N., Correia, J. R., Tita, Almeida-Fernandes, L., *Novel progressive failure model for quasi-orthotropic pultruded FRP structures: Application to compact tension and web-crippling case studies (Part II)*, Composite Structures 255 (2021) 112973.
23. Lamin, W. M., *Quasi-static translaminar fracture behavior of additively manufactured continuous carbon fiber reinforced thermoplastic*, MSc Dissertation, Aeronautical Institute of Technology, 2019.
24. Brito, C. B. G., Sales, R. C. M., Donadon, M. V., *Effects of temperature and moisture on the fracture behaviour of composite adhesive joints*, International Journal of Adhesion & Adhesives 100 (2020) 102607.
25. Marinho, N. R., Arbelo, M. A., Gonzalez, F., Candido, G. M., Sales, R. C. M., Donadon, M. V., *Experimental characterization of Mode I interlaminar fracture toughness in low-melt PAEK thermoplastic composite material*, 25th ABCM International Congress of Mechanical Engineering, October 20-25, 2019, Uberlândia – MG, Brazil.
26. Ramírez, F. M. G., Garpelli, F. P., Sales, R. C. M., Cândido, G. M., Arbelo, M. A., Shiino, M. Y., ; Donadon, M. V., *Hygrothermal effects on the fatigue delamination growth onset in interlayer toughened CFRP joints*. International Journal Of Fatigue, 138 (2020) 105729.
27. Van den Akker, B. P. H., Donadon, M. V., Loendersloot, R., De Oliveira, L. A., Arbelo, M. A., *The influence of hygrothermal aging on the fatigue behavior and residual strength of post-buckled co-bonded stiffened panels subjected to compressive loading*, Composites Part B 194 (2020) 108023.

Hybrid Materials and Structures

28. Borba, N. Z., *Design and mechanical integrity of friction riveted joints for thermoplastic composite*, PhD thesis, 2020.
29. Borba, N. Z., dos Santos, J. F., Amancio-Filho, S. T., *Hydrothermal aging of friction riveted thermoplastic composite joints for aircraft applications*, Composite Structures 255 (2021) 112871.

30. Borba, N. Z., Körbelin, J., Fiedler, B., dos Santos, J. F., Amancio-Filho, S. T., *Low-velocity impact response of friction riveted joints for aircraft application*, Materials and Design 186 (2020) 108369.
31. Borba, N. Z., Kötter, B., Fiedler, B., dos Santos, J. F., Amancio-Filho, S. T., *Mechanical integrity of friction-riveted joints for aircraft applications*, Composite Structures 232 (2020) 111542.
32. André, N. M., *Mechanical integrity and corrosion behavior of metalcomposite hybrid joints produced with Friction Spot Joining*, PhD Thesis, 2020.
33. Falck, R. M. M., *A new additive manufacturing technique for layered metal-composite hybrid structures*, PhD Thesis, 2020.

Structural Health Monitoring

34. Marques, D. E. T., Vandepitte, D., Tita, V., *Damage detection and fatigue life estimation under random loads: A new structural health monitoring methodology in the frequency domain*, Fatigue and Fracture of Engineering Materials and Structures, 2021;1–15.
35. Marques, D. E. T., Pagani Jr., C. C., Ribeiro, M. L., Tita, V., *Sensitivity analysis and damage identification in composite plates*, Proceedings of the 7th International Symposium on Solid Mechanics - MECSOL 2019, ABCM, Brazil.
36. Dorneles, L. L., Clarke, T. R., Dotta, F., Tamba, A. F. , Rulli, R. P., *Reliability of Lamb Wave SHM systems: influence of hydrostatic pressure, mechanical loading and fatigue on the value of a damage index*, 12th International Workshop on Structural Health Monitoring, 2019.
37. Gomes, G. F., Chaves, J. A. S., Almeida, F. A., *An inverse damage location problem applied to AS-350 rotor blades using bat optimization algorithm and multiaxial vibration data*, Mechanical Systems and Signal Processing 145 (2020) 106932.
38. Gomes, G. F., Pereira, J. V. Purcino, *Sensor placement optimization and damage identification in a fuselage structure using inverse modal problem and firefly algorithm*, Evolutionary Intelligence (2020) 13:571–591.
39. Gomes, G. F., Almeida, F. A., Junqueira, D. M., *Optimized damage identification in CFRP plates by reduced mode shapes and GA-ANN methods*, Engineering Structures 181 (2019) 111–123.
40. www.H2020-remap.eu

Loads

41. Moreira, T. M. M., *A modified cumulative damage approach accounting for plasticity effects on fatigue life*, MSc Dissertation, Aeronautics Institute of Technology, 2020.